Structural and mechanistic studies of the inhibitory effect of Liprin-α3 on mDia1 function

Inaugural - Dissertation

zur

Erlangung des Doktorgrades

der Mathematisch-Naturwissenschaftlichen Fakultät

der Universität zu Köln

vorgelegt von

Julian Brenig

aus Köln

Hundt Druck GmbH, Köln

2016

Structural and mechanistic studies of the inhibitory effect of Liprin-α3 on mDia1 function

Inaugural-Dissertation

zur

Erlangung des Doktorgrades

der Mathematisch-Naturwissenschaftlichen Fakultät

der Universität zu Köln

vorgelegt von

Julian Brenig

aus Köln

Berichterstatter:	Dr. Michael Lammers (Betreuer)
Gutachter:	Prof. Dr. Kay Hofmann

Tag der letzten mündlichen Prüfung: 04.12.2015

Zusammenfassung

Diaphanous-related formins (DRFs) sind Multidomänen-Proteine, die an der Nukleation und dem Zusammenbau von Aktinfilamenten beteiligt sind. Sie werden durch eine autoinhibitorische Interaktion der C-terminalen Domäne (*Diaphanous-autoregulatory domain*, $mDia_{DAD}$) mit der N-terminalen Domäne (*Diaphanous-inhibitory domain*, $mDia_{DID}$) reguliert. Durch die Bindung von aktivem RhoA wird dieser inhibitorische Zustand aufgelöst und das Formin gleichzeitig zur Plasmamembran rekrutiert. Eine aktuelle Studie indentifizierte Liprin-α3 als einen weiteren Interaktionspartner des Formins mDia1. Es konnte gezeigt werden, dass die Überexpression von Liprin-α3 zu einer Verringerung in der Menge an zellulärem Aktin sowie zu der Aufhebung der Lokalisierung von mDia1 an der Plasmamembran führte. Das Ziel dieser Arbeit war es, die Bindung von Liprin-α3 an mDia1 strukturell und mechanistisch zu charakterisieren, und zu analysieren welchen Einfluss dies auf die Aktivität von mDia1 hat.
Umfassende ITC Studien wurden durchgeführt, um ein minimales Liprin-α3 Fragment zu definieren, das noch immer dazu in der Lage ist an mDia1 zu binden und die Menge an zellulärem Aktin zu verringern. Dieses Fragment wurde dazu verwendet, die Kristallstruktur des mDia1 • Liprin-α3 Komplexes zu lösen. Mit Hilfe von thermodynamischen und kinetischen Analysen konnte gezeigt werden, dass Liprin-α3 die Bindung von RhoA an $mDia_N$ effizienter inhibiert als die Bindung von $mDia_{DAD}$ an $mDia_N$. Zusätzlich deuten die strukturellen Daten darauf hin, dass die Dissoziation von Liprin-α3 von mDia1 durch RhoA allosterisch erfolgt, während $mDia_{DAD}$ und Liprin-α3 um eine überlagernde Bindestelle an mDia1 konkurrieren. Überexpressionsstudien mit Liprin-α3 in HeLa und N2a Zellen zeigten Unterschiede in der Lokalisierung von Liprin-α3 und dem inhibitorischen Potential von Liprin-α3 auf die Funktion von mDia1. Diese Ergebnisse lassen auf Zelltyp abhängige Mechanismen schließen, welche die Funktion von Liprin-α3 regulieren.
Basierend auf den in der Studie gewonnenen Daten werden die folgenden Mechanismen bezüglich der Inhibierung von mDia1 durch Liprin-α3 postuliert. Erstens, die Wiederherstellung des autoinhibitorischen Zustandes wird unterstützt durch die veränderten Bindungsaffinitäten von RhoA und $mDia_{DAD}$ an $mDia_N$. Zweitens, RhoGAPs sind in der Lage effektiver mit $mDia_N$ um die Bindung von RhoA zu konkurrieren. Dadurch wird die Hydrolyse von gebundenem GTP in RhoA verstärkt, was zu einer Inaktivierung von RhoA und anschließend von mDia1 führt. Drittens, Liprin-α3 schwächt die Interaktion mit weiteren mDia1 aktivierenden Proteinen und ist in der

Lage zusätzliche mDia1 regulierende Proteine zu rekrutieren. Zusammengefasst präsentiert diese Arbeit ein Modell für die Inhibierung der Aktivität von mDia1 durch Liprin-α3 und verdeutlicht die Bedeutung vom Gerüstprotein Liprin-α3 für die Regulierung des Aktinzytoskeletts.

"Men love to wonder, and that is the seed of science"

Ralph Waldo Emerson, Philosopher

Abstract

Diaphanous-related formins (DRFs) are multi-domain proteins, that are involved in the nucleation and assembly of actin filaments. They are regulated by an autoinhibitory interaction of the C-terminal Diaphanous-autoregulatory domain ($mDia_{DAD}$) with the N-terminal Diaphanous-inhibitory domain ($mDia_{DID}$). Binding of active Rho proteins to the N-terminal domain leads to the release of the inhibitory state and plasma membrane localization of DRFs. Most recently, Liprin-α3 has been identified as a novel interaction partner of mDia1. It was shown, that overexpression of Liprin-α3 leads to a reduction in the amount of cellular F-actin and the translocation of mDia1 from the plasma membrane. The aim of this thesis was to structurally and mechanistically characterize the binding of mDia1 and Liprin-α3 and to investigate how the presence of Liprin-α3 influences the activity of mDia1.

Comprehensive *in vitro* studies were performed to define a minimal Liprin-α3 fragment (Liprin-core region, LCR), that still binds to mDia1 and is able to induce a reduction in the amount of cellular F-actin. Using this fragment the interaction of Liprin-α3 and mDia1 was also characterized structurally. Presence of Liprin-α3 reduced the binding affinity of RhoA to $mDia_N$ more efficiently than the binding of $mDia_{DAD}$ to $mDia_N$, as determined by thermodynamic and kinetic analysis. Furthermore, the structural data revealed, that the dissociation of Liprin-α3 from mDia1 by RhoA is mediated allosterically, while $mDia_{DAD}$ dissociates Liprin-α3 by competing for the a highly overlapping binding site on $mDia_N$. Additionally, overexpression of Liprin-α3 in HeLa and N2a cells displayed differences in Liprin-α3 localization and the reduction of the cellular amount of F-actin. This indicated the importance of cell-type dependent mechanisms that regulate the function of Liprin-α3.

Based on the data obtained in this study the following mechanisms explaining the inhibition of mDia1 by Liprin-α3 were postulated. Firstly, the re-establishment of the mDia1 autoinhibitory state is supported by the altered binding affinities of RhoA and $mDia_{DAD}$ for $mDia_N$. Secondly, RhoGAPs can compete more efficiently with $mDia_N$ for RhoA binding. This leads to the downregulation of RhoA activity due to enhanced GTP hydrolysis and subsequently the inactivation of mDia1. Thirdly, Liprin-α3 inhibits the interactions of mDia1 with additional activating proteins, besides RhoA, and is able to recruit further regulatory proteins of mDia1 function. In conclusion, this thesis presents a model for the inhibition of mDia1 function by Liprin-α3, emphasizing the impact of the scaffold protein Liprin-α3 on the regulation of the actin cytoskeleton.

Table of content

List of Figures

List of Tables

1. Introduction

1.1. Actin cytoskeleton

The cytoskeleton is essential for many cellular processes such as cell migration, mitosis, cell division, cell polarity and many more (Clarke & Spudich, 1977; Pollard, 1976). In vertebrates it can be composed of microfilaments, microtubules and intermediate filaments. All three work together to form highly organized networks and are thereby able to respond to and to mediate internal and external signals (Zigmond, 1996). Microtubules are polymeric structures that consist of α- and β-tubulin dimers. They are important for the establishment of the spindle apparatus, intracellular transport processes and macromolecular assemblies, such as flagella or cilia (Petry *et al.*, 2013; Vale, 2003). Important for the biological function is their polar organization. At their plus-end only β-subunits are present, whereas the minus-end is composed of α-subunits. The elongation rate is distinct faster at the plus-end, compared to the minus-end (Walker *et al.*, 1988). Intermediate filaments are assembled of two parallel coiled-coil dimers, that align in an anti-parallel orientation. In difference to microtubules and microfilaments this leads to a nonpolar organization, of so-called A11-tetramers (Herrmann *et al.*, 1996). The second notable difference is their distinct specificity for tissues and organisms (Block *et al.*, 2015). Based on their sequence homology, they are classified in five subfamilies. They all have in common to provide the cell with mechanical resilience and stability (Schopferer *et al.*, 2009). Well described members are Keratin, Desmin and Vimentin (Lin *et al.*, 2010; Pawelzyk *et al.*, 2014).

Microfilaments or filamentous actin (F-actin) are composed of polar, globular actin (G-actin) monomers. G-actin has a molecular weight of approximately 42 kDa and is the most abundant protein in eukaryotic cells (Figure 1.1) (Pollard, 1986). Similar to microtubules the filaments exhibit a structural polarity, accomplished by a unidirectional orientation of G-actin molecules. Based on this polarity the filament end where increased elongation occurs, is termed ”plus-end“ and the opposite site where the depolymerizaion happens is called ”minus-end“ (Small *et al.*, 1978; Woodrum *et al.*, 1975). The ”plus-end“ is also termed ”barbed end“ and the ”minus-end“ is also referred to as ”pointed end“. These annotations derive from their appearance in electron microscopy experiments using myosin decoration of microfilaments (Huxley, 1969).

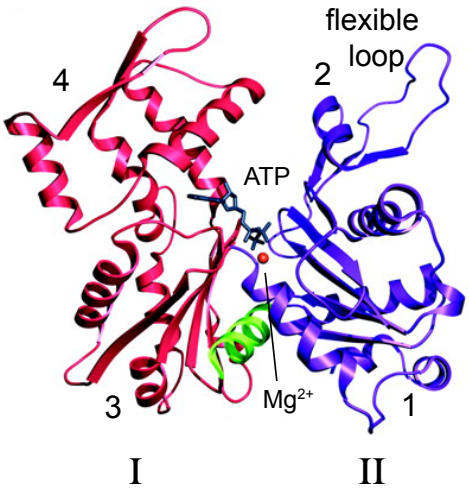

Figure 1.1 Ribbon representation of a G-actin monomer.
Crystal structure of a G-actin monomer of striated muscle tissue of a rabbit in complex with ATP and Mg^{2+}. The monomer is orientated with the minus-end on top and the plus-end at the bottom. The two domains I (subdomain 1 and 2, blue) and domain II (subdomain 3 and 4, purple) are depicted, as well as the bound ATP molecule in the middle of these domains. The linker α-helix is shown in green. Modified from Graceffa & Dominguez (2003).

Despite the globular structure of G-actin it is composed of two domains consisting of two subdomains each (Figure 1.1). The nucleotide binding pocket is at the interface of these four domains. Upon binding of ATP, ADP or in the nucleotide free state the monomer cycles between different structural conformations and can adapt open and closed states. Another special feature is the flexible DNase I binding loop in subdomain 2, that it most likely transitioned into an α-helix, upon ATP hydrolysis and the release of the γ-phosphate (Otterbein *et al.*, 2001).

1.1.1 F-actin polymerization

The polymerization of actin filaments is characterized by three different phases (Figure 1.2). Based on the instability of actin dimers and trimers spontaneous filament polymerization is an unlikely event (lag-period or nucleation phase). However, once a stable nucleus of three or more G-actin monomers has been formed the addition of further actin monomers occurs (elongation phase). The third phase (steady-state

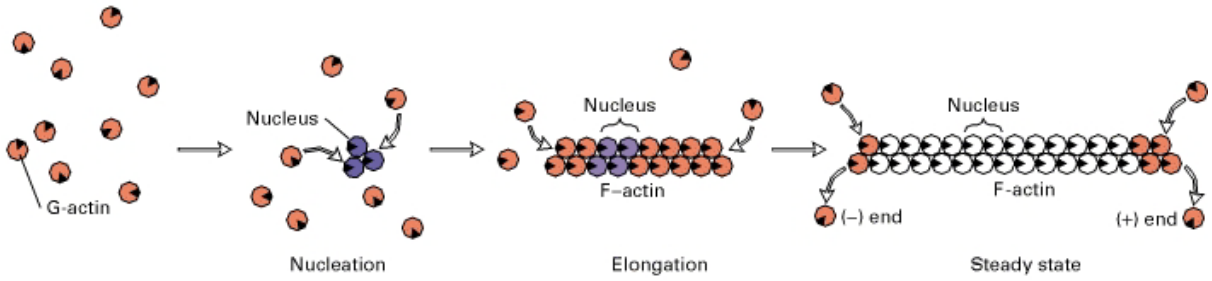

Figure 1.2 Three phases of *in vitro* actin polymerization.
Modified from Lodish *et al.* (2000).

phase) is defined by the decreasing concentration of free G-actin during the elongation process. At some point the concentration reaches a level at which the simultaneously polymerization equals the dissociation and no net change in filament length takes place. This indicates the importance of actin nucleation as a rate limiting step.

The ratio of the dissociation rate constant (k_{diss}) and the association rate constant (k_{ass}) of ATP-G-actin monomers to the filaments ends describes the so-called critical concentration C_c or equilibrium dissociation constant (K_D). At concentrations higher than C_c G-actin polymerizes. Polymerization assays have determined a C_c for the plus-end of 0.12 µM and 0.6 µM for the minus-end (Figure 1.3) (Wegner, 1976; Wegner & Engel, 1975). This shows that lower concentrations of free actin are needed for the elongation at the plus-end, compared to the minus-end. In consequence, during the steady-state actin elongation happens at the barbed-end while actin dissociation occurs at the pointed-end, resulting in a movement of bound G-actin filaments to the pointed-end. This effect is also called *treadmilling* effect (Kirschner, 1980; Wegner, 1976).

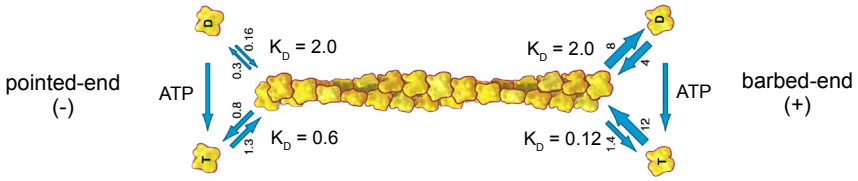

Figure 1.3 Treadmilling model after Wegner.
Association and dissociation rates at actin filaments. Association rates are depicted as µM $^{-1}$ s^{-1}, dissociation rates have the unit s^{-1} and the equilibrium dissociation constant is shown in µM. Modified from Pollard & Borisy (2003).

Additional to the polarity of the filaments, the nucleotide state of the G-actin monomer influences the actin assembly (Figure 1.3). While the incorporation of ATP-G-actin at the barbed-end is highly driven by the increased association rate constant compared to the pointed-end, the equilibrium constant for ADP-G-actin is the same at both filament ends. Following the incorporation, the bound ATP is rapidly and irreversible hydrolyzed (half time 2 s) (Blanchoin & Pollard, 2002; Carlier *et al.*, 1988). The subsequent phosphate dissociation is distinctly slower (half time 350 s), determining the filament lifetime. (Carlier & Pantaloni, 1986). ADP-P_i-actin intermediates in the filaments have similar properties as ATP-G-actin. Although the ATP-hydrolysis is not needed for the polymerization of actin filaments itself, it is a crucial step for the treadmilling effect, due to the altered kinetics at both ends of the filament. In the steady-state phase the elongation at the barbed-end depends on the amount of free G-actin, and is thereby limited by the dissociation at the pointed-send. Under these conditions the

filament growth is limited to approximately 0.04 µm min^{-1}. However, cell movement of 10 µm min^{-1} has been shown, indicating the requirement of additional regulatory mechanisms (Pollard & Borisy, 2003). One example is the conformational change of the G-actin monomers upon binding of cations, which increases the polymerization (Maruyma & Tsukagoshi, 1984; Selden *et al.*, 1983). Furthermore, more than 60 protein classes exist, that modulate the F-actin formation (Vale & Kreis, 1999). Elongation can be inhibited by F-actin capping proteins, that bind to the barbed end (Cooper & Schafer, 2000), or by binding of Thymosin β_4 to ATP-G-actin preventing binding to the filaments (Carlier *et al.*, 1993). Another actin binding protein named Profilin binds to ADP-actin monomers and enhances the exchange of ADP to ATP (Lu & Pollard, 2001). Secondly, Profilin bound ATP-G-actin is recruited to prolin rich regions of proteins, such as WASP family members and formins. This local increase of ATP-G-actin enhances the nucleus formation (Watanabe *et al.*, 1997). The protein class of formin homology proteins, especially mDia1 is introduced in greater detail in 1.2. Furthermore a range of microfilament regulatory processes involving Arp2/3-complexes and their activating proteins are introduced in 1.1.2.

1.1.2 Actin filament regulation and remodeling

As mentioned before the nucleation is a crucial step in the actin filament formation. Hitherto, three protein classes have been identified to aid in nucleation and promote polymerization of new actin filaments. These proteins belong to the actin-related protein 2/3 (Arp2/3) complex, formins and a protein class containing tandem repeats of G-actin binding motifs, such as Spire, Cordon-bleu or Leiomodin (Ahuja *et al.*, 2007; Goley & Welch, 2006). The Arp2/3 complex consists of seven subunits, including the Arp2 and Arp3 subfamilies (Machesky & Insall, 1998), and possesses a low nucleation activity on its own (Mullins *et al.*, 1998). So-called nucleation promotion factors (NPFs) are of importance for the activity of Arp2/3. These NPFs can be divided into two classes.

Class I NPFs mediate the actin nucleation via their C-terminally located Verprolin homology (V), central (C) and acidic (A) regions (Machesky *et al.*, 1999). The V-domain (also called W or WH2 for WASp homology 2) binds to actin monomers and the C and A motifs interact with multiple subunits of the Arp2/3 complex. Thereby, NPFs recruit actin monomers to the Arp2/3 complex. The Arp2 and Arp3 subunits form a trimeric structure with the actin monomer, inducing a different conformation of Arp2/3. This leads to more potent state to promote the actin nucleation step for new filaments (Chereau *et al.*, 2005; Marchand *et al.*, 2001).

Class I NPFs can be further classified into five groups

1. Wiskott-Aldrich Syndrome protein (WASP) and neuronal-enriched homologue of WASP (N-WASP)
2. WASP family Verprolin-homologous (WAVE) proteins (Suppressor of cAMP receptor [Scar])
3. WASP and Scar homologue (WASH)
4. WASP homologue associated with actin, membranes and microtubules (WHAMM)
5. Junction-mediating regulatory protein (JMY)

Class II NPFs contain proteins, such as Cortactin another activating protein of the Arp2/3 complex. However, Cortactin displays a weaker effect on the nucleation, compared to class I NPFs. Instead, it mainly aids in the stabilization of branch junctions and inhibits debranching (Weaver *et al.*, 2001).

In contrast to the class of Diaphanous-related formins (see 1.2) the activated Arp2/3 complex initiates 70° branching of existing actin filaments. In this process the new daughter filament is anchored by Arp2/3 with its pointed end to the mother filament (Rouiller *et al.*, 2008). As a result, Arp2/3 mediates the formation of a so-called dendritic network of branched actin filaments (Blanchoin *et al.*, 2000), and is thereby regulating the cell morphology. The branching of actin filaments has been shown to be crucial for many cellular processes, including cell migration and adhesion (DeMali *et al.*, 2002; Machesky *et al.*, 1997), phagocytosis (May *et al.*, 2000) and trafficking events (Stamnes, 2002).

1.2. Diaphanous-related formins

Formin homology (FH) proteins, or short formins, are multidomain proteins consisting of more than 1000 amino acids. The first formin genes (FMN1/2) were identified by mutations of the *limb deformity* gene locus in mouse, that induced severe defects cell polarity and morphogenesis (Maas *et al.*, 1990). Although, more recent studies ascribed the phenotype to *gremlin*, a gene located on the same chromosomal locus (Zuniga *et al.*, 2004). Subsequent studies showed, that mutations of the *Drosophila* gene *dia* lead to impaired cytokinesis, with a gene product (Diaphanous) homologous to formin (Castrillon & Wasserman, 1994). Additionally, studies in budding yeast (*Saccharomyces cerevisiae*) displayed the importance of the formin Bni1 for the assembly of microfilaments (Evangelista *et al.*, 2002). A comparison of the FMN1/2 proteins of

mice, Diaphanous of flies and Bni1 of yeast showed a high sequence homology of two regions termed formin-homology FH1 and FH2. These domains are present, albeit in different sizes, in all known formins with the exception of ForC in *Dictyostelium discoideum*, which consists only of the FH2 domain (Castrillon & Wasserman, 1994). The conservation of these domains indicates their functional importance in formins. Indeed, both domains are involved in the regulation and formation of microfilaments and microtubules during a variety of cellular processes (Palazzo *et al.*, 2001; Wallar & Alberts, 2003).

Hitherto, in mammals 15 different formins are described, that can be classified into eight groups: (Breitsprecher & Goode, 2013; Schönichen & Geyer, 2010)

1. Dia (Diaphanous homolog formin)
2. DAAM (dishevelled-associated activator of morphogenesis)
3. FMNL (formin-like protein)
4. WHIF (WH2 domain-containing formin)
5. INF (inverted formin)
6. FHOD (formin homology domain-containing)
7. Delphilin
8. FMN (formin)

Besides the conserved FH1 and FH2 domains a third domain FH3 was identified at the N-terminus of Fus1 in *Schizosaccharomyces pombe* (Petersen *et al.*, 1998). The FH3 has been further divided into the diaphanous-inhibitory domain (DID) and the subsequent dimerization-domain (DD), and is a special feature of a formin class that is regulated by autoinhibition. These Diaphanous-related formins (DRFs) are autoregulated by an intramolecular interaction between the C-terminal Diaphanous-autoregulatory domain (DAD) and the N-terminal DID domain (Alberts, 2001; Li & Higgs, 2003; Nezami *et al.*, 2006; Otomo *et al.*, 2010). Another characteristic domain of DRFs is the N-terminally located GTPase-binding domain (GBD), which is located C-terminally of the DID (Rose *et al.*, 2005). Upon binding of active Rho GTPases to the GBD the DID-DAD interaction and thereby autoinhibition is relieved (Lammers *et al.*, 2005; Rose *et al.*, 2005; Seth *et al.*, 2006; Westendorf, 2001).

An overview of the domain organization of one formin of each class is shown in Figure 1.4.

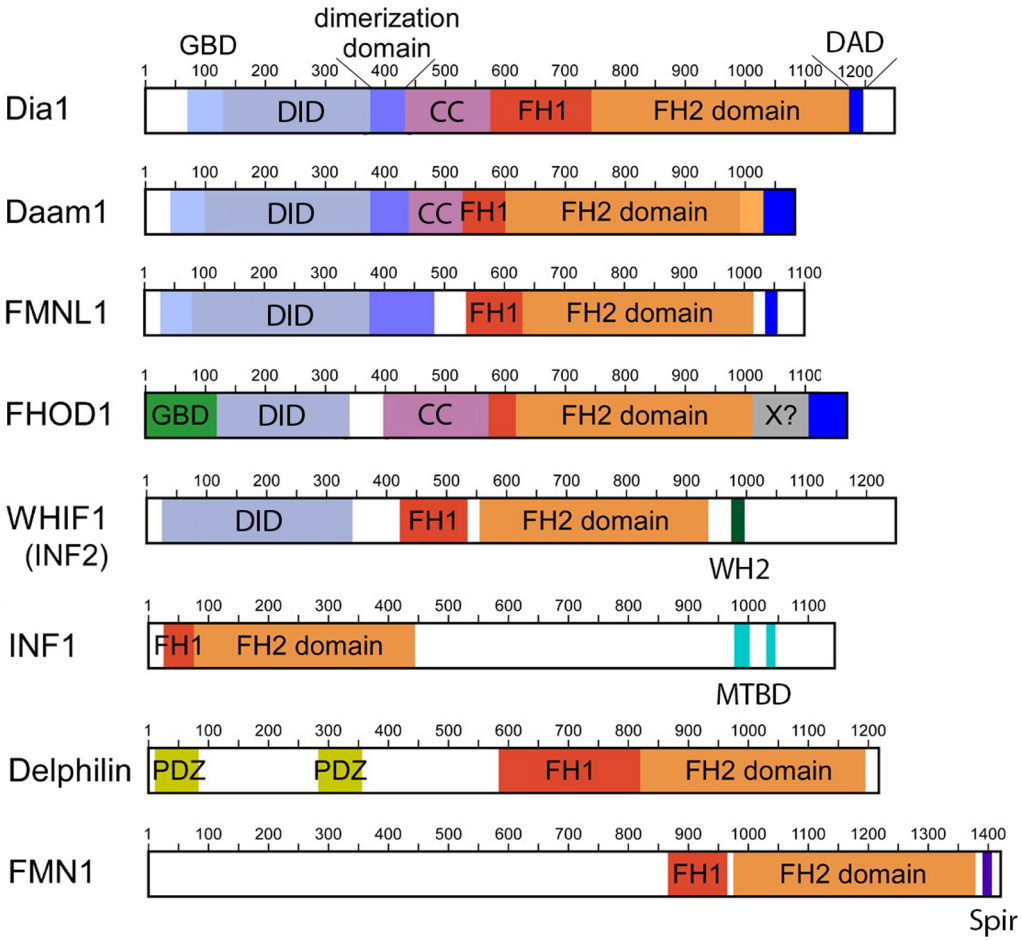

Figure 1.4 Modular domain organization of human formins.
Overview of the domain organization of one example for each formin class. Showing the GTPase binding domain (GBD), Diaphanous-inhibitory domain (DID), dimerization domain, coiled-coil domain (CC), formin homology domains 1,2,3 (FH1, FH2, FH3), Diaphanous- autoregulatory domain (DAD), Wiskott-Aldrich syndrome homology region 2 (WH2), microtubule-binding domain (MTBD) and PDZ homology domain. Modified from Schönichen & Geyer (2010).

The DRFs Dia1, Daam1, FMNL1 and FHOD1 display a typical GTPase binding domain and a Diaphanous-inhibitory domain (DID) at their N-terminus, followed by the FH1 and FH2 domains and the C-terminal Diaphanous-autoregulatory domain (DAD). It has been shown, that GBD/DAD deletion mutants of DRFs are constitutively active and induce the formation of actin stress fibers, in presence of ROCK (Rho associated coiled-coil kinase) (Copeland & Treisman, 2002; Watanabe *et al.*, 1999). Delphilin is the only formin containing PDZ domains, that are required for binding of the glutamate receptor delta 2 subunit (GluRδ2) (Miyagi *et al.*, 2002), thus shown to be important

for the localization at dendritic spines of Purkinje cells (Matsuda *et al.*, 2006). INF1 is able to interact directly with microtubules via a C-terminal microtubule-binding domain (MTBD), which leads to co-alignment of microtubules with actin filaments (Young *et al.*, 2008). Instead of DAD the formin WHIF1 (INF2) has an C-terminally located WH2 (WASP homology 2) domain. Similar to the DAD the WH2 domain binds to the DID, but additionally binds to actin monomers, accelerating F-actin nucleation (Chhabra & Higgs, 2006). Interestingly, the binding of WH2 to the DID solely impacts actin polymerization and not nucleation processes (Chhabra *et al.*, 2009).
Since formins are able to interact with small GTPases of the Rho-family and simultaneously with proteins regulating the actin cytoskeleton (e.g. F-BAR proteins, Profilin) they display important effector proteins that mediate signal transduction. The regulation of DRFs and their impact on F-actin nucleation and polymerization will be discussed in the subsequent sections.

1.2.1 Autoinhibition and activation of DRFs by Rho GTPases

Although the autoinhibitory interaction of the Diaphanous-inhibitory domain (DID) and the Diaphanous-autoregulatory domain (DAD) is a common feature of all Diaphanous-related formins (DRFs) (Alberts, 2001; Liu *et al.*, 2008; Vaillant *et al.*, 2008), so far only the structure of the mDia1 inhibition has been solved by X-ray crystallography (Lammers *et al.*, 2005; Nezami *et al.*, 2006; Otomo *et al.*, 2010). A simplified model of the autoinhibitory state of mDia1 is depicted in Figure 1.5. The DAD binds to the DID adjacent to the GTPase binding domain (GBD_N), leading to the formation of a closed state and the inactivation of the formin.

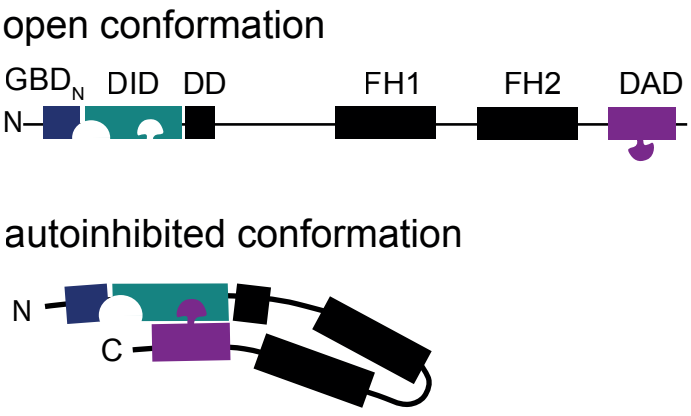

Figure 1.5 Model of the autoregulatory mechanism of mDia1.
Presented are the open and closed (autoinhibited) conformation of mDia1. Shown are the GTPase-binding domain (GBD_N), the Diaphanous-inhibitory domain (DID), dimerization domain (DD), Formin-homology domain (FH1,2) and the Diaphanous-autoinhibitory domain (DAD).

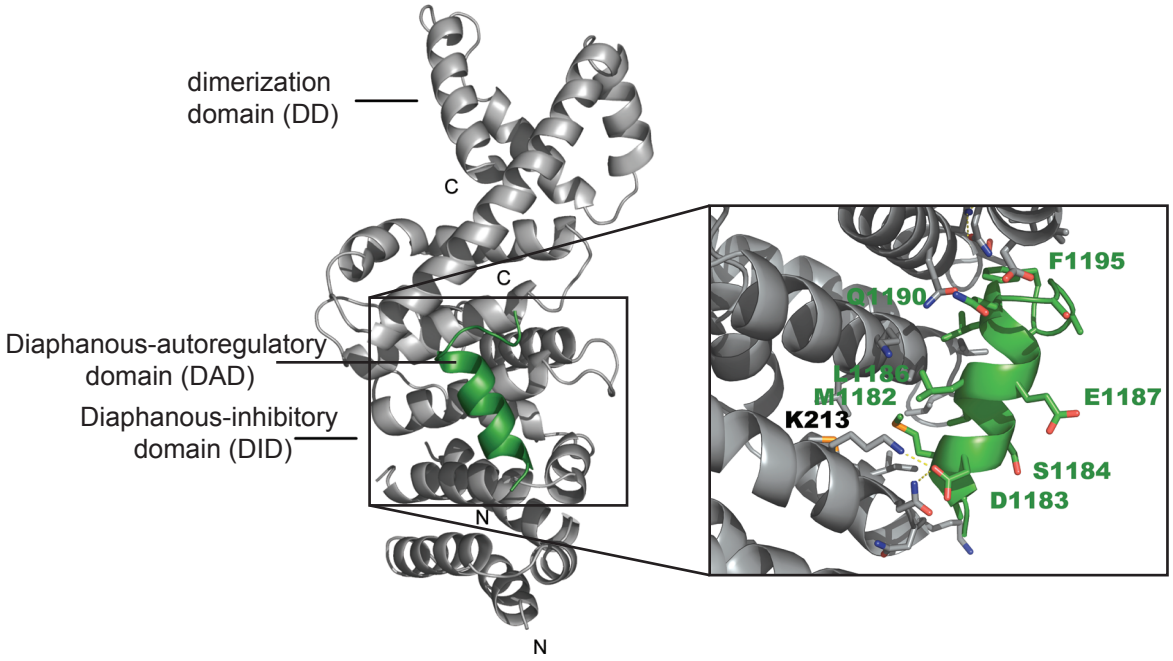

Figure 1.6 Crystal structure of the $mDia_{DID}$ • $mDia_{DAD}$ complex.
Left: The ribbon presentation shows the $mDia_{DID}$ domain in complex with the $mDia_{DAD}$ core region exhibiting the amino acids 1180-1195 (PBD: 2BAP). *Right:* Zoom in on the binding interface, depicting some of the major amino acids involved in the binding. Modified from Lammers *et al.* (2005).

The DAD of mDia1 can be divided into the DAD core region (DCR; aa 1175-1195) and a subsequent basic region, which varies in length and sequence (Lammers *et al.*, 2005; Wallar *et al.*, 2006). In the first solved crystal structure of the DID • DAD complex, only the DCR is visible forming an amphipathic helix that binds to the hydrophobic concave side of the armadillo repeat region (ARR) of the DID (Figure 1.6) (Lammers *et al.*, 2005). Although the subsequent amino acids of the DAD are not visible in the structure they are important for the binding affinity (Wallar *et al.*, 2006). It has been postulated that the C-terminal part of the DAD contacts the negatively charged patches on $mDia_N$ along the α-helix (interdomain helix, α17), connecting the DID domain with the dimerization domain (DD) (Nezami *et al.*, 2010; Otomo *et al.*, 2010). This binding mechanism seems to be similar in all DRFs sharing the following consensus sequence for DAD (G/A)(V/A)MDXLLEXL(K/R/Q)X(G/A)(S/G/A)(A/P) (Alberts, 2001).

Binding of active Rho GTPases to the regulatory N-terminus ($mDia_N$, GBD_N-DID-CC) leads to the release of the DID-DAD interaction and resolves the autoinhibited state. The formin p140mDia was the first to be identified as effector protein of small GTPases (Watanabe *et al.*, 1997). In recent years the binding specificity and the interaction has been studied intensively with biochemical, structural and cell dependent methods. Especially, the activation of mDia1 isoforms and their interaction with various GTPases

has been characterized in great detail (Lammers *et al.*, 2008). Described interactions of formins with specific Rho GTPases are summarized in Table 1.1.

Table 1.1 DRFs and their GTPases. Modified from Kühn & Geyer (2014).

Formin	binding domain	Rho GTPases	Reference
mDia1, mDia2	GBD-FH3	RhoA	(Alberts *et al.*, 1998; Watanabe *et al.*, 1999, 1997)
mDia1, mDia2	GBD-FH3	RhoB	(Wallar *et al.*, 2007; Watanabe *et al.*, 1999)
mDia1	GBD-FH3	RhoC	(Rose *et al.*, 2005; Watanabe *et al.*, 1999)
mDia2, mDia3	GBD-FH3	Cdc42	(Alberts *et al.*, 1998; Peng *et al.*, 2003; Yasuda *et al.*, 2004)
mDia1, mDia2	GBD-FH3	Rac1,2	(Ji *et al.*, 2008; Lammers *et al.*, 2008; Rose *et al.*, 2005)
hDia2	n.d.	RhoD	(Gasman *et al.*, 2003)
mDia2	n.d.	Rif	(Pellegrin & Mellor, 2005)
Daam1	N-terminus (aa 41-477)	RhoA, -B, -C	(Habas *et al.*, 2001; Higashi *et al.*, 2008)
Daam1	N-terminus (aa 1-698)	Rac1	(Matusek *et al.*, 2008)
Daam1	n.d.	Cdc42	(Aspenström *et al.*, 2006)
FMNL1	n.d.	Rac1	(Favaro *et al.*, 2013; Gomez *et al.*, 2007; Yayoshi-Yamamoto *et al.*, 2000)
FMNL1	N-terminus (aa 1-450)	Cdc42	(Seth *et al.*, 2006)
FMNL2	N-terminus (aa 27-276)	RhoC	(Kitzing *et al.*, 2010)
FMNL2	GBD-FH3 (aa 1-379)	Cdc42	(Block *et al.*, 2012)
FMNL3	n.d.	RhoC	(Vega *et al.*, 2011)
FHOD1	FH1 (aa 422-717)	Rac1	(Gasteier *et al.*, 2003; Westendorf, 2001)
INF2	FH3 (aa 1-340)	Cdc42	(Madrid *et al.*, 2010)

The first crystal structure of a GTPase in complex with a formin was solved by the group of Wittinghofer (Figure 1.7) (Rose *et al.*, 2005). In accordance with other effector proteins, these data revealed that active, GppNHp loaded RhoC binds mainly via switch I and II. While switch I binds interacts with mDia1 via the GBD_N, switch II contacts residues in the ARR of the DID. Moreover, the Rho-insert helix also locates in close approximation to the fifth armadillo repeat of the DID. Notably, the residues located in the switch I and II regions involved in formin binding, are conserved throughout the Rho GTPases (Kühn & Geyer, 2014). A major contribution to the specificity of the mDia1-GTPase interaction seems to be created by the triple asparagine motif in the loop connecting the third helix of ARM1 and the first helix of ARM2 in $mDia_{DID}$. Mutating the motif to the residues TSH (Thr, Ser, His) of mDia2 and mDia3, increases

the affinity of mDia1 for Cdc42. Further specificity of the DRF-GTPase interaction is created by the Rho-insert helix (Lammers *et al.*, 2008). The specific interactions of the switch I and II region of RhoC with the ARR and GBD_N are shown in Figure 1.7.

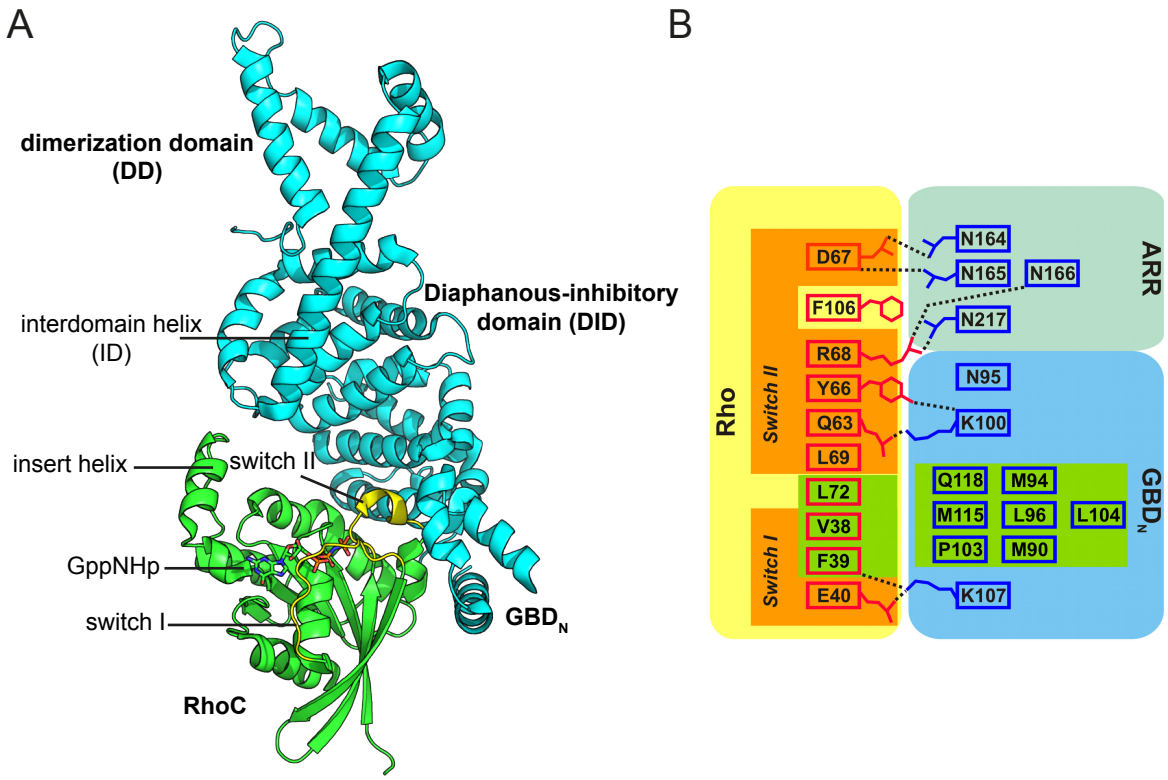

Figure 1.7 Interaction between mDia1 and RhoC. A: Ribbon presentation of the mDia1 • RhoC • GppNHp complex of PDB: 1Z2C. B: Interactions created between Rho and the armadillo repeat region (ARR, DID) and the GTPase binding domain (GBD_N) of mDia. Modified from Rose *et al.* (2005).

As depicted in Figure 1.8 the binding interfaces of $mDia_{DAD}$ and RhoC on $mDia_N$ only partially overlap. However, the formation of a putative ternary complex of $mDia_{DID}$ • $mDia_{DAD}$ • Rho has been experimentally ruled out in several studies (Lammers *et al.*, 2008, 2005; Nezami *et al.*, 2006; Otomo *et al.*, 2005a). A two step mechanism for the dissociation of $mDia_{DAD}$ from $mDia_{DID}$ by RhoA has been suggested, that includes an initial weak binding of RhoA to mDia1, followed by a tighter association. This would subsequently lead to the dissociation of $mDia_{DAD}$ from $mDia_{DID}$ by steric interference and additional charge-charge repulsion (Lammers *et al.*, 2005). Whether the initial loose binding is initiated by the Rho-insert helix and is thereby also important the specificity, or if the RhoA first binds loosely to the GBD_N and then forms stronger contacts to the $mDia_{DID}$ remains unclear.

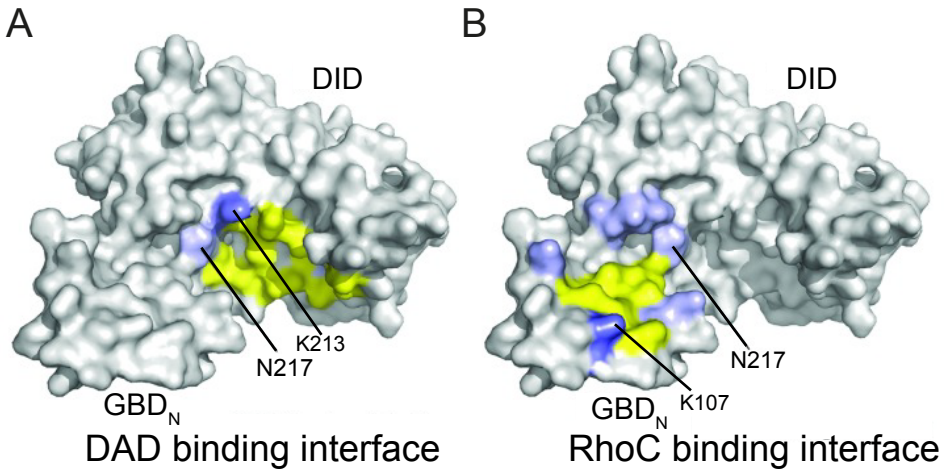

Figure 1.8 mDia1 binding interface of DAD and RhoC .
A: mDia$_{DAD}$ (mDia Diaphanous-autoinhibitory domain) binding interface on mDia1. Shown are the residues of the mDia$_{DID}$ (mDia Diaphanous-inhibitory domain) involved in the binding of mDia$_{DAD}$ (PDB: 2F31) (Nezami *et al.*, 2006). Depicted in light blue are the residues N217, N310 and Q352 that mediate hydrogen bonds with mDia$_{DAD}$. K213 of mDia$_{DID}$, which forms a salt bridge with D1183 of mDia$_{DAD}$ is shown in blue. Hydrophobic interactions of I222, K252, L253, A256, I259, L260, Q307, A311, T314, V351, and V355 are colored yellow. B: RhoC binding interface on mDia1. Shown are the residues of the GBD$_N$-DID involved in the binding of RhoC (PDB: 1Z2C). Hydrophobic interactions of M90, M94, N95, L96, P103, L104, and M115 are depicted in yellow, polar interactions of K100 and Q118 (GBD) and N164, N165, N166 and N217 (mDia$_{DID}$) in light blue. The created salt bridge of K107 is marked in blue color. Modified from Kühn & Geyer (2014).

1.2.2 Formin induced actin nucleation and elongation

Mandatory for the activity of Diaphanous-related formins (DRFs) are the release of the autoinhibitory state by Rho GTPase binding and the distinct features of the dimeric formin structure. DRFs accelerate F-actin formation by enhancing the nucleation process and by supporting the elongation at the barbed end. These effects are mainly driven by their FH1 and FH2 domain.

Actin nucleation

It has been shown, that the isolated FH2 domain is able to nucleate actin filaments *in vitro* (Pring *et al.*, 2003; Pruyne *et al.*, 2002). Based on structural data it was postulated that the nucleation is accelerated by the recruitment and stabilization of actin dimers and trimers (Figure 1.9). The crystal structure of the FH2 domain of the formin Bni1p of *S. cerevisiae* displays the complete α-helical composition. The monomers are arranged head-to-tail in the dimer, forming a donut-shaped ring (Xu *et al.*, 2004). Important for the dimerization of the FH2 is the N-terminally located region, also referred

to as lasso, which contacts the post domain of the other monomer (Xu *et al.*, 2004) (Figure 1.9). Furthermore, this region displays minor differences between the structure of Bni1p and mDia1. Additionally, Otomo *et al.* could show by crystallization with tetramethylrhodamine-actin (TMR-actin), that the dimeric FH2 domain contacts three actin molecules, while each FH2 monomer exhibits two actin binding sites. (Otomo *et al.*, 2005b). Crucial for the actin binding are a conserved isoleucine (in Bni1p I1431) and lysine (in Bni1p K1601) (Lu *et al.*, 2007; Otomo *et al.*, 2005b) and mutations of these residues results in reduced activity of the formin (Bartolini *et al.*, 2008; Ramabhadran *et al.*, 2012).

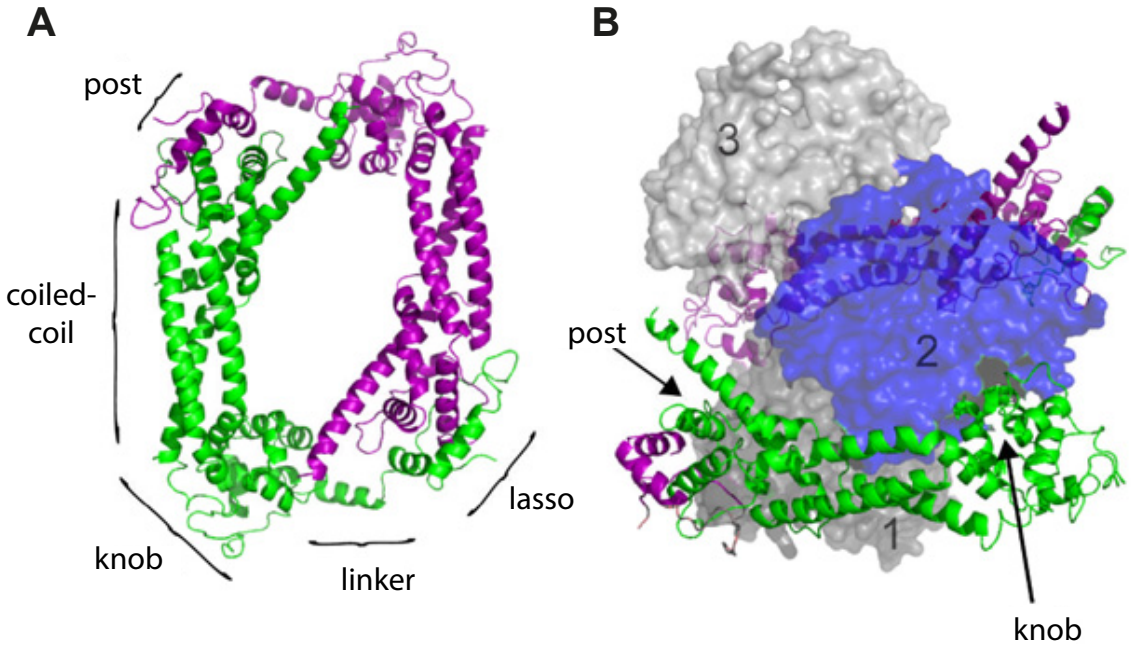

Figure 1.9 Dimeric FH2 structure in complex with actin. A: Crystal structure of the FH2 domain of the *S. cerevisiae* formin Bni1p showing the residues 1350-1760 (PDB: 1UX5, Xu *et al.* (2004)). The FH2 monomers are presented in green and purple. Labeled are the lasso, linker, knob, coiled-coil, and post regions of the green FH2 subunit. B: Ribbon representation of the FH2 domain of Bni1p (residues 1350-1760) in complex with muscle actin (PDB: 1Y64, Otomo *et al.* (2005b). The three actin subunits of the polymer are depicted as surface representation in blue and gray, labeled 1 to 3 from the barbed- to the pointed-end. Modified from Paul & Pollard (2009b).

The knob region of FH2 domains contact the actin molecules in the hydrophobic groove between the subdomains 1 and 3. Additionally, the post site of the FH2 forms electrostatic contacts along subdomain 1 of actin subunits (Figure 1.9 B). However, the reported binding affinities of the FH2 domain for single G-actin monomers are rather low (>5 µM) (Evangelista *et al.*, 2003; Zigmond, 2004) or not present at all (Chesarone *et al.*, 2010). On the other hand the affinity for the barbed end is very high (low nanomolar K_D, Moseley *et al.* (2004)). Together with the slow *in vitro* nucleation

rate of the FH2 domain it is therefore hypothesized that the FH2 is needed for the stabilization of spontaneously formed actin dimers or trimers *in vitro* and additional regions of formins are involved in actin nucleation *in vivo*. An alternative nucleation mechanism has been postulated involving the FH1 domain. The FH1 domain, which is predicted to be mostly unstructured contains several proline-rich motifs (Kovar *et al.*, 2003; Michelot *et al.*, 2005). These motifs are known to be recognition areas for Profilin and SH3 (Src-homology 3) and WW domains (WWP repeating motif) (Bedford *et al.*, 1997; Imamura *et al.*, 1997; Macias *et al.*, 2002). Especially the binding and recruitment of Profilin bound ATP-G-actin at the FH1 was believed to initiate nucleation (Sagot *et al.*, 2002). More recent studies indicate that the interaction of the FH1 domain and Profilin • G-actin might only play minor role in the nucleation (Paul & Pollard, 2008). Latest data reveal the emerging importance of the formins tail regions. Sequences located C-terminally of the FH2 domain bind actin monomers and thereby effectively enhance nucleation (Gould *et al.*, 2011; Heimsath & Higgs, 2012). In addition, an increasing number of regulatory proteins, that bind to the tail regions have been identified (Graziano *et al.*, 2011; Okada *et al.*, 2010). These proteins include so-called nucleation promoting factors (NPFs) (1.2.3).

Actin elongation

Formins fulfill several functions, that lead to a regulated elongation at the barbed end of actin filaments. They prevent the binding of capping proteins, which would block further elongation (Harris *et al.*, 2004; Kovar *et al.*, 2005; Zigmond *et al.*, 2003), they prevent the annealing of barbed filament ends to pointed ends (Kovar *et al.*, 2003) and finally they recruit actin monomers to the growing barbed end. It has been emphasized, that the FH1 domain is needed for Profilin • G-actin recruitment to the FH2 domain, resulting in accelerated elongation at the barbed-end (Paul & Pollard, 2009a). Early electron micrographs and additional kinetic assays indicated that formins stay bound to the barbed end during the processive elongation (Pruyne *et al.*, 2002; Zigmond *et al.*, 2003). This would require an intensively debated translocation of the FH2 domain for each actin monomer that is added to the barbed end. The initial theory explaining this mechanism is known as ”stair stepping“ model. (Otomo *et al.*, 2005b; Xu *et al.*, 2004). These models were based on structural information of the FH2 domain and indicated that formins act as leaky capping proteins. Due to conformational changes of the FH2 dimer, formins can switch between an ”open state“ and a ”closed state“. During the closed state both parts of the dimer bind tightly to the actin subunits at the barbed end, which are orientated in a planar structure with a 180° rotation between consecutive subunits. This unfavorable conformation presents no contacts for further actin subunits. Partial dissociation of the FH2 (step off) would lead to a more

relaxed rotation of 167° of actin subunits and enable one free G-actin in the solution to bind to the exposed FH2, as well as the barbed end. Assembly of the actin monomer subsequently leads to the re-establishment of the closed state (Kozlov & Bershadsky, 2004; Paul & Pollard, 2009a; Vavylonis *et al.*, 2006; Zigmond *et al.*, 2003). The time span between the alternating open and close states is defined as the "gating factor" (Paul & Pollard, 2009b). This value varies from almost 1 (uninhibited) for mDia1 to nearly 0 (capping) for Cdc12 in *S. pombe* (Kovar *et al.*, 2006) and could explain differences in the elongation rates of different formins (Block *et al.*, 2012; Kovar *et al.*, 2003; Neidt *et al.*, 2008).

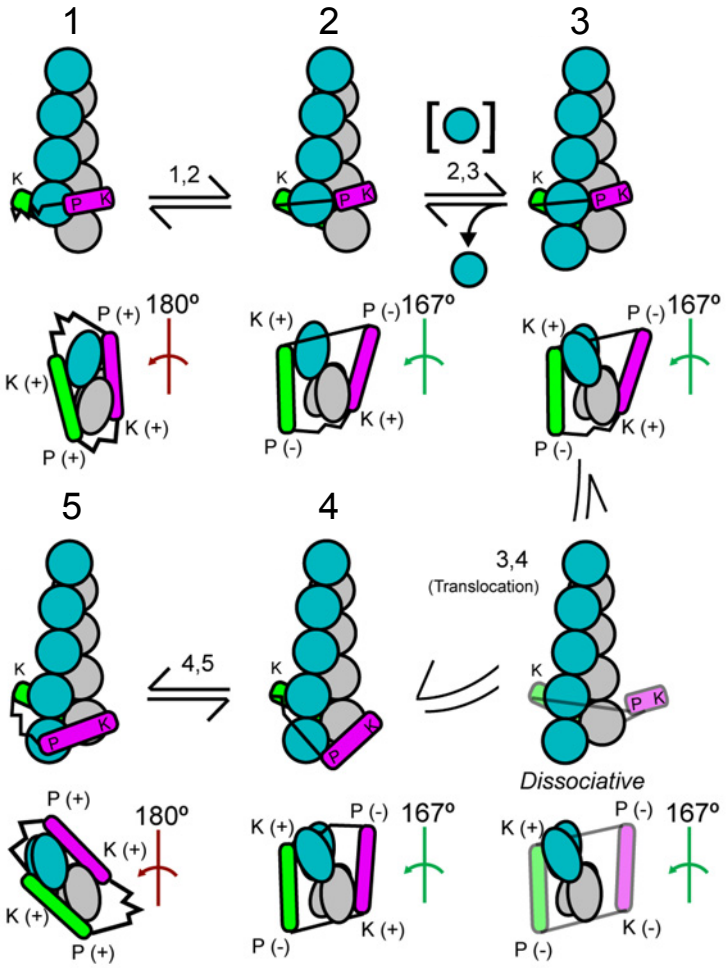

Figure 1.10 "Stepping second" mechanism of actin elongation. This model shows the hypothesized FH2 induced 5 step elongation of actin at the barbed end in regard of the FH2 dimer translocation. In green depicted is the leading half of the FH2 dimer and the trailing part is shown in magenta. K, P refer to the knob and post site of the FH2 domain. Actin monomers are blue and silver and interactions with the knob or post site are indicated as (+) or (-). The 5 steps are illustrated as the side view of the filament with the barbed end orientated downwards (upper image) and the top view of the barbed end (lower image). The closed and open state of the FH2 dimer is indicated by the green and red angle symbols. Images 1,2 and 4,5 are equivalent images of the cycle. Modified from Paul & Pollard (2009b).

However, the initial ”stair stepping“ model did not take the helical twist of F-actin into account. Induced by the helical structure the FH2 needs to rotate relatively to the filament in an angle of 14° per elongation cycle. Therefore, the stair stepping model was expanded by the ”screw mode“ (Shemesh *et al.*, 2005) and also the ”stepping second” hypothesis has been emphasized (Paul & Pollard, 2009b). The latter is displayed in Figure 1.10.

The ”stepping second“ model is based on the new structure data of incorporated actin subunits provided by Oda *et al.* (2009). Upon incorporation into the microfilament the actin monomers become flattened. This lead to the conclusion that the bound FH2 dimer might influence the orientation as well as the conformation of the actin subunits and *vice versa* (Paul & Pollard, 2009b). Paul and Pollard propose, that following each open state and actin subunit insertion, the formin subunit is transiently bound to the interior actin in the microfilament. Subsequently, the tense FH2 domain translocates to the newly build end and shifts into the closed state, lowering its free energy (Paul & Pollard, 2008). Similar to the ”stair stepping“ model the ”stepping second“ mechanism includes several steps of partially dissociation of the FH2 domain. In comparison to the ”stair stepping“ model, during the ”stepping second“ model the dissociation and translocation occurs after the incorporation of actin monomers. Notably, recent studies using single-molecule fluorescence polarization could confirm the rotational movement of mDia1 during the elongation of actin filaments (Mizuno *et al.*, 2011).

1.2.3 mDia1 localization and interacting proteins

Besides the activation, the localization of DRFs is also influenced by Rho GTPases. This has been shown for many different formins and GTPases (Evangelista *et al.*, 1997; Martin *et al.*, 2007; Tolliday *et al.*, 2002). The prenylated GTPases bind to the GBD domain and recruit the activated DRFs to the membrane. Notably, recent studies identified several new mechanisms mediating the plasma membrane localization of formins, that are independent of Rho GTPases. Another protein, that binds to the $mDia_N$ region upon the release of the autoinhibitory state is the scaffolding protein IQGAP1. The interaction with IQGAP1 is mandatory for the proper localization of mDia1 in phagocytic cup formation and phagocytosis (Brandt *et al.*, 2007). Furthermore, scaffolding proteins containing membrane associated BAR domains could have an impact on formin localization (Frost *et al.*, 2009). These interactions have been found for mDia1, which binds with the FH1 domain to the SH3 domain of IRSp53 (BAR-domain protein) (Fujiwara *et al.*, 2000; Goh *et al.*, 2012) and Daam1, which interacts with SH3 domain of Cip4 (Aspenström *et al.*, 2006). Other sequences, important for the localization of formins, have been postulated for Bnr1 in *S. cerevisiae* and Cdc12 in *S.*

pombe (Gao *et al.*, 2010). These regions are also located at the N-terminus of the formin and interact with septin-associated kinases, regulating the function of Bnr1 (Buttery *et al.*, 2012).
Alongside the phosphorylation by septin-associated kinases a variety of post translational modification (PTM) has been described for formins. Phosphorylation by Prk1p of both tails is involved in the release of the autoinhibitory state of Bni1 in *S. cerevisiae* (Wang *et al.*, 2009). The formins mDia2 (Diaphanous homolog 3) and FHOD1 are activated upon interaction with the Rho-associated protein kinase (ROCK) (Dean *et al.*, 2011; Hannemann *et al.*, 2008; Takeya *et al.*, 2008). Additionally, the formin mDia3 is phosphorylated and regulated by the kinase Aurora B (Cheng *et al.*, 2011) and the formins FHOD1 and FHOD3 are targets of CK2 (casein kinase 2 subunit α) and PRKG1 (cGMP-dependent protein kinase 1) (Iskratsch *et al.*, 2010, 2013). The described farnesylation and myristoylation of INF2 (inverted formin-2) and FMNL2 (formin-like protein 2), have a more direct impact on the membrane localization (Block *et al.*, 2012; Chhabra *et al.*, 2009)
Notably, in mDia1 and mDia2 polybasic clusters at the N- and C-terminus have been identified, that might directly associate with phospholipids through electrostatic interactions (Gorelik *et al.*, 2011; Ramalingam *et al.*, 2010). The direct interaction with phospholipids has also been confirmed for the plant formins AFH1, formin1 and class II formins (Cheung *et al.*, 2010; Martiniere *et al.*, 2011; van Gisbergen *et al.*, 2012), indicating a general mechanism of several species.
Another protein, that binds to the N-terminal region of mDia1 and is involved in F-actin regulation is is the scaffolding protein Liprin-α3 (Sakamoto *et al.*, 2012a). This new class of mDia1 interaction proteins will be further introduced in 1.4.

1.3. Guanine nucleotide binding proteins

The signal transduction of extracellular stimuli to the intracellular compartments is an important step for many cellular functions. These processes are often controlled and mediated by guanine nucleotide binding proteins (GNBP), also named G-Proteins. Based on their structural and sequential similarities they can be divided into TRAFAC (translation factor) and SIMIBI (signal recognition GTPases, MinD and BioD) (Leipe *et al.*, 2002). Well known examples of the TRAFAC GNBPs are the translation factor IF-2, the Ras-superfamily (*e.g.* Rho, Ras, CDC42) and the myosin-kinesin superfamily. Proteins associated with the SIMBI-GNBPs are often involved in protein localization and targeting. Besides their structural categorization GNBPs can also be classified regarding their function, which results in five distinct groups.

1. α-subunits of heterodimeric G-proteins (G_αs)
2. Translation factors (e. g. IF-2, elongation factor Tu)
3. Ras superfamily (e. g. Rho, Ras, Cdc42)
4. Signal recognition particle (SRP) and SRP-receptor
5. Large GNBPs (e. g. Dynamin)

Hitherto, in humans more than 150 members of the Ras superfamily are known. Most of them are structurally and functionally described in great detail. They have a molecular weight of approx. 20-25 kDa and can be further divided into five major subfamilies based on structural and functional similarities (Table 1.2). The first member and eponym of the superfamily, Ras (rat sarcoma) , was identified by Chien *et al.* (1979) as the product of a proto-oncogene.

Table 1.2 The five major subfamilies of the Ras superfamily. Classification based on Wennerberg *et al.* (2005) and Rojas *et al.* (2012).

	Ras	**Rho**	**Rab**	**Arf**	**Ran**
quantity	39	22	65	30	1
function	morphology, differentiation, apoptosis, proliferation	cytoskeleton, gene expression, polarity, growth	vesicle-trafficking	vesicle-trafficking	nuclear transport, mitotic spindle-formation
examples	(H/K/N)-Ras Rap Rheb Ral	Rho (A/B/C) Rac1 Cdc42 Rif	Rab1A Rab2 Rab3A	Arf1 Arf6 Sar1	Ran

Proteins of the Ras-subfamily mediate cell-proliferation, -apoptosis, -morphology and -differentiation (Vojtek & Der, 1998). Concerning their diverse functions it is not surprising, that mutations of Ras can be found in diverse tumors and in fact 20-30 % of all human tumors carry a Ras-activating mutation (Prior *et al.*, 2012). Rho-proteins (Ras-homologous) play important roles in the regulation of the cytoskeleton, cell growth and also gene expression (Kitayama *et al.*, 1989; Sander & Collard, 1999). Regulation of vesicular transport is controlled by ADP-ribosylation factor (Arf) family proteins and Ras-like proteins in brain (Rab) (Moss & Vaughan, 1998; Schimmöller *et al.*, 1998). The ran-related nuclear (Ran) proteins are involved in the nucleocytoplasmic transport of proteins and RNA (Weis, 2003).

Their common feature is the ability to cycle between an active GTP-bound state and an inactive GDP-bound state (1.3.3), which is determined by conformational changes of the G-domain (1.3.2). Only in the GTP-bound form effector proteins can bind, which leads to their activation (*e.g.* DRFs) and signal transduction events occur. The state of GPTases is highly regulated by the hydrolysis (1.3.4) and the exchange (1.3.5) of the guanine nucleotide.

1.3.1 Small GTPases of the Rho-family

Based on their sequence homology and functional similarities proteins of the Rho-family can be subdivided into six major groups (Table 1.3) (Wennerberg & Der, 2004). In mammals the first described Rho proteins of the Rho-family were the isoforms RhoA, B and C (Madaule & Axel, 1985). Today, the most noted and well characterized members are RhoA (ras homologous A), Rac1 (ras-related C3 botulinum toxin substrate) and Cdc42 (cell division cycle 42) (Hall, 1998).

Table 1.3 The Rho subfamily of Ras proteins. Classification based on Wennerberg & Der (2004).

Rho	**Rac**	**Cdc42**	**Rnd**	**Miro**	**RhoBTB**
RhoA	Rac1	Cdc42	Rnd1	Miro1	RhoBTB1
RhoB	Rac1b	TCL	Rnd2	Miro2	RhoBTB2
RhoC	Rac2	Wrch1	Rnd3		RhoBTB3
	Rac3	Chp			
	RhoG	TC10			

The small GTPases of the Rho-family are involved in a wide range of cellular processes, such as cell-cell adhesion, cell polarity, cell migration and gene transcription. Many of these processes are mediated by the activation of effector proteins, involved in the regulation of the actin cytoskeleton (Chimini & Chavrier, 2000; Kaibuchi *et al.*, 1999; Van Aelst & DSouza-Schorey, 1997). RhoA, Cdc42 and Rac1 display distinct effects on the actin cytoskeleton if activated in cells (Figure 1.11).

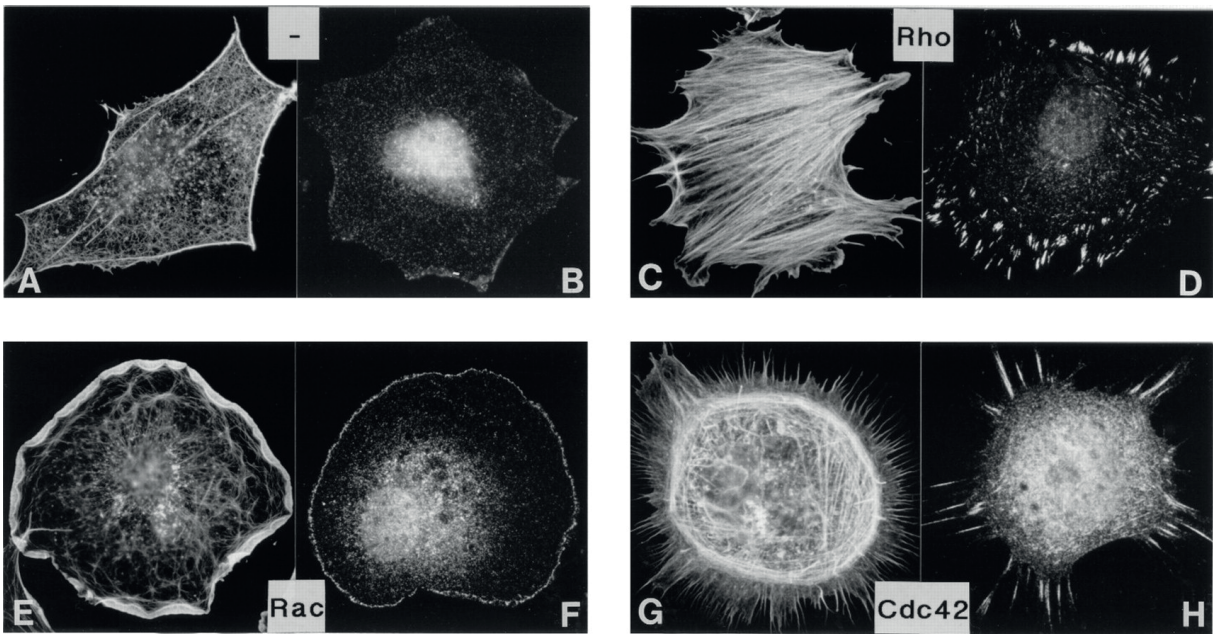

Figure 1.11 Impact of RhoA, Rac and Cdc42 on the actin cytoskeleton.
Quiescent, serum-starved Swiss 3T3 fibroblasts cells with activated RhoA by lysophosphatidic acid addition (C,D), microinjection of constitutively active Rac (E,F) and microinjection of the Cdc42 exchange factor FGD1 (G,H). Staining of actin in (A), (C), (E) and (G) vinculin staining in (B), (D), (F) and (H). Modified from Hall (1998).

Activation of RhoA leads to an increase in the amount of F-actin (Figure 1.11 C) and to the formation of focal adhesions (Figure 1.11 D). The effector protein mDia1, involved in acceleration of actin nucleation and elongation, is activated upon RhoA binding (Hill *et al.*, 1995). In comparison, Cdc42 mediates filopodia formation (Figure 1.11 G) and Rac induces the formation of lamellipodia, by the activation of the Arp2/3 complex through binding to NPFs (*e.g.* WASP, WAVE)(Figure 1.11 E) (Bishop & Hall, 2000; Ridley *et al.*, 1992). Moreover, the small GTPases are regulated by a cross-talk between the Rho proteins. It has been shown that Cdc42 can also activate Rac, while Rac in turn is able to activate Rho (Nobes & Hall, 1995; Ridley *et al.*, 1992)

1.3.2 The G-domain of the Ras-superfamily

The G-domain is the central structural motif of Ras-superfamily proteins and determines nucleotide and effector protein binding (Figure 1.12 A). It consists of six β-sheets and five adjacent α-helices, which are linked by ten loop regions. A distinct feature of Rho proteins is the insert helix (α3), that has been shown to be important for the activation of ROCK (Rho-associated protein kinase) (Zong *et al.*, 2001). Five of the loop regions (G1-G5) hold the key elements for specific nucleotide and effector binding (Bourne *et al.*, 1991; John *et al.*, 1990; Schmidt *et al.*, 1996; Via *et al.*, 2000). The

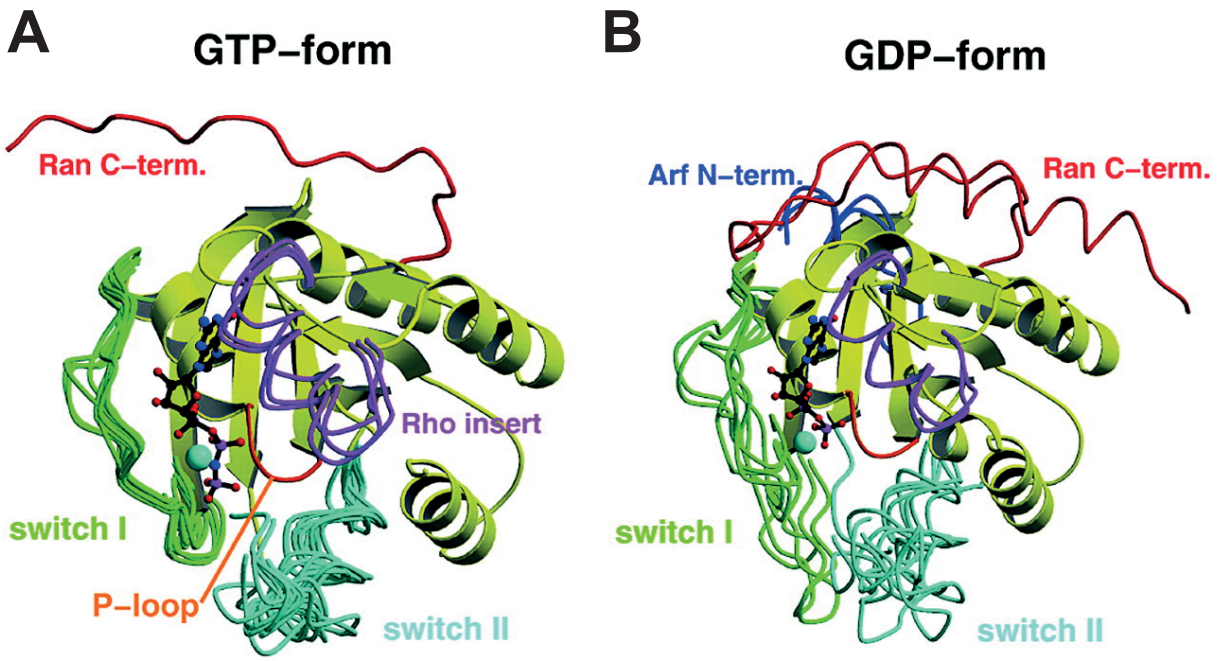

Figure 1.12 Superposition of several GNBP G-domains in their GTP- and GDP-bound state. The ribbon presentation displays the difference of the switch I and II region, dependent on the guanine nucleotide bound state. A: In the GTP-bound active state the switch I and II adopt a rigid conformation. B: In the Inactive GDP-bound state the switches are more flexible. Additional, structural features of Ran (red), Arf (blue) and Rho (purple) are highlighted. Modified from Vetter & Wittinghofer (2001).

P-loop (G1) with the consensus sequence GxxxxGK(S/T) mediates the high affinity binding of the nucleotide by interactions with the β- and γ-phosphates (Saraste *et al.*, 1990). Interaction with effector and regulatory proteins depend on the switch I and switch II regions (G2, G3). They bind to the γ-phosphate of GTP and Mg^{2+}. Upon hydrolysis the binding is disrupted and conformational changes occur explaining the molecular switch mechanism (Figure 1.12 B) (Spoerner *et al.*, 2001; Wittinghofer & Pal, 1991). Guanine-binding specificity is created by the G4 and G5 loop motifs due to the formation of specific hydrogen bonds with the guanine base (Zhong *et al.*, 1995).

1.3.3 Regulatory cycle

Small GNBPs are binary molecular switches with nucleotide dependent conformations. They are able to cycle between a GTP- and GDP-bound form (Figure 1.13). In the GTP-bound active state the conformation of the switch I and switch II regions are stabilized by the interaction with the γ-phosphate. The intrinsic hydrolysis rate and nucleotide dissociation of small GTPases are extremely low. Without additional proteins that support and regulate these processes, GTPases would not be a molecular switch of biological significance.

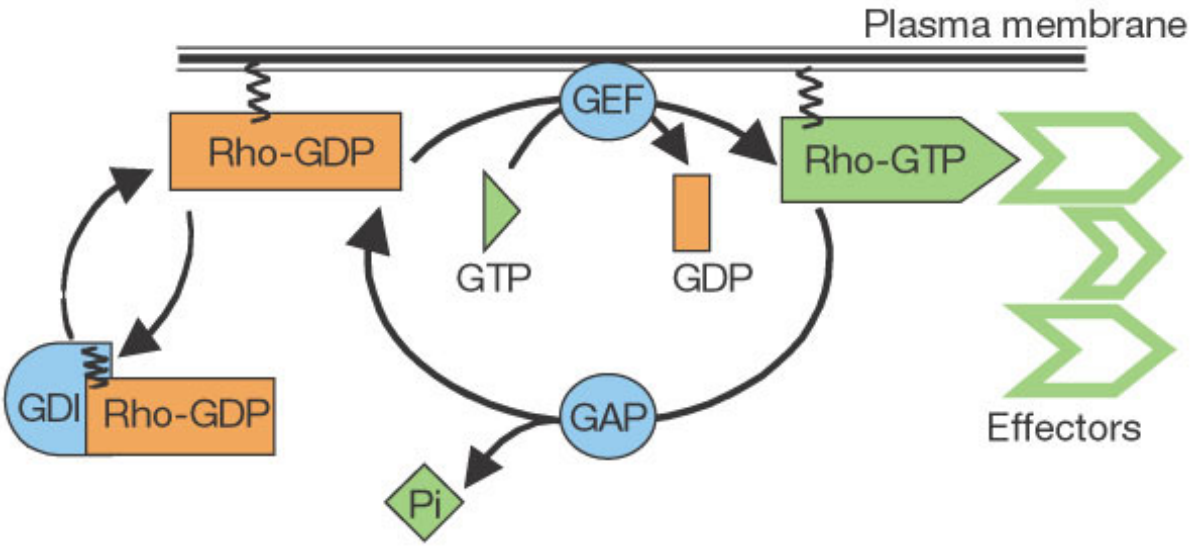

Figure 1.13 Regulatory cycle of Rho GTPases.
Small GNBPs are regulated by three distinct protein classes. The guanine nucleotide exchange is mediated by GEFs (guanine nucleotide exchange factors), the hydrolysis of GTP to GDP is accelerated by GAPs (GTPase activating proteins) and GDIs (guanine nucleotide dissociation inhibitors) extract the inactive prenylated GTPases from the membrane. Modified from Etienne-Manneville & Hall (2002).

Active GTP-bound Rho GTPases are inhibited by RhoGAPs (1.3.4). These proteins accelerate the hydrolysis rate of GTP to GDP. The activation of Rho GTPases is mediated by so-called GEFs (guanine-nucleotide exchange factors), that accelerate the nucleotide dissociation (1.3.5). In addition the localization of GTPases is regulated by GDIs (guanine nucleotide dissociation inhibitors), which are able to extract prenylated Rho proteins from lipid bilayers (Figure 1.13).

1.3.4 RhoGAPs

RhoGAPs play a crucial role to switch off signaling transduction pathways. Without RhoGAPs the slow intrinsic GTP-hydrolysis rate of GNBPs would lead to an ongoing downstream signaling, which would result in drastic consequences for cell functions. Since the discovery of the first RhoGAP more then 25 years ago (Trahey & McCormick, 1987), over 70 members of yeast to human RhoGAPs have been identified today and some of them are structurally and functionally characterized (Bernards, 2003; Peck *et al.*, 2002). The RhoGAPs of specific GTPases are conserved, however among the different Rho subfamilies they display different mechanisms to accelerate to the GTP-hydrolysis (Scheffzek *et al.*, 1997; Seewald *et al.*, 2002). Three of these mechanisms are depicted in Figure 1.14.

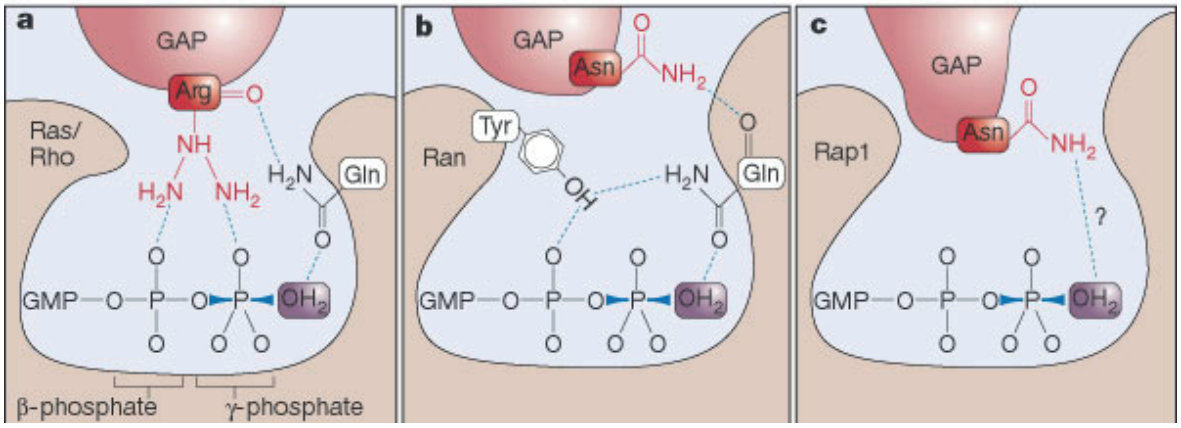

Figure 1.14 Differences in the GAP-accelerated GTP-hydrolysis of Rho proteins.
Essential for the effectiveness of the different GAPs is the positioning of a H_2O molecule for the nucleophilic attack on the γ-phosphate. a: The catalytic glutamine of Ras/Rho is positioned by the arginine of RasGAP (Scheffzek *et al.*, 1997). b: RanGAPs use an asparagine to stabilize the glutamine (Seewald *et al.*, 2002). c: Rap1 specific GAPs use an asparagine to position the water molecule directly (Daumke *et al.*, 2004). Illustration from Rehmann & Bos (2004).

The successful crystallizations of several small GTPases in complex with GAPs made it possible to gain further insights into the catalytic mechanisms. Ras- and RhoGAPs insert a positively charged arginine ("arginine finger") into the active site. One effect is the neutralization of the negative charge of the phosphates. As a second important function the arginine positions the glutamine (position 61 in Ras and 63 in RhoA) in *trans*. This glutamine on the other hand, orients the water molecule that attacks the γ-phosphate (Figure 1.14 a). RhoA exhibits an intrinsic hydrolysis rate of $0.022\,\mathrm{min}^{-1}$, which is increased to nearly $100\,\mathrm{min}^{-1}$ by p190RhoGap (Zhang & Zheng, 1998). Despite their structural differences, a similar mechanism seems to be the basis for all RhoGAP catalyzed hydrolysis reactions in GTPases. In RanGAPs the arginine is replaced by a asparagine, that stabilizes the glutamine of Ran, while the catalytic effect remains basically the same (Figure 1.14 b). Furthermore, the asparagine releases the inhibitory effect of the tyrosine 39 in Ran, that contacts the β-phosphate and orients the catalytic glutamine in *cis* (Brucker *et al.*, 2010). A distinct mechanisms is used for Rap1, which does not possess a catalytic glutamine. In Rap proteins the H_2O molecule is positioned directly by the asparagine of the GAP ("asparagine thumb"), as postulated by Daumke *et al.* (2004) and Scrima *et al.* (2008).

1.3.5 Activation by guanine nucleotide exchange factors

The intrinsically slow dissociation of bound nucleotides is the rate determining step in the transition of GNBPs into the active GTP-bound conformation. Hence, the

dissociation rate is increased by guanine nucleotide exchange factors (GEFs). Although, the different GEFs display structural differences the general reaction mechanism is functionally similar. Induced by GEFs the guanine nucleotide dissociation rate is accelerated by several orders of magnitude (Hutchinson & Eccleston, 2000; Klebe *et al.*, 1995). The concentration of GTP in the cell is approximately tenfold increased compared to GDP. Thus, upon dissociation of GDP, the GTPase is preferentially binding GTP instead of GDP. The GEFs p190RhoGEF and PDZ-RhoGEF increase the nucleotide exchange from 4.8×10^{-4} min^{-1} to 1930×10^{-4} min^{-1} (van Horck *et al.*, 2001), and from 5.5×10^{-4} min^{-1} to 1179×10^{-4} min^{-1}, respectively (Gasmi-Seabrook *et al.*, 2010).

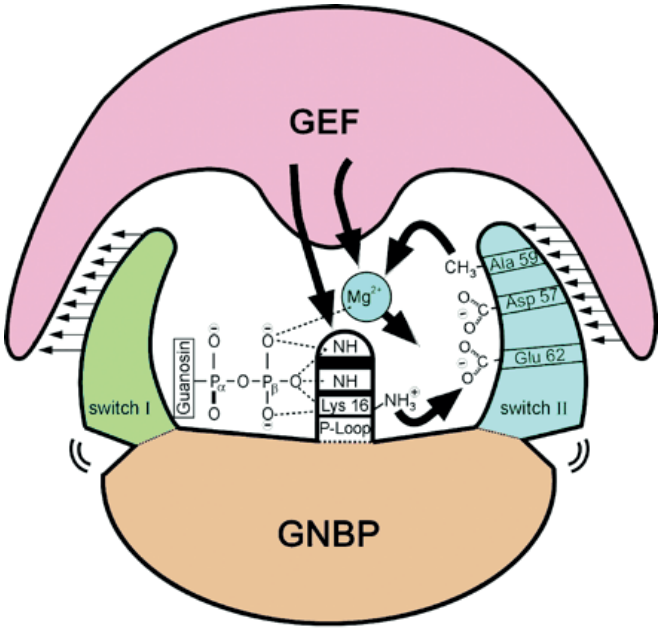

Figure 1.15 Schematic presentation of the *"push and pull"* mechanism of GEFs.
GEFs reduce the binding affinity of nucleotides to GNBPs. The insertion of several side chains into the active site impair the positioning of the P-loop and Mg^{2+}. Furthermore the switch I region is pulled out and the switch II region is pushed in the catalytic site. Modified from Vetter & Wittinghofer (2001).

During the course of the so-called "push and pull" mechanism the switch I region is pulled out and the switch II region is pushed in the nucleotide binding site (Vetter *et al.*, 1999). The insertion of additional amino acids into the nucleotide binding site by GEFs alters the conformation of the P-loop and displaces the Mg^{2+}-Ion, which is needed for the high nucleotide binding affinity (Gasper *et al.*, 2008; Lenzen *et al.*, 1998). This ultimately lowers the nucleotide affinity. Upon GEF-binding the P-loop lysine (K16 in Ras; K18 in Rho) is not able to interact with the negative charges of the phosphates but instead is orientated to the switch II (Figure 1.15). Notably, GEFs have no influence on the binding selectivity of GTPases regarding GTP or GDP. The insertion of guanine nucleotides is only driven by their intracellular concentration.

1.4. Scaffold protein Liprin-α3

Liprin-α has been firstly described as binding partner of leukocyte common antigen-related (LAR) family of receptor protein tyrosine phosphatases (LAR-RPTPs) (Pulido *et al.*, 1995; Serra-Pages *et al.*, 1995). Based on their primary structure the liprin protein family can be subdivided into Liprin-α, Liprin-β, Kazrin, and Liprin-γ. In mammals four different Liprin-α have been found, namely Liprin-α1, -α2, -α3 and -α4 together with Liprin-β1 and -β2 and KazrinE (Groot *et al.*, 2004; Serra-Pages *et al.*, 1998). For *Drosophila melangolaster* only one Liprin-β and Dliprin-α as the only Liprin-α have been described (Kaufmann *et al.*, 2002). Additionally, Liprin-γ (ortholog of KazrinE) has been found in *D. melangolaster* (Astigarraga *et al.*, 2010). The only Liprin-α in *C. elegans* is Syd-2 (synapse-defective 2) (Zhen & Jin, 1999). Especially, Liprin-α displays a high degree of conservation with approximately 50 % amino acid similarity between the human Liprin-α1 and Syd-2 (Spangler & Hoogenraad, 2007).
Liprin-α2 and -α3 are mainly expressed in the brain, whereas Liprin-α1 is ubiquitously expressed and Liprin-α4 is predominantly present in muscle tissues (Zürner *et al.*, 2011; Zürner & Schoch, 2009). The expression of the different Liprin-α isoforms in brain lysates has been further characterized. It has been shown, that Liprin-α1 is most abundant in the olfactory gland and in cultured glia cells, Liprin-α2 and -α3 are predominant in the hippocampus and Liprin-α4 is abundantly expressed at parallel fiber-Purkinje cell synapses (Spangler *et al.*, 2011).

1.4.1 Domain organization and interaction partner of Liprin-α

The subfamily of Liprin-α is composed of a predicted N-terminal coiled-coil domain and three C-terminal SAM (steril-α-motif) domains, also referred to as liprin homology (LH) domain (Pulido *et al.*, 1995; Serra-Pages *et al.*, 1995). Homodimerization of Liprin-α occurs via the N-terminal domain (Taru & Jin, 2011), whereas heterodimerization with Liprin-β is mediated by the SAM domains (Serra-Pages *et al.*, 1995). The N-terminal region of Liprin-α binds additionally to the ELKS protein family (ERC/CAST, ELKS-Rab6-interacting protein-CAST) (Dai *et al.*, 2006; Ko *et al.*, 2003b), RIM (Rab3-interacting molecul)(Schoch *et al.*, 2002), GIT1 (G-protein coupled receptor kinase interactor) (Ko *et al.*, 2003a), KIF1A (kinesin family member 1A) (Shin *et al.*, 2003) and most recently discovered also to mDia1 (Diaphanous) (Sakamoto *et al.*, 2012a). The SAM domains are involved in the binding of LAR-RPTPs (Pulido *et al.*, 1995; Serra-Pages *et al.*, 1995), CASK (calmoduin-dependent serine protein kinase) (Olsen *et al.*, 2005; Samuels *et al.*, 2007), ATP (Serra-Pagès *et al.*, 2005), CaMKII (Ca^2+/calmodulin-dependent protein

kinase II) (Hoogenraad *et al.*, 2007) and GRIP (glutamate receptor interacting protein) (Wyszynski *et al.*, 2002). The interactions are also summarized in Table 1.4.

Table 1.4 Overview of Liprin-α binding proteins. Modified and completed from Spangler & Hoogenraad (2007)

Binding partner	Liprin-	Function	Reference
Liprin-β	α1-3	Unknown	(Serra-Pages *et al.*, 1998)
LAR-RPTP	α1-3	presynaptic active zone formation	(Dunah *et al.*, 2005; Serra-Pages *et al.*, 1995, 1998)
GIT1	α1-4	AMPAR trafficking	(Ko *et al.*, 2003a,b)
GRIP1	α1-4	AMPAR trafficking	(Wyszynski *et al.*, 2002)
CASK	α2	neurotransmitter release	(Olsen *et al.*, 2005)
CaMKII	α1	dendrite and spine development	(Hoogenraad *et al.*, 2007)
CAST/ERC	α1-4	presynaptic scaffolding	(Dai *et al.*, 2006; Ko *et al.*, 2003b)
RIM	α3,4	neurotransmitter release	(Schoch *et al.*, 2002)
KIF1A	α1,2,4	microtublar transport	(Shin *et al.*, 2003)
mDia1	α3	microfilament formation	(Sakamoto *et al.*, 2012a)

1.4.2 Liprin-α functions

The proteins of the Liprin-α family have been shown to be involved in many processes, that regulate cellular and synaptic functions. Thereby, they mainly act as scaffolding proteins, linking specific components into larger protein complexes. Their versatile functions for the development and morphology at synapses is described briefly in the following. Additionally, the new emerged role of Liprin-α3 for the regulation of the F-actin formation is elucidated.

Pre- and postsynaptic development and the release of neurotransmitter

The subfamily of Liprin-α has been shown to be involved in the assembly of presynaptic components of many organisms. Loss-of-function mutation studies of the *liprin-α* homologue gene, *syd-2* in *C. elegans* caused severe defects in presynaptic structures (Zhen & Jin, 1999). The mutation led to translocalization of several synaptic vesicle proteins and increased the length of the active zones. Further studies showed, that SYD-2 additionally recruits GIT (G-protein-coupled interactor), SAD-1 (synapses of amphids defective-1), ELKS-1 (CAST/ERC) and SNN-1 (synapsin-1) to the presynaptic site (Patel *et al.*, 2006). A similar effect was observed in *Drosophila* using the *liprin-α*

homologue *Dliprin-α*. Mutations of *Dliprin-α* led to an impaired morphology of the active zone and the reduction of synaptic boutons (Kaufmann *et al.*, 2002).
The *syd-2* and *Dliprin-α* mutants did also influence the synaptic transmission, indicating an impact on the neurotransmitter release and vesicle cycling (Kaufmann *et al.*, 2002; Zhen & Jin, 1999). Two proteins involved in these processes, CAST and RIM (Rab3-interacting molecule), are linked by Liprin-α and co-localized at the synapses. Another complex that assembles in the presence of Liprin-α is composed of CASK (Ca^{2+}/calmodulin-dependent serine protein kinase), MALS (mammalian LIN-seven protein) and Mint1. The disruption of this complex decreased the excitatory postsynaptic currents (Olsen *et al.*, 2005).
At the postsynaptic site Liprin-α interacts with GRIP1 (glutamate receptor-interacting protein 1) (Wyszynski *et al.*, 2002), an AMPAR (AMPA (α-amino-3-hydroxy-5-methylisoxazole-4-propionic acid) receptor) binding protein (Dong *et al.*, 1997). The interaction of Liprin-α with this receptor is required for a proper localization and expression of AMPAR. Additionally, the binding of Liprin-α to leukocyte common antigen-related (LAR) receptors regulates AMPAR and the morphology of dendritic spines (Dunah *et al.*, 2005).

Intracellular transport mechanism

Liprin-α has an additional role in the trafficking of synaptic proteins. It has been reported that Liprin-α binds to the Kinesin-like protein KIF1A, an axonal transporter of synaptic vesicles (Miller *et al.*, 2005; Shin *et al.*, 2003). Mutations of *liprin-α* in *Drosophila*, resulted in impaired movement of synaptic vesicles (Miller *et al.*, 2005). In complex with GRIP1, Liprin-α is also connected to cadherins and β-catenin, proteins involved in the maintenance of focal adhesions. Therefore, postulated models indicate, that Liprin-α is able to recruit structure-bearing protein complexes, such as cadherin-β-catenin and also functional complexes (AMPAR) to the synapse (Dunah *et al.*, 2005; Spangler & Hoogenraad, 2007).

Inhibition of stress fiber formation

The interaction of Liprin-α3 and the Diaphanous formin mDia1 has most recently been described by Sakamoto *et al.* (2012a). They showed via pulldown assays, that Liprin-α3 binds with its N-terminal coiled-coil domain to $mDia_{DID}$-DD (Diaphanous-inhibitory domain, Dimerization-domain) of mDia1. Furthermore, they postulated a competition of Liprin-α3 with the $mDia_{DAD}$ (Diaphanous autoregulatory domain) for $mDia_{DID}$ binding. Overexpression of Liprin-α3 resulted in reduced RhoA activated stress fiber formation and delocalization of mDia1 from the plasma membrane. In accordance with

these results knowndown of Liprin-α3 by RNAi resulted in enhanced microfilament formation. However, the exact binding mechanism of Liprin-α3 and mDia1, and the influence on the mDia1 activity remained unclear.

2. Aim of this thesis

Liprin-α3 has recently been identified as a novel interaction partner of the formin mDia1. It has been shown that Liprin-α3 inhibits the mDia1 induced formation of F-actin and that it translocates mDia1 from the plasma membrane. However, the underlying mechanisms remained unclear. In order to gain further insights into the inhibitory potency of Liprin-α3 on the mDia1 function, the following questions were addressed in this thesis.

1. How and where binds Liprin-α3 to mDia1?
The first aim of this study was to functionally and structurally characterize the interaction sites of Liprin-α3 and mDia1. Based on these data determinants of specificity underlying the interaction were further investigated.

2. Is the autoregulation of mDia1 affected by Liprin-α3?
In order to study how Liprin-α3 downregulates the mDia1 function, the influence of Liprin-α3 on mDia1 activation by RhoA, as well as its impact on the mDia1 autoinhibition were analyzed thermodynamically and kinetically. This included the question of potential ternary complexes and the possible dissociation of Liprin-α3 from $mDia_N$ by RhoA and $mDia_{DID}$.

3. Is the minimal mDia1-binding Liprin-α3 fragment able to mediate the F-actin reducing effect?
The last part of this thesis addressed the question, whether the overexpression of the shortest mDia1-binding Liprin-α3 fragment is sufficient to obtain the same reducing effect on the amount of cellular F-actin as full-length Liprin-α3. Additionally, the question arose, if cell type specific mechanisms exist, that regulate the activity and the inhibitory potential of Liprin-α3.

3. Materials and Methods

3.1. Materials

3.1.1 Cell strains

Name	Supplier
E.coli BL21 (DE3) T1	New England Biolabs®
E.coli DH5a	New England Biolabs®

3.1.2 Antibiotics

Antibiotic	Final concentration
Ampicillin	$100\,\mu g\,mL^{-1}$
Kanamycin	$25\,\mu g\,mL^{-1}$

3.1.3 Vectors

Vector	Supplier
pGEX4T5-TEV*	GE Healthcare
pEGFP-N3	BD bioscience
mCherry-C1	Clontech Laboratories

* This vector was designed on basis of the commercially available pGEX4T1 vector. An additional TEV (tabacco etch virus) restriction site was inserted between Thrombin cleavage site and the multiple cloning site (MCS). Neither the Thrombin cleavage site, nor the reading frame were affected.

3.1.4 Buffers and solutions

Name	Components
phosphate buffered saline (PBS)	10 mM Na_2HPO_4, 2 mM KH_2PO_4, 137 mM NaCl, 2.7 mM KCl, pH 7.4
phosphate buffered saline - Tween (PBST)	10 mM Na_2HPO_4, 2 mM KH_2PO_4, 137 mM NaCl, 2.7 mM KCl, 0.1 % Tween-20, pH 7.4
protein buffer	25 mM Tris/HCl, 150 mM NaCl, 5 mM $MgCl_2$, 2 mM β-ME, pH 7.4
protein wash buffer	25 mM Tris/HCl, 500 mM NaCl, 5 mM $MgCl_2$, 2 mM β-ME, pH 7.4
exchange buffer	50 mM Tris/HCl, 100 mM NaCl, 5 mM EDTA, pH 7.4
GSH elution buffer	25 mM Tris/HCl, 150 mM NaCl, 5 mM $MgCl_2$, 2 mM β-ME, 30mM GSH, pH 7.4
Laemmli sample buffer	50 mM Tris/HCl, pH 6.8, 50 % (v/v) Glycerol, 500 mM DTT, 10 % (w/v) SDS, 0.5 % (w/v) Bromphenolblue
coomassie staining solution	40 % (v/v) methanol, 10 % (v/v) acetic acid, 0.4 % (w/v) Coomassie-R250. 0.4 % (w/v) Coomassie-G250
coomassie destaining solution	40% (v/v) ethanol, 10% (v/v) acetic acid
anode buffer	200 mM Tris/HCl, pH 8.9
cathode buffer	100 mM Tris/HCl, 100 mM tricine, 0.1 % (w/v) SDS , pH 8.2
RIPA buffer	50 mM Tris/HCl, 150 mM sodium chloride, 1.0 % Triton X-100, 0.5 % sodium deoxycholate, 0.1 % (w/v) SDS, pH 8.0
mild stripping buffer	1.5 % (w/v) glycine, 0.1 % (w/v) SDS, 1 % (v/v) Tween20, pH 2.2
transfer buffer	25 mM Tris, base, 150 mM glycine, 10% (v/v) methanol

3.1.5 Media

Media	Components (1L)
LB	10 g peptone, 5 g yeast extract, 10 g NaCl, pH 7.4
LB agar	10 g peptone, 5 g yeast extract, 10 g NaCl, 16 g agar, pH 7.4

3.1.6 Crystallization Screens

Name	Manufacturer
Additive Screen HT™	Hampton Research
Crystal Screen™	Hampton Research
Crystal Screen 2™	Hampton Research
PEG/Ion Screen™	Hampton Research
PEG/Ion 2 Screen™	Hampton Research
Index™	Hampton Research
JCSG-*plus*	Molecular Dimensions
PACT Premier™	Molecular Dimensions
Morpheus® HT-96	Molecular Dimensions
Crystal Strategy Screen™ I HT-96	Molecular Dimensions
Crystal Strategy Screen™ II HT-96	Molecular Dimensions
PGA-LM HT-96 Screen™	Molecular Dimensions
Structure Screen I	Molecular Dimensions
Structure Screen II	Molecular Dimensions

3.1.7 Antibodies and actin filament staining

Antigen	Origin	Manufacturer	Catalog no.	Dilution
mCherry	rabbit	abcam®	ab167453	1:1250
eGFP	mouse	Acris Antibodies	AM20710PU-N	1:1250
α-tubulin	rat	abcam®	ab6160	1:1000
rabbit-IgG (HRP)	goat	abcam®	ab6721	1:10000
mouse-IgG (HRP)	rabbit	abcam®	ab6728	1:10000
rat-IgG (HRP)	rabbit	abcam®	ab6734	1:10000
Phalloidin		Biotium	00041	1:60

3.1.8 Enzymes

Name	Supplier
Digest	
EcoRI-HF	New England BioLabs
BamHI-HF	New England BioLabs
XhoI	New England BioLabs
HindIII-HF	New England BioLabs
BglII-Hf	New England BioLabs
PCR	
Phusion® High-Fidelity DNA Polymerase	New England BioLabs
Ligation	
T4 DNA ligase	New England BioLabs

3.1.9 Chromatography columns

Name	Supplier
Superdex 75 10/300 GL	GE Healthcare
Superdex 200 10/300 GL	GE Healthcare
Superdex 75 16/60 GL	GE Healthcare
Superdex 75 26/60 GL	GE Healthcare
Superdex 200 16/60 GL	GE Healthcare
Superdex 200 26/60 GL	GE Healthcare

3.1.10 Cloning primer

All primers were purchased from MW-Biotech and are listed in the table below.

Primer for cloning into expression vectors

Table 3.1 Primers used for cloning into the pGEX4T5-TEV vector.

protein	size	vector	sense / antisense	enzyme
mDia1 *mouse*	79-369	pGEX4T5-TEV	5′−GGAATTCTCAGACGAGCAAGTTCTTGTC−3′ 5′−CCGCTCGAGCGGTTATCCCTTCAGATCAAAG−3′	EcoRI XhoI
mDia1 *mouse*	74-369	pGEX4T5-TEV	5′−GGAATTCTCATTGCAGGACATCTCAGAC−3′ 5′−CCGCTCGAGCGGTTATCCCTTCAGATCAAAG−3′	EcoRI XhoI
mDia1 *mouse*	69-369	pGEX4T5-TEV	5′−GGAATTCGACCCCACTGCTCAGTCATTGCAGG−3′ 5′−CCGCTCGAGCGGTTATCCCTTCAGATCAAAG−3′	EcoRI XhoI
mDia1 *mouse*	79-435	pGEX4T5-TEV	5′−GGAATTCTCAGACGAGCAAGTTCTTGTC−3′ 5′−CCGCTCGAGCGGTTAGTGTAGAACTATCTGAGAAAC−3′	EcoRI XhoI
mDia1 *mouse*	79-443	pGEX4T5-TEV	5′−GGAATTCTCAGACGAGCAAGTTCTTGTC−3′ 5′−CCGCTCGAGCGGTTAGAAGTCAGGATCAGTTCCATTTTTG−3′	EcoRI XhoI
mDia1 *mouse*	74-443	pGEX4T5-TEV	5′−GGAATTCTCATTGCAGGACATCTCAGAC−3′ 5′−CCGCTCGAGCGGTTAGAAGTCAGGATCAGTTCCATTTTTG−3′	EcoRI XhoI
mDia1 *mouse*	69-443	pGEX4T5-TEV	5′−GGAATTCGACCCCACTGCTCAGTCATTGCAGG−3′ 5′−CCGCTCGAGCGGTTAGAAGTCAGGATCAGTTCCATTTTTG−3′	EcoRI XhoI
mDia1 *mouse*	69-435	pGEX4T5-TEV	5′−GGAATTCGACCCCACTGCTCAGTCATTGCAGG−3′ 5′−CCGCTCGAGCGGTTAGTGTAGAACTATCTGAGAAAC−3′	EcoRI XhoI
mDia1 *mouse*	69-451	pGEX4T5-TEV	5′−GGAATTCGACCCCACTGCTCAGTCATTGCAGG−3′ 5′−CCGCTCGAGCGGTTAATCAATCTGCAGGTGTCGG−3′	EcoRI XhoI
mDia1 *mouse*	69-570	pGEX4T5-TEV	5′−GGAATTCGACCCCACTGCTCAGTCATTGCAGG−3′ 5′−CCGCTCGAGCGGTTAAGCAGCACTGCTAGAAAC−3′	EcoRI XhoI
mDia1 *mouse*	135-369	pGEX4T5-TEV	5′−GGAATTCTCTGCCATGATGTACATCC−3′ 5′−CCGCTCGAGCGGTTATCCCTTCAGATCAAAG−3′	EcoRI XhoI
mDia1 *mouse*	135-525	pGEX4T5-TEV	5′−GGAATTCTCTGCCATGATGTACATCC−3′ 5′−CCGCTCGAGCGGTTATTTCTGTGCAGTGATCTGCTGC−3′	EcoRI XhoI
mDia1 *mouse*	135-570	pGEX4T5-TEV	5′−GGAATTCTCTGCCATGATGTACATCC−3′ 5′−CCGCTCGAGCGGTTAAGCAGCACTGCTAGAAAC−3′	EcoRI XhoI
mDia1 *mouse*	135-500	pGEX4T5-TEV	5′−GGAATTCTCTGCCATGATGTACATCC−3′ 5′−CCGCTCGAGCGGTTAAAAGTCATTTTCCATCTTTTTC−3′	EcoRI XhoI
mDia1 *mouse*	135-550	pGEX4T5-TEV	5′−GGAATTCTCTGCCATGATGTACATCC−3′ 5′−CCGCTCGAGCGGTTACTTGGCATCTTCTAGTTCTTTTG −3′	EcoRI XhoI
mDia1 *mouse*	135-475	pGEX4T5-TEV	5′−GGAATTCTCTGCCATGATGTACATCC−3′ 5′−CCGCTCGAGCGGTTACAGCTCTGTAGCTTTGGCCTC −3′	EcoRI XhoI
mDia1 *mouse*	135-451	pGEX4T5-TEV	5′−GGAATTCTCTGCCATGATGTACATCC−3′ 5′−CCGCTCGAGCGGTTAATCAATCTGCAGGTGTCGG−3′	EcoRI XhoI
mDia1 *mouse*	WW-1145-1200	pGEX4T5-TEV	5′−CGGGATCCTGGTGGATGCGGAGAGCAAAATTAGC−3′ 5′−CCGCTCGAGCGGTTACCCTCTCTTCCGTCGGAATG −3′	EcoRI XhoI
mDia1 *mouse*	WW-1145-1209	pGEX4T5-TEV	5′−CGGGATCCTGGTGGATGCGGAGAGCAAAATTAGC−3′ 5′−CCGCTCGAGCGGTTACCCAGCCTTCCTGTTG−3′	EcoRI XhoI
Liprin-α3 *mouse*	20-587	pGEX4T5-TEV	5′−CGGAATTCGGCCCGGACGAGGCC−3′ 5′−CCGCTCGAGCGGTTACGGTGACCCTGCTTGC −3′	EcoRI XhoI
Liprin-α3 *mouse*	25-587	pGEX4T5-TEV	5′−GGAATTCGGCGAGCTGGAGCGCCTCATG−3′ 5′−CCGCTCGAGCGGTTACGGTGACCCTGCTTGC−3′	EcoRI XhoI
Liprin-α3 *mouse*	77-587	pGEX4T5-TEV	5′−CGGAATTCGCTCTGCCTCAGGAG−3′ 5′−CCGCTCGAGCGGTTACGGTGACCCTGCTTGC−3′	EcoRI XhoI
Liprin-α3 *mouse*	90-587	pGEX4T5-TEV	5′−CGGAATTCAACTTATGTCGGGAAC−3′	EcoRI

Continued

protein	size	vector	sense / antisense	enzyme
			5′−CCGCTCGAGCGGTTACGGTGACCCTGCTTGC−3′	XhoI
Liprin-α3 *mouse*	110-587	pGEX4T5-TEV	5′−CGGAATTCCGAAACAACACCCGG−3′ 5′−CCGCTCGAGCGGTTACGGTGACCCTGCTTGC−3′	EcoRI XhoI
Liprin-α3 *mouse*	217-587	pGEX4T5-TEV	5′−CGGAATTCGCCGAGACCTTACCA−3′ 5′−CCGCTCGAGCGGTTACGGTGACCCTGCTTGC−3′	EcoRI XhoI
Liprin-α3 *mouse*	271-587	pGEX4T5-TEV	5′−CGGAATTCATGAACGATGACCAC−3′ 5′−CCGCTCGAGCGGTTACGGTGACCCTGCTTGC−3′	EcoRI XhoI
Liprin-α3 *mouse*	306-587	pGEX4T5-TEV	5′−GGAATTCGAGGAGAAGAACTC−3′ 5′−CCGCTCGAGCGGTTACGGTGACCCTGCTTGC−3′	EcoRI XhoI
Liprin-α3 *mouse*	457-587	pGEX4T5-TEV	5′−GGAATTCGAGGAGAAGAACTCCCTGAGCGAGGA−3′ 5′−CCGCTCGAGCGGTTACGGTGACCCTGCTTGC−3′	EcoRI XhoI
Liprin-α3 *mouse*	W-532-587	pGEX4T5-TEV	5′−CGGGATCCTGGGGAGGAAGTCCTGCCCGGGAG−3′ 5′−CCGCTCGAGCGGTTACGGTGACCCTGCTTGC−3′	EcoRI XhoI
Liprin-α3 *mouse*	W-541-587	pGEX4T5-TEV	5′−CGGGATCCTGGGGAACCAACCATGTCTCTAAG−3′ 5′−CCGCTCGAGCGGTTACGGTGACCCTGCTTGC−3′	BamHI XhoI
Liprin-α3 *mouse*	W-561-587	pGEX4T5-TEV	5′−CGGGATCCTGGGGAGGAGACACCCCACCACCCAC−3′ 5′−CCGCTCGAGCGGTTACGGTGACCCTGCTTGC−3′	EcoRI XhoI
Liprin-α3 *mouse*	W-443-498	pGEX4T5-TEV	5′−CGGGATCCTGGGGAGGAAGTGGGCAAGCTGATGTGC−3′ 5′−CCGCTCGAGCGGTTAGTACCGGCCCAGCGAG−3′	BamHI XhoI
Liprin-α3 *mouse*	W-443-491	pGEX4T5-TEV	5′−CGGGATCCTGGGGAGGAAGTGGGCAAGCTGATGTGC−3′ 5′−CCGCTCGAGCGGTTAGCCAGAACTGGACAC−3′	BamHI XhoI
Liprin-α3 *mouse*	W-491-560	pGEX4T5-TEV	5′−CGGGATCCTGGGGAGGAGGCCTTGACTCGCTGG−3′ 5′−CCGCTCGAGCGGTTATGGAACGGCTGGACCCTC−3′	EcoRI XhoI
Liprin-α3 *mouse*	W-541-571	pGEX4T5-TEV	5′−CGGGATCCTGGGGAACCAACCATGTCTCTAAG−3′ 5′−CCGCTCGAGCGGTTAGGCAGAGCGGGGCGTG−3′	BamHI XhoI
Liprin-α3 *mouse*	25-217	pGEX4T5-TEV	5′−GGAATTCGGCGAGCTGGAGCGCCTCATG−3′ 5′−CCGCTCGAGCGGTTAGGCCTTCTGCAGGGTCTGTTGC−3′	EcoRI XhoI
Liprin-α3 *mouse*	25-817	pGEX4T5-TEV	5′−GGAATTCGGCGAGCTGGAGCGCCTCATG−3′ 5′−CCGCTCGAGCGGTTAGGGCAGCCCAAGGCTG−3′	EcoRI XhoI
Liprin-α3 *mouse*	25-737	pGEX4T5-TEV	5′−GGAATTCGGCGAGCTGGAGCGCCTCATG−3′ 5′−CCGCTCGAGCGGTTAGGACCCCGCCTGCAGTGCC−3′	EcoRI XhoI
Liprin-α3 *mouse*	W-561-581	pGEX4T5-TEV	5′−CGGGATCCTGGGGAGGAGACACCCCACCACCCAC−3′ 5′−CCGCTCGAGCGGTTACGCCAAAGCCTGGGCCATCCTCTCAAGAC−3′	EcoRI XhoI
Liprin-α3 *mouse*	W-561-582	pGEX4T5-TEV	5′−CGGGATCCTGGGGAGGAGACACCCCACCACCCAC−3′ 5′−CCGCTCGAGCGGTTACAGCGCCAAAGCCTGGGCCATCCTCTCAAG−3′	EcoRI XhoI
Liprin-α3 *mouse*	1-737	pGEX4T5-TEV	5′−GGAATTCATGATGTGCGAGGTG−3′ 5′−CCGCTCGAGCGGTTAGGACCCCGCCTGCAGTGCC−3′	EcoRI XhoI
Liprin-α3 *mouse*	1-817	pGEX4T5-TEV	5′−GGAATTCATGATGTGCGAGGTG−3′ 5′−CCGCTCGAGCGGTTAGGGCAGCCCAAGGCTG−3′	EcoRI XhoI
RhoA *human*	1-193	pGEX4T5-TEV	5′−CGGGATCCATGGCTGCCATCCGG−3′ 5′−CGGAATTCCGTTACAAGACAAGGCAACCAG−3′	BamHI EcoRI

Primer for cloning into cell culture expression vectors

Table 3.2 Primers used for cloning into the pEGFP-N3 and mCherry-C1 vectors.

protein	size	vector	sense / antisense	enzyme
Liprin-α3 *mouse*	1-1043	mCherry-C1	5′−CCCAAGCTTGGGTTAGCAGGAGTAAGTCCGGACCGAAAC−3′ 5′−GAAGATCTATGATGTGCGAGGTGATGCCTAC−3′	BglII HindIII
Liprin-α3 *mouse*	1-817	mCherry-C1	5′−CCCAAGCTTGGGTTAGCAGGAGTAAGTCCGGACCGAAAC−3′ 5′−GGAATTCCTTAGGGCAGCCCAAGGCTG−3′	HindIII EcoRI
Liprin-α3 *mouse*	561-587	mCherry-C1	5′−GAAGATCTGGAGACACCCCACCACCCAC−3′ 5′−AAGCTTGGGTTACGGTGACCCTGCTTGCAGCGC−3′	BglII HindIII

Continued

protein	size	vector	sense / antisense	enzyme
Liprin-α3 *mouse*	567-587	mCherry-C1	5′−GAAGATCTACGCCCCGCTCTGCCCGTCTTG−3′ 5′−AAGCTTGGGTTACGGTGACCCTGCTTGCAGCGC−3′	BglII HindIII
Liprin-α3 *mouse*	(3GS)567-587	mCherry-C1	5′−GAGGATCCGGAACGCCCCGCTCTGCCCGTC−3′ 5′−AAGCTTGGGTTACGGTGACCCTGCTTGCAGCGC−3′	BglII HindIII
Liprin-α3 *mouse*	561-582	mCherry-C1	5′−GAAGATCTGGAGACACCCCACCACCCAC−3′ 5′−AAGCTTGGGTTACAGCGCCAAAGCCTG−3′	BglII HindIII
RhoA *human*	1-193	pEGFP-N3	5′−GAAGATCTATGGCTGCCATCCGGAA −3′ 5′−GGATCCCAAGACAAGGCAAC−3′	BglII BamHI

QuikChange® Site-Directed-Mutagenesis Primer

Table 3.3 Primers used for site-directed mutagenesis.

protein	mutation	sense / antisense
Liprin-α3 *mouse*	R569E	5′−CACCACCCACGCCCGAATCTGCCCGTCTTGAG−3′ 5′−CTCAAGACGGGCAGATTCGGGCGTGGGTGGTG−3′
Liprin-α3 *mouse*	R572E	5′−GCCCCGCTCTGCCGAACTTGAGAGGATG−3′ 5′−CATCCTCTCAAGTTCGGCAGAGCGGGGC−3′
Liprin-α3 *mouse*	L573E	5′−CGCTCTGCCCGTGAGGAGAGGATGGCCCAG−3′ 5′−CTGGGCCATCCTCTCCTCACGGGCAGAGCG−3′
Liprin-α3 *mouse*	L575E	5′−CTGCCCGTCTTGAGGAAATGGCCCAGGCTTTG−3′ 5′−CAAAGCCTGGGCCATTTCCTCAAGACGGGC−3′
Liprin-α3 *mouse*	M576E	5′−GCCCGTCTTGAGAGGGAGGCCCAGGCTTTGG−3′ 5′−CCAAAGCCTGGGCCTCCCTCTCAAGACGGGC−3′
Liprin-α3 *mouse*	L580E	5′−GAGGATGGCCCAGGCTGAGGCGCTGCAAGCAGGGTC−3′ 5′−GACCCTGCTTGCAGCGCCTCAGCCTGGGCCATCCTC−3′
Liprin-α3 *mouse*	T563E	5′−GATCCTGGGGAGGAGACGAACCACCACCCACGC−3′ 5′−GCGTGGGTGGTGGTTCGTCTCCTCCCCAGGATC−3′
Liprin-α3 *mouse*	T567E	5′−GACACCCCACCACCCGAGCCCCGCTCTGCCCGTC−3′ 5′−GACGGGCAGAGCGGGGCTCGGGTGGTGGGGTGTC−3′
Liprin-α3 *mouse*	T563/567E	5′−GACGAACCACCACCCGAGCCCCGCTCTGCCCGTC−3′ 5′−GACGGGCAGAGCGGGGCTCGGGTGGTGGTTCGTC−3′
mDia1 *mouse*	N165D	5′−GAGTCTCTCTCAACGACAACCCTGTCAGTTG−3′ 5′−CAACTGACAGGGTTGTCGTTGAGAGAGACTC −3′
mDia1 *mouse*	A256D	5′−CAAAGCTGCTGTCTGACCTCTGTATCCTGC−3′ 5′−GCAGGATACAGAGGTCAGACAGCAGCTTTG−3′
mDia1 *mouse*	I259D	5′−GTCTGCCCTCTGTGACCTGCCGCAGCCGGAG−3′ 5′−CTCCGGCTGCGGCAGGTCACAGAGGGCAGAC−3′
mDia1 *mouse*	E317R	5′−CTCATCACTCCAGCTAGGGAACTGGACTTCCGAG−3′ 5′−CTCGGAAGTCCAGTTCCCTAGCTGGAGTGATGAG−3′
mDia1 *mouse*	E358R	5′−CTGTGCGTGTTTGATAGACAAGGGGATGAAGATTTC−3′ 5′−GAAATCTTCATCCCCTTGTCTATCAAACACGCACAG−3′
mDia1 *mouse*	E362R	5′−GATGAACAAGGGGATAGGGATTTCTTTGATCCTG−3′ 5′−CAGGATCAAAGAAATCCCTATCCCCTTGTTCATC−3′
mDia2 *mouse*	K369C	5′−CTGGATATACAACTTTGTGTCTTTGATGAGCAC−3′ 5′−GTGCTCATCAAAGACACAAAGTTGTATATCCAG−3′
RhoA *human*	Q63L	5′−GGGACACAGCTGGGCTGGAAGATTATGATCGC−3′ 5′−GCGATCATAATCTTCCAGCCCAGCTGTGTCCC−3′
RhoA *human*	G14V	5′−GGTGATTGTTGGTGATGGAGCCTGTGG−3′ 5′−CCACAGGCTCCATCACCAACAATCACC−3′

3.2. Molecular Biological Methods

3.2.1 Cloning

The cloning of specific protein fragments into the desired vectors required several steps. The DNA was amplified, purified, restricted, again purified, ligated into the vector and finally transformed into *E. coli*. Each step is described in the following.

Polymerase chain reaction

In the first step the inserts were amplified by polymerase chain reaction (PCR) using the indicated primer (Table 3.1, 3.2) with the specific restriction sites. The primer were pipetted together with the template DNA in a 50 µL reaction mixture as indicated.

PCR reaction mixture	
Phusion buffer (5x)	10 µL
DMSO	1.5 µL
10 x dNTP (2 mM)	1 µL
5′-primer (10 pmol/µL)	1 µL
3′-primer (10 pmol/µL)	1 µL
Phusion® High-Fidelity DNA Polymerase	0.5 µL
template DNA (20-200 ng)	1 µL
H_2O	ad 50 µL

DNA amplification was performed using a thermal cycler with the following setup. Subsequently, the DNA samples were purified.

Table 3.4 PCR Settings.

step	duration	temperature	number of cycles
denaturation	30 sec	94 ℃	1
denaturation	30 sec	94 ℃	
annealing	30 sec	55-75 ℃	30
elongation	20 sec/ kb	72 ℃	
elongation	10 min	72 ℃	1

DNA purification

During the cloning procedure the DNA was purified at two steps. After the initial PCR to ensure proper restriction the DNA was purified using the QIAquick PCR Purification Kit (Quiagen). The digested DNA fragments and vectors were purified using the QIAquick Gel Extraction Kit (Quiagen). Both protocols were done according to the manufactures manual.

Restriction

The amplified and purified DNA strands were restricted with the corresponding enzymes (Table 3.1, 3.2). Therefore, the samples were incubated at 37 ℃ for 1 h in CutSmart® buffer. Simultaneously, 1 µg of the target vector was digested with the same enzymes prior to the ligation.

Ligation

Ligation was performed according to the manufacturers protocol using the T4 DNA ligase (NEB). Therefore, 50 ng of the vector DNA and a fivefold molar excess of insert DNA were incubated with the ligase for 10 min at RT. The following heat inactivation of the enzyme was performed at 65 ℃ for another 10 min. Afterwards, the sample was transformed into *E. coli* cells as described in section 3.3.

Colony PCR

Correct and complete ligation of the desired DNA fragments into the vector was controlled by Colony PCR. Following the transformation and cultivation the grown *E. coli* colonies were picked and used as the template for a PCR using the 5 Prime Mastermix (5Prime) and vector specific primers. The amplified fragments were analyzed by agarose gelelectrophoresis and stained with SYBR® Safe (Life technologies).

3.2.2 Site-directed mutagenesis

The exchange, deletion and insertion of specific nucleotides was performed using the QuikChange® Site-Directed-Mutagenesis Protocol (Stratagene, Amsterdam, Belgium). Therefore two reverse-complementary primer with the desired mutation flanked by approximately 15 bases at each site were designed. To optimize the annealing, the primer ended with an 5′ and 3′ guanosin or cytosin and had a melting temperature of approximately 70 ℃. The primer were pipetted together with the template DNA in a 50 µL reaction mixture as indicated.

QuikChange reaction mixture	
Phusion buffer (5x)	10 µL
DMSO	1.5 µL
10 x dNTP (2 mM)	1 µL
5′-primer (10 pmol/µL)	2.5 µL
3′-primer (10 pmol/µL)	2.5 µL
Phusion® High-Fidelity DNA Polymerase	0.5 µL
template DNA (2 ng)	1 µL
H_2O	ad 50 µL

The site directed mutagenesis was performed using a thermal cycler with the following setup (Table 3.5). Subsequently, the sample was incubated with Dpn1 (NEB) for 2 h at 37 ℃. This enzyme cleaves only at methylated sites (template), keeping the PCR product intact. Afterwards the sample was transformed into *E. coli* cells as described in section 3.3.

Table 3.5 QuikChange PCR cycler settings.

step	duration	temperature	number of cycles
denaturation	60 sec	94 ℃	1
denaturation	60 sec	94 ℃	
annealing	60 sec	55 ℃	30
elongation	30 sec/ kb	72 ℃	
elongation	10 min	72 ℃	1

3.2.3 Purification of plasmid DNA

The used constructs were amplified using DH5α *E. coli* strains. These transformed cells were cultivated in 4 mL LB-medium at 37 ℃ O/N and the plasmid DNA was purified with the QIAprep Spin Miniprep Kit (Quiagen). For vectors used in cell culture assays 100 mL of LB-medium and the QIAGEN Plasmid Midi kit (Quiagen) were used. This resulted in higher amounts of plasmid DNA with a high degree of purity suitably for adequate transfection efficiencies.

3.2.4 Denaturing SDS-polyacrylamid gelelectrophoresis

Discontinuous denaturing SDS-polyacrylamid gelelectrophoresis (SDS-PAGE) was used to separate protein mixtures and to examine the different steps of the protein purification process. Composition of the gels is shown in Table 3.6.

Table 3.6 SDS-PAGE gel composition.

	stacking gel	**separation gel**
acrylamide (%)	3.1	12
acrylamide solution 30 % / mL	2.48	12.4
tricine-buffer / mL	6	13.4
glycerol 86 % / mL		6.2
TEMED / µL	30	30
APS 10 % / µL	300	300

Before the samples were loaded on the SDS gels they were incubated with Laemmli sample buffer and boiled at 96 ℃ for 5 min. The electrophoresis was performed in the anode/cathode buffers for 45-60 min at 160 V. Subsequently, the gels were stained with coomassie staining solution for approximately 30 min and then destained with coomassie destaining solution.

3.2.5 Analysis of protein expression by immunoblotting

In order to control the expression of the mCherry-Lip_{fl} and pEGFP-RhoA Q63L constructs in N2a and HeLa cells, the cells were seeded in 6-well plates and transfected the next day (3.7.2). After 18 h the cells were lyzed in 50 µL RIPA buffer per well and incubated with Laemmli sample buffer. Of these, 15 µg were used for the SDS-PAGE. Proteins were transferred onto a methanol-activated PVDF membrane (GE Healthcare) by semidry electrotransfer for 45 min at 150 mA in transfer buffer. The membrane was blocked in 5 % (w/v) milk powder in PBS-T for 60 min at RT. Primary antibodies were diluted in 3 % (w/v) milk powder in PBS-T according to Table 3.1.7 and used for incubation at 4 ℃ O/N. The next day, the membrane was washed three times with PBS-T for 10 min and subsequently incubated with the corresponding secondary HRP-coupled antibody, which was also diluted in 3 % (w/v) milk powder in PBS-T. The secondary antibodies were incubated for 60 min at RT and thereafter the membrane was washed three times with PBS-T for 10 min. Signal development was induced with Roti®-Lumin (Roth) in the darkroom.

Stripping of the membrane for detection with additional antibodies was accomplished by incubation and careful heating with the mild stripping buffer for 2 x 10 min. After three following washing steps with PBS-T for 10 min the membrane was again blocked with 5 % (w/v) milk powder in PBS-T for 60 min and incubated with another primary antibody. Successful stripping of the membrane was controlled by incubation with Roti®-Lumin (Roth) after the first washing step.

3.2.6 Peptide synthesis

All synthesized peptides used in this study were kindly provided by the group of Ines Neundorf according to the protocol described in Brenig *et al.* (2015). The following peptides were synthesized and finally used.

label	**amino acid sequence**	**molecular weight**
$Lip_{567–587}$	TPRSARLERMAQALALQAGSP	2223.6 Da
$Lip_{567–587}$ T567E	EPRSARLERMAQALALQAGSP	2251.61 Da
F-$Lip_{567–587}$	CF-GSGTPRSARLERMAQALALQAGSP	2784.11 Da
F-$Lip_{567–582}$	CF-GSGTPRSARLERMAQALAL	2343.65 Da

3.3. *E.coli* transformation and cryopreservation

3.3.1 Preparation of competent *E.coli* cells

Preparation of chemically competent *E. coli* strains was accomplished with the $CaCl_2$-method (Mandel & Higa, 1970). As the first step 400 mL LB medium, inoculated with 5 mL of a preculture, was grown to $OD_{600} = 0.3$. The cells were pelleted for 10 min at 500 x *g* and resuspended in 25 mL of an ice-cold and sterile 0.1 M $CaCl_2$ solution. After incubation for 20 min on ice the cells were again centrifuged for 10 min at 500 x *g* . This time the cells were resuspended in 2 ml ice-cold 0.1 M $CaCl_2$ solution supplemented with 15 % glycerol. Samples were divided in 200 µL aliquots, flash frozen in liquid N_2 and stored at -80 ℃.

3.3.2 Transformation

For cloning strategies *E. coli* DH5α cells were transformed, for protein expression BL21 (DE3) were used. Of these cells 100 µL were incubated with 50 ng Plasmid-DNA, or 10 µL ligation sample, respectively. The samples were chilled on ice for 30 min and subsequently heatshocked at 42 ℃ for 2 min. Afterwards the cells recovered for

45 min at 37 °C. Eventually, they were pelleted and plated on agar plates with the corresponding selection antibiotic.

3.3.3 *E. coli* cryopreservation

The agar plates with the grown *E. coli* cells were used for short-term storage of 1–2 weeks at 4 °C. For long-term storage 700 µL of the *E. coli* strains were supplemented with 300 µL glycerine (86 %) and stored in CryoTubes™ (Sigma-Aldrich) at -80 °C.

3.4. Protein Purification

3.4.1 Expression of recombinant proteins

Up to five colonies from the agar plate were picked and used to inoculate 200 mL pre-culture LB-medium. These cultures were grown at 37 °C, 140 rpm O/N. The final 10 L expression culture with LB-medium was inoculated 1:100 with the pre-culture and cultivated at 37 °C, 160 rpm until an optical density at 600 nm (OD_{600}) of 0.6–0.8 was reached. At this point the protein expression was induced by addition of 200 µM isopropyl-β-D-thiogalactopyranoside (IPTG). The induced cultures were grown O/N at 18 °C. The next day the *E. coli* cells were pelleted at 4000 x *g* for 20 min, resuspended in 100-150 mL protein buffer and stored at -80 °C.

3.4.2 Cell lysis

The *E. coli* cells were lyzed by sonication using a Branson Sonifier 250. Therefore, the thawed pellets were sonicated 3 x 2 min with 60 % duty cycle and a micro tip limit of 8. Afterwards, the lysate was centrifuged at 50 000 x *g* for 45 min at 4 °C to separate the cell debris from soluble protein.

3.4.3 Affinity purification

For all proteins used in this study GST-affinity purification was performed as initial step. At first the column packed with approximately 40 mL of PureCube Glutathion Agarose (Cube Biotech) was equilibrated with protein buffer. The equilibrated beads were then loaded with the cleared protein lysate and the flowthrough was collected. In order to get rid of non-specifically bound protein the column was washed with 5–10 column volumes (CV) protein wash buffer. Prior to the TEV-cleavage the buffer

was again exchanged to protein buffer. Once the TEV-protease was added, the buffer circulation was started and continued at 4 ℃ O/N. The protein was eluted the next day. Since the TEV-protease was obtained by Ni-affinity purification the unwanted protein could be removed with Ni-Sepharose 6 Fast Flow columns (GE healthcare). The euluted protein was concentrated using ultrafiltration with AmiconUltra centrifugal devices with the adequate pore size (molecular weight cut-off of 3, 10 or 30 kDa). If the following size exclusion chromatography was not performed the same day, the proteins were flash frozen and stored at -80 ℃.

Column material regeneration

The GSH-column was rinsed with 2 CV GSH elution buffer, to remove the still bound GST from the beads. A sample of this elution was taken to control the GST expression by SDS-PAGE. Afterwards the column was washed with 2-3 CV water, before 2 CV of 6 M guanidinium hydrochloride was added. At the end the column was washed again with 5 CV water.

3.4.4 Size exclusion chromatography

Following the affinity purification the proteins were further purified by size exclusion chromatography (SEC). Thereby, possible existing impurities could be removed and a proper folding of the protein was guaranteed. The size exclusion chromatographies were performed with the ÄKTApurifier system (GE healthcare) and a set of Superdex S75 and S200 columns. This system allows the protein elution at a constant flow and pressure, as well as the monitoring of absorption at 220 nm and 280 nm. For each run 2 mL of the protein sample were loaded and eluted with protein buffer in 2–4 mL fractions. The eluted fractions were tested via SDS-PAGE and the fractions showing high purity were pooled, concentrated, flash frozen and finally stored at -80 ℃.

Analytical size exclusion chromatography

Besides the purification of proteins size exclusion chromatography can be used to get a hint of the molecular size and oligomeric state of proteins. For this purpose 100 µL of each sample was loaded onto either a Superdex S75 10/300 or Superdex S200 10/300 column and eluted with protein buffer at a flowrate of 0.5 mL/min. The Superdex S75 column was calibrated with Aprotinin (6.5 kDa), Ribonuclease A (13.7 kDa), Carbonic Anhydrase (29 kDa), Ovalbumin (43 kDa) and Conalbumin (75 kDa). Additionally, Aldolase (158 kDa), Ferritin (440 kDa) and Tyhroglobulin (669 kDa) were used for the S200 column.

3.4.5 Determination of protein concentration

The protein concentration was determined by measuring the absorption at 280 nm. Using the Lambert-Beer law the concentration can be calculated as indicated.

$$A = \epsilon * c * l \tag{3.1}$$

with the absorbance A, absorption coefficient ϵ ($M^{-1}\,cm^{-1}$), the concentration c (M) and the cell path length l (cm). The applied extinction coefficients for the mDia1 and Liprin-α3 fragments are summarized in Table 4.1.

In case of the protein RhoA another method was used due to the additional absorption of the bound nucleotide at 280 nm. The concentration of RhoA was determined with the BradfordUltra assay (Expedeon) measuring the reaction of the amino acid side chains with Coomassie brilliant blue G-250 at 595 nm. Bovine serum albumin (BSA) was used for the calculation of a standard curve.

3.4.6 Nucleotide exchange on RhoA

The bound nucleotide of RhoA was exchanged to 2‘/3‘-O-(N-Methylanthraniloyl)-GppNHp (mant-GppNHp, Jena Bioscience) (Figure 3.1). Fluorescence of this non-hydrolyzable nuleotide can be excited at 355 nm and detected at 448 nm.

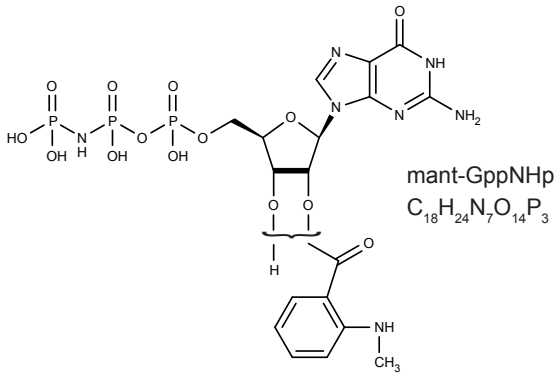

Figure 3.1 Structure of 2‘/3‘-O-(N-Methylanthraniloyl)-GppNHp.

For the nucleotide exchange 500 µL with 2 mg/mL of purified RhoA were incubated with a fourfold molar excess of mant-GppNHp and 1 µL of calf intestinal phosphatase (CIP, New England Biolabs®) at 4 ℃ O/N. The EDTA in the exchange buffer binds the Mg^{2+} Ions, that are needed for the high affinity binding of small GTPases to GTP and GDP. Furthermore, GTP and GDP are removed from the exchange equilibrium due to

CIP induced hydrolysis. Analytical size exclusion chromatography with protein buffer was used to remove the excess of unbound mant-GppNHp, and CIP. Additionally, the nucleotide bound state was stabilized by the $MgCl_2$ in the buffer. The obtained RhoA • mant-GppNHp was aliquoted, flash frozen and stored at -80 ℃ for stopped-flow fluorescence spectroscopy assays.

3.5. Biophysical Methods

3.5.1 Isothermal Titration Calorimetry

The protein-protein interactions were characterized by isothermal titration calorimetry (ITC). A simple binding reaction of two components A and B can be described as:

$$A + B \rightleftharpoons AB \tag{3.2}$$

The association constant (K_A) is defined as:

$$K_A = \frac{[AB]}{[A][B]} \tag{3.3}$$

Additionally, K_A is connected to the Gibbs free energy ΔG.

$$\Delta G = -RTlnK_A = \Delta H - T\Delta S \tag{3.4}$$

with the Gibbs free energy ΔG, the ideal gas constant R, the absolute temperature T, the equilibrium association constant K_A, the reaction enthalpy ΔH and the reaction entropy ΔS.

Every reaction is associated with a change in the reaction enthalpy and this change can be measured indirectly. The binding ligand A is titrated step-wise to the reaction partner B inside the measurement cell. Thereby, heat is either released (negative ΔH, exothermic) or absorbed (positive ΔH, endothermic). The instrument determines the energy that is needed to keep the temperature difference between the measurement cell and the reference cell, filled with water at the exact same level (isothermal). This supplied heat is integrated and plotted against the increasing concentration of A against B. Fitting with a one-side model of these data results directly in the equilibrium association constant (K_A), stoichiometry (N) and reaction enthalpy (ΔH) of the investigated binding. The Gibbs free energy (ΔG) and the reaction entropy (ΔS) can be derived from the equation 3.4.

For this study an ITC_{200} (GE healthcare) was used. All measurements were performed at 20 ℃. Since, this method is highly sensitive, even small differences in the protein buffers can lead to dilution heat signals. Therefore, all proteins used were purified in the same buffer. In each experiment 2–3 µL of protein in the syringe was step-wise titrated to the protein inside the measurement cell. Typically, the concentration in the syringe was between 200–500 µL and ten fold increased compared to the protein inside the cell (20–50 µL). A spacing of 120 sec between the injections was set with an initial delay of another 120 sec. The differential power (DP) of six was initialized at the beginning. Standard EDTA-$CaCl_2$ sample tests were used to assess the statistical significance of our observations, as described by MicroCal. The obtained values were within the manufactures tolerance with ± 20 % for the K_A and ± 10 % for ΔH.

The data analysis was performed with the software provided by the manufacturer (MicroCAL Origin version 7.0).

ITC competition assays

In the case of the ITC competition assays an initial complex was preformed in an ITC experiment. Therefore a tenfold molar excess of the ligand A was titrated to the protein B in the sample cell. This resulted in saturated complexes with a twofold molar excess of the ligand inside the sample cell. Abundant solution was removed from the cell and the third binding partner C was added to the complex with a tenfold molar excess.

3.5.2 Fluorescence polarization assay

Fluorescence polarization assays were used to determine whether mDia1, RhoA and Liprin-α3 can form ternary complexes. The method is based on the observation that a fluorophore, which is exited with polarized light, will emit polarized light (Perrin, 1926). However, this is only the case for stationary molecules. A rotating and moving molecule in solution will emit light that is largely depolarized and in a different plane from the excitation light. The actual polarization of a fluorophore is thereby proportional to the rotation, which in turn depends on the absolute temperature, viscosity and for this purpose most important the molecular volume. A small molecule in solution has a higher degree of movement and rotation and thus a high amount of depolarized emitted light. Accordingly, in case of larger molecules the emitted light remains polarized to a higher degree.

Using a Paradigm Detection Platform (Beckman Coulter) with a detection cartridge for fluorescein, the fluorophore was excited with polarized light and the emitted light was monitored in the vertical and horizontal plane. The polarization signal is defined as:

$$P = \frac{I_{\parallel} - I_{\perp}}{I_{\parallel} + I_{\perp}} \tag{3.5}$$

with:
$I_{\parallel}$: Intensities with parallel polarizers
$I_{\perp}$: Intensities with perpendicular polarizers

The small Liprin-α3 fragments $Lip_{567–582}$ and $Lip_{567–587}$ were N-terminally labeled with 5,6-carboxyfluorescein (CF). The fluorophore was excited at 485 nm and the emission was detected at 535 nm. Blank measurements were performed with Liprin-α3 fragments without the fluorophore. Each experiment was performed at 37 ℃ in protein buffer with an integration time of 500 ms. The first measurement was performed with 100 nM of each single Liprin-α3 fragments. In the second step 10 µM of mDia1 and in the third step additional 15 µM of RhoA Q63L were added. The solutions were incubated until a stable polarization signal was reached. Data analysis was done with GraphPad Prism 6.0 and each condition was measured independently three times.

3.5.3 Stopped-flow fluorescence spectroscopy

Stopped-flow fluorescence spectroscopy allows the analysis of fast interaction kinetics. Thereby, the change of fluorescence signals is measured in a microsecond time-scale, with a dead time of approximately 2-3 ms. The reaction partner are loaded into two drive syringes. They are forced by a drive ram through a mixing chamber into the observation cell. Simultaneously, this flow leads to a filling of the stop syringe, adjacent to the observation cell. The flow is interrupted once the pistol of the stop syringe hits the trigger switch, which is also the trigger of the data acquisition. Using this method the association and dissociation rate constants (k_{on}, k_{off}) of two reaction partners can be determined. They are defined as:

$$A + B \underset{k_{off}}{\overset{k_{on}}{\rightleftharpoons}} AB \tag{3.6}$$

Thus resulting in the rate of the complex formation of A and B:

$$\frac{d[AB]}{dt} = k_{on}[A][B] - k_{off}[AB] \tag{3.7}$$

In a typical conducted stopped-flow experiment one reaction partner is used in a much higher molar concentration than the other one. As a result, the concentration can be assumed to be constant, leading to pseudo-first order reaction. The second-order reaction kinetic $v = k[A][B]$ can, hence, be simplified to $v = k_{obs}[B]$, resulting in

$$\frac{d[AB]}{dt} = k_{obs}[B] - k_{off}[AB] \tag{3.8}$$

with $k_{obs} = k_{on}[A]$. The solution of the differential equation is given by

$$[AB] = \frac{k_{obs}[B]_0}{k_{obs} + k_{off}} - \frac{k_{obs}[B]_0}{k_{obs} + k_{off}} * e^{-t(k_{obs}+k_{off})} \tag{3.9}$$

with $[B]_0$: the concentration of B at time point zero

The changes in the fluorescence signal were plotted against the time and exponentially fitted, which resulted in k_{obs}. Due to the assumption of a pseudo-first order reaction it can be further simplified to:

$$k_{obs} = k_{on}[A] + k_{off} \tag{3.10}$$

The values of k_{obs} were plotted against the concentration of A and a linear fit was applied, leading to k_{on}. Furthermore, k_{off} can be obtained from the y-intercept. However, the k_{off} determined this way are often not precise and were therefore calculated from separate experiments. A complex of A and the fluorescently labeled binding partner B was preformed and titrated with a high molar excess of non-labeled protein B. The dissociation of the labeled protein was measured and single-exponentially fitted.

In this study the experiments were performed at 20 ℃ using a SX20 Applied Photophysics spectrometer (Leatherhead). The mantGppNHp nucleotide, which was bound to RhoA (3.4.6), was excited at 350 nm and the emission was recorded using a 420 nm cut-off filter. In order to determine the association rate constant 250 nM of RhoA • mant-GppNHp were titrated with increasing $mDia_N$ concentration (0.6–40.7 µM). The effect of Liprin-α3 on the binding kinetics was analyzed by adding a twofold molar excess of different fragments to the $mDia_N$. For the dissociation rate constant a 100 nM complex of $mDia_N$ • RhoA • mant-GppNHp was mixed with 10 µM constitutively active unlabeled RhoA Q63L in presence or absence of 10 µM Liprin-α3. Data analysis was done with GraphPad Prism 6.0.

3.6. Protein structure determination

3.6.1 Crystallization

The crystallization of proteins is a crucial step in the protein structure determination by X-rays. This is most commonly achieved by a gradually decrease of the protein solubility. As depicted in Figure 3.2 a higher saturated state can be reached by either increasing the protein concentration or the precipitant concentration. However, protein precipitation can occur if this transition happens too fast. Only in a certain cases it will lead to nucleation of crystalline structures, that may be followed by further growth up to three-dimensional crystals suitable for X-ray crystallography. Consequently, the formation of proper crystals depends on the protein concentration, as well as the pH value, ionic strength, composition of the precipitant and the temperature.

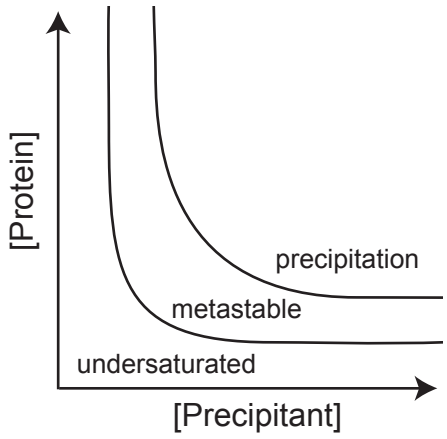

Figure 3.2 Crystallization phase diagram.
Simplified two-dimensional phase diagram depicting the importance of the protein concentration and precipitant.

Frequently used methods to obtain protein crystals are vapor diffusion crystallization (sitting drop, hanging drop) and crystallization by dialysis. In this study sitting drop vapor diffusion crystallization was used. Complexes with 5–10 mg/mL mDia1 with a fivefold molar excess of Liprin-α3 were preformed and 150 nL of this protein solution were mixed with 150 nL reservoir solution (Mosquito, TTPLabtech). The different complexes used for the crystallization attempts are collected in Table 3.7 and the tested crystallization screens are shown in Table 3.1.6.

Table 3.7 mDia1 • Liprin-α3 complexes used for crystallization screens.

mDia1	Liprin-α3	concentration of mDia1
$mDia_{135\text{-}570}$	$Lip_{532\text{-}587}$	10 mg/mL
$mDia_{135\text{-}570}$	$Lip_{491\text{-}587}$	10 mg/mL
$mDia_{79\text{-}369}$	$Lip_{561\text{-}587}$	10 mg/mL
$mDia_{79\text{-}369}$	$Lip_{567\text{-}587}$	10 mg/mL
$mDia_{79\text{-}435}$	$Lip_{567\text{-}587}$	10 mg/mL
$mDia_{79\text{-}443}$	$Lip_{567\text{-}587}$	10 mg/mL
$mDia_{135\text{-}443}$	$Lip_{567\text{-}587}$	10 mg/mL
$mDia_{135\text{-}435}$	$Lip_{567\text{-}587}$	10 mg/mL
$mDia_{135\text{-}369}$	$Lip_{532\text{-}587}$	10 mg/mL
$mDia_{135\text{-}369}$	$Lip_{567\text{-}587}$	10 mg/mL
$mDia_{135\text{-}369}$	$Lip_{567\text{-}587}$	15 mg/mL
$mDia_{135\text{-}369}$	$Lip_{561\text{-}587}$	10 mg/mL
$mDia_{135\text{-}369}$ (brown color)	$Lip_{567\text{-}587}$	10 mg/mL

Some of these tested conditions resulted in crystal formation of needle like structures, that were not suitable for X-ray analysis. In these cases the commercial screening solution was further varied, regarding pH or precipitant, in up-scaled hanging-drop vapor diffusion crystallization screens using 1 µL of the protein complex and 1 µL of the reservoir solution. However, no optimization in crystal formation could be observed. Finally, the crystals obtained from the $mDia_{135\text{-}369}$ (brown color) • $Lip_{567\text{-}587}$ were fished with a 0.05-0.1 mm loop and prepared for cryoprotection.

Cryoprotection

To ensure long-term storage and a higher degree of stability during the measurement, the protein crystals are flash frozen. Therefore, the crystals need to be in a cryogenic solution. This was achieved by transferring the crystals into the same solution with additional 30 % (w/v) of D-glucose as cryoprotectant. Afterwards they were flash frozen and stored in liquid N_2.

3.6.2 Data collection and processing

Data collection was performed at the Swiss Light Source (SLS), Paul Scherrer Institute in Villigen, Switzerland. The crystal was mounted on the goniometer head and orientated in the beamline X06DA. Finally, a dataset was collected at a wavelength

of 1.0 Å at 100 K. A Dectris Pilatus 2M detector was in a distance of 165 mm and the crystal rotated 0.1 ° for 1800 frames.

Further data processing was done with the program suite Ccp4 (Bailey, 1994). Mosflm 7.0.9 was used for the data indexing and integration. Scaling was performed with SCALA 3.3.20 (Evans, 2006; Leslie & Powell, 2007; Steller *et al.*, 1997). The quality of the data was judged by the completeness of the collected reflexes, redundancy, the signal to noise ratio of $I/\sigma I$ and data resolution. Additionally, the data were evaluated by R_{sym}:

$$R_{sym} = \frac{\sum_{hkl} \sum_{i=1}^{N} |I_{i,hkl} - \langle I_{i,hkl} \rangle|}{\sum_{hkl} \sum_{i=1}^{N} I_{i,hkl}} \tag{3.11}$$

with the reflex intensities I and miller indices hkl.

Phase determination

The electron density as function of position x,y,z can be expressed as the Fourier transformation of the structure factors F_{hkl}:

$$p(xyz) = \frac{1}{V} \sum_{hkl} F_{hkl} \, \mathrm{e}^{-2\pi i(hx+ky+lz)} \tag{3.12}$$

Separating the structure factor F_{hkl} into its amplitude $|F_{hkl}|$ and the phase of the diffracted beams α_{hkl} results in:

$$p(xyz) = \frac{1}{V} \sum_{hkl} |F_{hkl}| \, \mathrm{e}^{-2\pi i(hx+ky+lz)+i\alpha_{hkl}} \tag{3.13}$$

This elucidates the importance of the structure factor amplitudes, as well as the corresponding phases. Each reflex of the diffraction pattern corresponds to a wave with a specific amplitude and phase. However, while the amplitude can be calculated from the collected intensity, no information about the phase can be obtained. The loss of information is also termed as the phase problem. In this study molecular replacement was used as one possible solution to overcome this problem. It can be assumed that in a complex the $\mathrm{mDia_{DID}}$ has a much higher impact on the diffraction pattern than the Liprin-α3 fragment $\mathrm{Lip_{567\text{-}587}}$. Therefore, the residues 135–369 of chain B of the $\mathrm{mDia_N} \bullet$ RhoC structure (PDB: 1Z2C) were suitable for the program Phaser,

performing a search for two molecules per asymmetric unit (McCoy *et al.*, 2007). Using translation and rotation events an approximation of the unknown phases was possible.

3.6.3 Model building and refinement

The program Coot 0.7.1 was used to build the model into the $2F_o - F_c$ (countered at $1.0\,\sigma$) and $F_o - F_c$ (countered at $3.0\,\sigma$) electron density maps in iterative rounds of refinement (Emsley & Cowtan, 2004). After the initial phasing and model building, refinements are mandatory to improve the geometry of the model and the approximation of the phases. Through statistical adjustment of the atomic coordinates, the refinement leads to a higher accordance with the diffraction data. Based on the refinement, new amplitudes and phases are calculated for the structure factor F_{hkl}. Quality of the refinement can be estimated by R_{work}. This value describes the difference between the calculated amplitudes from the structure F_{calc} and the observed amplitudes F_{obs}.

$$R_{work} = \frac{\sum \big||F_{obs}| - |F_{calc}|\big|}{|\sum F_{obs}|} \tag{3.14}$$

Notably, possible model bias can occur, since incorrect build areas of the atomic model are also used to calculate the new structure factors. For this reason 5–10 % of the reflections are excluded from the refinement and used for the calculation of R_{free}, in analog to R_{work} (Brunger, 1992).

In this study the refinement was conducted with REFMAC5 (Murshudov *et al.*, 1997) and evaluated using MolProbity (Davis *et al.*, 2007). All structure figures presented here were made with PyMOL 1.6.9.0 (DeLano, 2002).

3.7. Immunocytochemistry

3.7.1 Cell cultivation

HeLa cells were grown in DMEM (Gibco) and N2a cells 1:1 DMEM/OptiMEM (Gibco). Both media were supplemented with 10 % (v/v) fetal calf serum (FCS, PAN Biotech), 100 U/mL penicillin (Gibco) and 100 U/mL streptomycin (Gibco) and 1 % non-essential amino acids (Gibco) at 37 ℃ with 5 % CO_2. At a confluency of more than 70 % the cells were trypsinated (0.25 % trypsin-EDTA, Sigma) and splitted. Long term storage was performed at -80 ℃ in cell culture medium supplemented with 10 % (v/v) DMSO.

3.7.2 Cell transfection and staining

Prior to the transfection 0.4×10^5 HeLa cells/mL and 0.5×10^5 N2a cells/mL were seeded on cover glasses in 24-well plates and cultured in 1 mL medium for 24 h. For the overexpression experiments 0.5 µg of each plasmid DNA was mixed together with 1 µL Plus Reagent™ in 100 µL Opti-MEM and incubated for 25 min. Finally, 1.5 µL Lipofectamine® LTX (Invitrogen) was added for another 5 min incubation time, before the mixture was pipetted to the cells. After 18 h the cells were washed with ice cold PBS and fixed with 3 % paraformaldehyde for 20 min. Before the cells were permeabilized with 0.5 % Triton X-100 for 15 min, they were washed again three times. Blocking of unspecific binding was accomplished with 3 % BSA in PBS for 60 min. Subsequently, the cell nuclei were stained with DAPI (1:20000, Santa Cruz Biotechnology) and staining of filamentous actin was done with CF647-phalloidin (1:60, Biotium). Three washing steps later, the cover slips were embedded in ProLong® Gold Antifade Reagent (Invitrogen) for 24 h. At the end, the cover slips were sealed with nail polish and stored in the dark.

3.7.3 Microscopy and quantification

The immunofluorescence images were taken with an UltraView VoX, PerkinElmer Life Sciences spinning disc confocal microscope. For data processing and quantification the software ImageJ (National Institutes of Health) was used. In the first step, the maximum Z-stack projection of the images was calculated before the CF647 intensity of each cell was quantified. Normalization was done to non-transfected cells under the same conditions. The mock transfected cells served as a reference to analyze the effect of RhoA G14V and Liprin-α3 overexpression. At least 20 cells for each construct were used for the analysis and each construct was tested at least two times. GraphPad Prism 6.0 was used for statistical analysis.

4. Results

The binding of Liprin-α3 to mDia1 has been firstly described by Sakamoto *et al.* (2012a). They narrowed down the binding sites to the amino acids 457–737 of Liprin-α3 and the amino acids 135–570 of mDia1. In their work it was further concluded that the binding of Liprin-α3 to mDia1 interferes with the binding of RhoA to mDia1. Yet, the mechanisms how Liprin-α3 exerts its effect leading to a reduction in cellular F-actin remains elusive. As a first step of this work the binding sites were narrowed down. Using these minimal mDia1 and Liprin-α3 fragments their binding was thermodynamically, kinetically and structurally characterized, as well as the interplay of Liprin-α3 with RhoA and the autoinhibitory state of mDia1.

4.1. Definition of the interaction sites of mDia1 and Liprin-α3

4.1.1 Design and examination of soluble mDia1 and Liprin-α3 fragments

In order to find the regions, that are necessary and sufficient for the interaction of Liprin-α3 and mDia1, several constructs were cloned and purified. The different fragments are shown in Table 4.1 with the according remark if expression and purification was successful in regard of the quality and quantity of material, to perform biophysical studies including X-ray crystallography.

Table 4.1 Cloned and purified fragments of mDia1 and Liprin-α3.

protein	fragment aa	size kDa	extinction coefficient (ϵ) M^{-1} cm^{-1}	purification
mDia1				
	79–369	34	9970	+
	74–369	34	9970	
	69–369	35	9970	
	79–437	41	14440	
	79–435	41	14440	+
	79–443	42	14440	+
	74–443	43	14440	
	69–443	43	14440	
	69–435	42	14440	
	69–451	44	14440	+
	69–570	58	14440	+
	135–369	27	8480	+
	135–525	45	12950	
	135–570	50	12950	+
	135–500	42	14400	
	135–550	48	12950	
	135–475	39	12950	
	135–451	37	12950	+
	WW-1145–1200	7	11000	+
	WW-1145–1209	8	11000	+
Liprin-α3				
	20–587	64	23950	
	25–587	63	23950	
	77–587	57	23950	
	90–587	56	23950	
	110–587	53	23950	
	217–587	41	16960	+
	271–587	34	16960	+
	306–587	30	16960	+
	457–587	14	1490	+
	457–737	22	23490	+
	W-532–587	6	5500	+
	W-541–587	5	5500	+
	W-561–587	3	5500	+
	W-443–498	6	6990	
	W-443–491	6	5500	+
	W-491–560	7	6990	+
	W-541–571	5	5500	
	25–217	20	6990	
	25–817	88	70930	
	25–737	80	47440	
	W-561–581	3	5500	+
	W-561–582	3	5500	+
	1–737	82	47440	
	1–817	90	70930	

4.1.2 Purification of mDia1 and Liprin-α3 peptides

For each fragment the purification process was performed according to the work-flow shown in Figure 4.1 A. The genes on the cloned pGEX4T5-TEV plasmids encoding for the proteins were expressed in *E. coli* BL21 (DE3) cells after induction with IPTG. After sonication the lysates were loaded onto a GSH-affinity chromatography column and washed prior to TEV-cleavage over night (O/N). Finally, the samples were concentrated and further purified using size exclusion chromatography (SEC), frozen in liquid N_2 and stored at -80 ℃. As an example the affinity purification of the $mDia_N\Delta GCC$ fragment (aa 135–570) is shown (Figure 4.1 B). The protein expression, as well as the TEV-cleavage have been controlled by SDS-PAGE. The overexpressed GST-fusion-protein is visible as a dominant band at 76 kDa in the lysate after induction with IPTG (lane 2). This band is still present in the soluble fraction after sonication (lane 4). After the TEV-cleavage the fusion-protein is cleaved to yield the desired mDia1 protein with 50 kDa (lane 6) and the cleaved GST-tag with 26 kDa (lane 7). In the next purification step the protein was further separated from potential impurities by SEC. The first peak (void volume) contains impurities, that are either by themselves or due to aggregation, too large to enter the column pores. Purified and correctly folded proteins could be collected from the second elution peak (Figure 4.1 C).

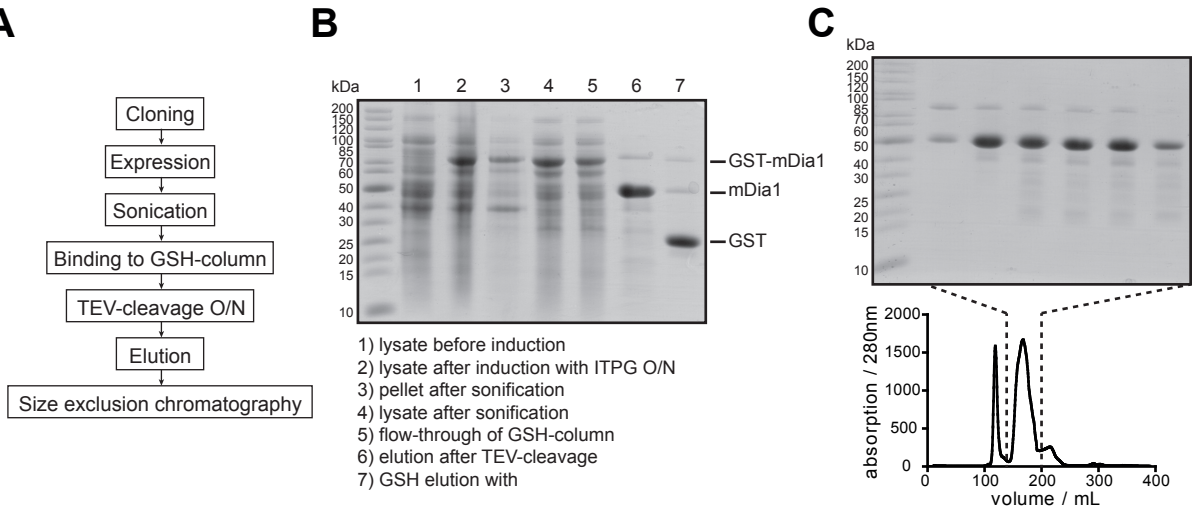

Figure 4.1 Example of the two-step purification protocol using affinity columns and size exclusion chromatography.
A: Work-flow of the different protein purification steps. B: GSH-column purification of $mDia_N\Delta GCC$. The figure shows the SDS-PAGE with the overexpression of the gene plasmid in *E. coli* BL21 (DE3) cells, the protein solubility after sonication and the successful TEV-cleavage. C: Size exclusion chromatography (S200, 26/60) of the concentrated protein following the GSH-purification. Elution of the protein was monitored using the absorption at 280 nm. Impurities and correct size of the protein fragment are controlled by SDS-PAGE.

The fragments that were finally used in this study to characterize the mDia1-Liprin-α3 binding are depicted in Figure 4.2. These fragments were expressed and purified to sufficient yields and to a high level of purity (Figure 4.3) and were thereby suitable for subsequent analyses.

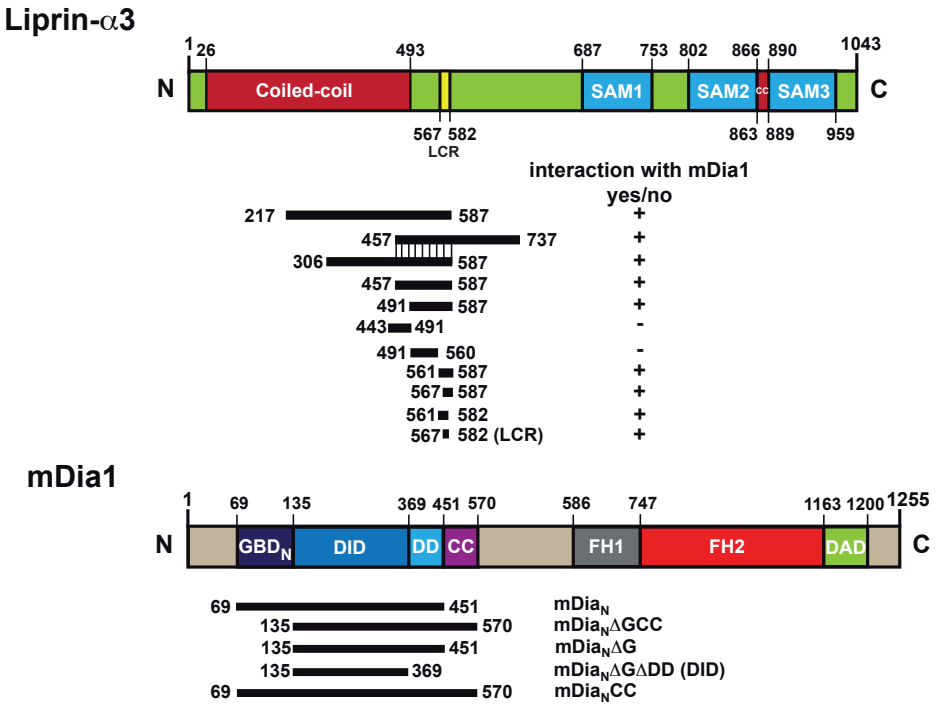

Figure 4.2 Overview of the mDia1 and Liprin-α3 domains and the used constructs. Illustrated are the different domains of mDia1 and mouse Liprin-α3 and the constructs that were used for the characterization of the protein interactions.

Quality control of the purified samples was performed by SDS-PAGE (Figure 4.3).

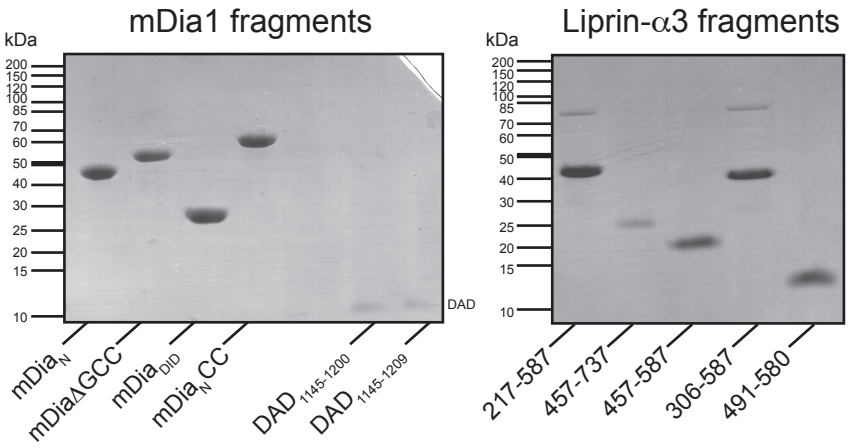

Figure 4.3 SDS-PAGE of the mDia1 and Liprin-α3 fragments used for further studies. Approximately 5 µg of each indicated protein was loaded per lane.

All fragments used for the definition of the binding site exhibit a high degree of purity. The samples show clear defined protein bands and a migration behavior according to their molecular weight.

4.1.3 Definition of the mDia1-lip binding site by isothermal titration calorimetry

Isothermal titration calorimetry (ITC) was used to define the minimal Liprin-α3 and mDia1 interaction sites. All measured combinations of Liprin-α3 and mDia1 fragments are collected in Table 4.2 and Figures A.3 to A.5. Sakamoto *et al.* restricted the binding site in pull-down assays to the N-terminal coiled-coil of Liprin-α3 (aa 457–737, $Lip_{457–737}$) and the N-terminal region of mDia1 lacking the guanine-nucleotide binding domain (GBD_N) $mDia_N\Delta GCC$ (aa 135–570). These fragments bind in ITC measurements in an exothermic reaction with an affinity of 3.0 µM and a molar ratio of 1.0, indicating a 1:1 binding stoichiometry (N). A fragment containing GBD_N ($mDia_NCC$) showed no further increase of the binding affinity (5.9 µM, Figure 4.4 A), suggesting that this region is indeed not needed for the binding of Liprin-α3. The N-terminal elongated and C-terminal shortened Liprin-α3 fragment (aa 217–587, $Lip_{217–587}$) binds towards $mDia_N\Delta GCC$ and $mDia_NCC$ with a slightly decreased affinity of 13.5 µM and 13.6 µM, respectively and an N-value of 0.5. Binding stoichiometry and binding affinity could be restored by N-terminal deletion of the $Lip_{217–587}$ fragment, resulting in fragment $Lip_{306–587}$ with binding affinities towards different mDia1 fragments of 2.9–11.0 µM and N-values of 0.7–0.9. As a result, the overlapping region of $Lip_{306–587}$ and $Lip_{457–737}$, namely $Lip_{457–587}$ was purified and tested regarding its binding capacity towards mDia1. This fragment binds $mDia_N\Delta GCC$ with an affinity of 5.7 µM. Further C-terminally truncated fragments of Liprin-α3 spanning the residues 443–491 ($Lip_{443–491}$) and 491–560 ($Lip_{491–560}$) showed no binding in ITC measurements. Whereas the fragment $Lip_{561–587}$ (aa 561–587) still binds to $mDia_NCC$ with an affinity of 6.2 µM. Finally, the essential amino acids of Liprin-α3, needed for the mDia1 binding, could be narrowed down to the region 567–587 ($Lip_{567–587}$). This peptide was synthesized and exhibits a 4.4 µM binding affinity towards $mDia_N$, suggesting that this fragment contains all residues needed for mDia1 binding (Figure 4.4 B).

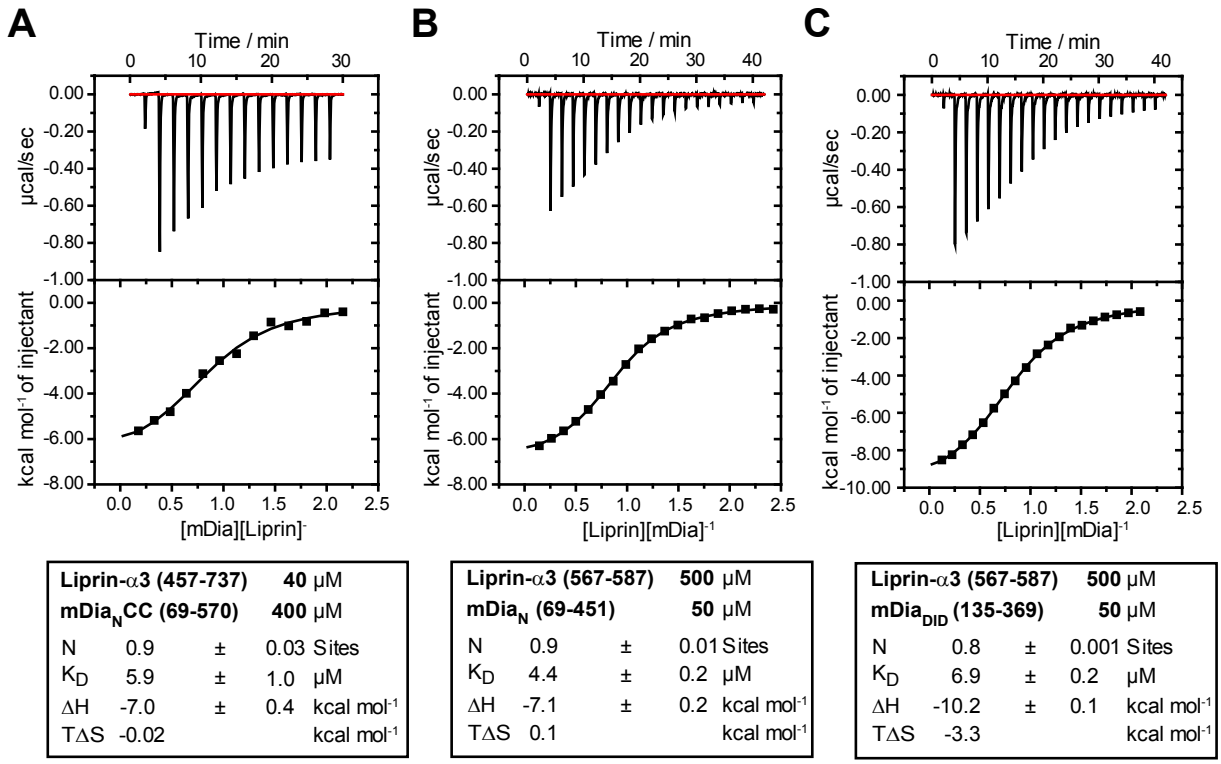

Figure 4.4 Determination of the Liprin-α3-mDia1 binding site by ITC.
ITC measurements of the depicted mDia1 and Liprin-α3 fragments at 20 °C in protein buffer. Shown are the interactions of A: $mDia_NCC$ (aa 69–570) with $Lip_{457–737}$, B: $mDia_N$ (aa 69–451) with $Lip_{567–587}$ and C: $mDia_{DID}$ (aa 135–369) with $Lip_{567–587}$. $Lip_{567–587}$ binds with a similar affinity to $mDia_{DID}$ as $Lip_{457–737}$ to $mDia_NCC$. (K_D: equilibrium dissociation constant; ΔH: change in reaction enthalpy; ΔS: change in reaction entropy; N: stoichiometry of binding; T: temperature in Kelvin)

The next aim was to further specify the binding area on the N-terminal mDia1 region. As indicated by Sakamoto *et al.* and confirmed by ITC analysis the GBD_N plays no direct role in Liprin-α3 binding and can therefore be excluded. Performing ITC measurements with the two shortest Liprin-α3 fragments ($Lip_{561–587}$ and $Lip_{567–587}$) showed that the mDia1 Diaphanous-inhibitory domain ($mDia_{DID}$, aa 135–369) contains all essential Liprin-α3 interaction residues. The determined binding affinities of $mDia_{DID}$ to $Lip_{561–587}$ and $Lip_{567–587}$ were 8.3 µM and 6.9 µM, respectively (Figure 4.4 C, Table 4.2).

In summary using ITC analyses the binding site of mDia1 and Liprin-α3 could be narrowed down to $mDia_{DID}$ and $Lip_{567–587}$ with a binding affinity of approx. 7 µM, showing an exothermic heat profile. Furthermore, all reactions were driven by favorable enthalpic interactions, while most of the reactions were also entropically favorable (Table 4.2).

Table 4.2 ITC measurements for the identification of the mDia1–Liprin binding-site. All ITC measurements were performed in protein buffer at 20 °C. The protein concentration in the cell (superscript: C) was between 30–50 µM, the concentration in the syringe (superscript: S) was between 300–500 µM. (K_D: equilibrium dissociation constant; ΔH: change in reaction enthalpy; ΔS: change in reaction entropy; N: stoichiometry of binding; T: temperature in Kelvin)

Interaction		K_D	ΔH	TΔS	N
		µM	*kcal mol^{-1}*	*kcal mol^{-1}*	
Liprin 217–587	$^{C}Lip_{217–587}$-$^{S}mDia_{DID}$	12.0 ±0.8	−8.3 ±0.6	−1.8	0.5
	$^{C}Lip_{217–587}$-$^{S}mDia_{N}$ΔGCC	13.6 ±1.1	−9.3 ±0.5	−2.8	0.5
	$^{C}Lip_{217–587}$-$^{S}mDia_{N}$CC	13.5 ±0.9	−6.6 ±0.3	−0.04	0.5
Liprin 306–587	$^{C}Lip_{306–587}$-$^{S}mDia_{N}$ΔGCC	2.9 ±0.2	−4.9 ±0.1	2.4	0.7
	$^{C}Lip_{306–587}$-$^{S}mDia_{N}$	8.0 ±0.8	−5.2 ±0.1	1.6	0.9
	$^{C}Lip_{306–587}$-$^{S}mDia_{N}$ΔG	11.0 ±0.9	−5.9 ±0.1	1.6	0.9
Liprin 457–587/737	$^{C}Lip_{457–737}$-$^{S}mDia_{N}$CC	5.9 ±1.0	−7.0 ±0.4	−0.02	0.9
	$^{C}Lip_{457–737}$-$^{S}mDia_{N}$ΔGCC	3.0 ±0.4	−5.1 ±0.2	2.3	1.0
	$^{C}Lip_{457–587}$-$^{S}mDia_{N}$CC	9.1 ±1.1	−4.6 ±0.1	2.2	0.6
	$^{C}Lip_{457–587}$-$^{S}mDia_{N}$ΔGCC	5.7 ±0.4	−4.3 ±0.2	0.8	0.8
	$^{C}Lip_{457–587}$-$^{S}mDia_{N}$	7.7 ±0.8	−3.8 ±0.2	3.1	0.8
	$^{C}Lip_{457–587}$-$^{S}mDia_{DID}$	9.9 ±0.3	−8.9 ±0.2	−2.2	0.6
Liprin 491–587	$^{C}Lip_{491–587}$-$^{S}mDia_{N}$ΔGCC	6.4 ±0.8	−5.6 ±0.3	1.4	0.8
Liprin 443–491	$^{C}Lip_{443–491}$-$^{S}mDia_{N}$	no binding			
Liprin 491–560	$^{C}Lip_{491–560}$-$^{S}mDia_{N}$	no binding			
Liprin 561/567–587	$^{C}Lip_{561–587}$-$^{S}mDia_{N}$CC	6.2 ±1.1	−4.2 ±0.3	2.7	1.1
	$^{S}Lip_{561–587}$-$^{C}mDia_{DID}$	8.3 ±0.5	−10.4 ±0.2	−3.6	0.9
	$^{S}Lip_{561–587}$-$^{C}mDia_{N}$	2.6 ±0.2	−7.1 ±0.1	0.4	0.9
	$^{S}Lip_{567–587}$-$^{C}mDia_{N}$	4.4 ±0.2	−7.1 ±0.2	0.1	0.9
	$^{S}Lip_{567–587}$-$^{C}mDia_{DID}$	6.9 ±0.2	−10.2 ±0.1	−3.3	0.8

4.1.4 Oligomeric states of Liprin-α3 and mDia1

The oligomeric state of a protein can have an impact on its biological function. Therefore, the purified mDia1 and Liprin-α3 fragments were analyzed by coiled-coil predictions and size exclusion chromatography (Figure 4.5).

As expected and supported by available structural data the coiled-coil predictions of mDia1 show the presence of putative coiled-coil regions spanning the residues 452–570, that are adjacent to the dimerization domain (Figure 4.5 A). Moreover, further coiled-coil regions are predicted to be localized near the C-terminus. Liprin-α3 has a high probability of N-terminal coiled-coil domains that are known to mediate homooligomerization (Serra-Pages *et al.*, 1998). The peptide $Lip_{457–737}$ defined by Sakamoto *et al.* is overlapping with these regions. However, in this study the essential binding region of Liprin-α3 could be narrowed down to the peptide $Lip_{567–587}$, which is not contributing to the formation of the predicted coiled-coils.

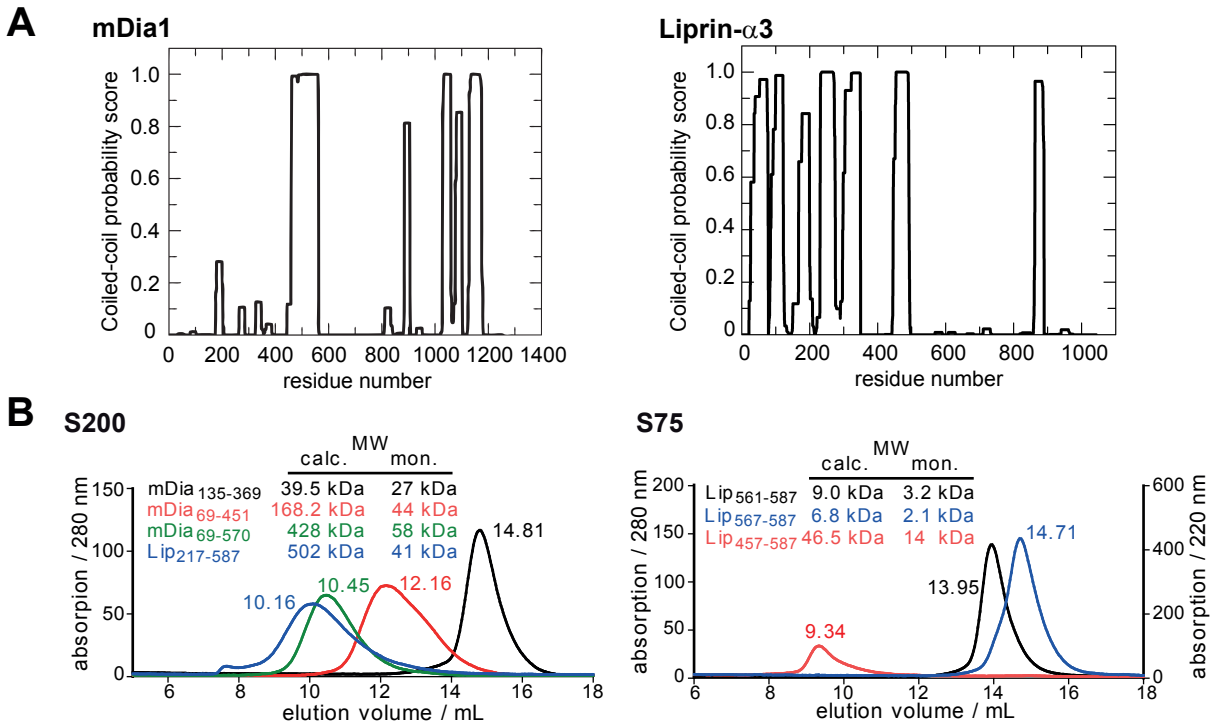

Figure 4.5 Coiled-coil predictions and oligomeric states of mDia1 and Liprin-α3 fragments. A: Coiled-coil predictions of mDia1 and Liprin-α3 calculated with COILS version 2.1 B. Different oligomeric states of the mDia1 and Liprin-α3 fragments as determined by size exclusion chromatography with 5 mg/mL protein in protein buffer using different columns (S75 10/300, S200 10/300). Elution was monitored by the absorption at 280 nm, except for the peptide $Lip_{567–587}$ which was monitored at 220 nm. The molecular weight (MW) of the fragments is shown as the calculated value from the calibrated column (calc.) and the predicted size for the respective monomers (mon.).

Additionally, the oligomeric states of the different mDia1 and Liprin-α3 fragments were determined and compared (Figure 4.5 B). To that end, the constructs that were used for the binding studies were analyzed by analytical size exclusion chromatography (SEC). Depending on the expected molecular weight of a monomer fragment (MW mon.) either a S75 10/300 or S200 10/300 column was used. The shortest mDia1 fragment, $mDia_{DID}$ (aa 135–369), lacking the dimerization domain elutes as an elongated monomer in solution. In comparison $mDia_N$ (aa 69–451) and $mDia_NCC$ (aa 69–570) seem to form higher oligomers, although structural data suggest the formation of elongated dimers. For the fragments $Lip_{561–587}$, $Lip_{567–587}$ and $Lip_{457–587}$ possible trimeric elution profiles could be observed. Whether these peptides form trimers or this running behavior is caused by a low content of secondary structure remains unclear from these data. Strikingly, however, is the tenfold increase of the calculated MW in the case of $Lip_{217–587}$. This fragment is overlapping with the predicted N-terminal coiled-coil region and seems to form a higher oligomer in solution, which would also be consistent with the reduced binding stoichiometry as shown by ITC.

4.2. Crystal structure of the mDia1 • Liprin-α3 complex

4.2.1 Crystallization attempts of different mDia1 • Liprin-α3 complexes

The first crystallization setups were performed using $Lip_{457–587}$ in complex with a variety of mDia1 fragments ($mDia_N\Delta GCC$, $mDia_N$, $mDia_{DID}$ and $mDia_{79–443}$). Since the extensive screenings did not lead to any successful protein crystal formation, smaller Liprin-α3 fragments were used, namely $Lip_{561–587}$ and the synthesized $Lip_{567–587}$. Although this did result in protein crystal formation (Figure 4.6 A,B), none of these needle shaped crystals could be further optimized to result in evaluable X-ray diffraction. Finally, using the fragments $Lip_{567–587}$ and $mDia_{DID}$ in complex with Ni^{2+}-Ions, led to suitable crystal formation (Figure 4.6 C). These crystals had a final size of approximately $50 * 50 * 20\,\mu M$. They were shock frozen in liquid nitrogen using 0.2 M sodium chloride, 0.1 M Tris pH 8.0, 20 % w/v PEG 6k containing 30 % (w/v) dextrose as cryoprotectant.

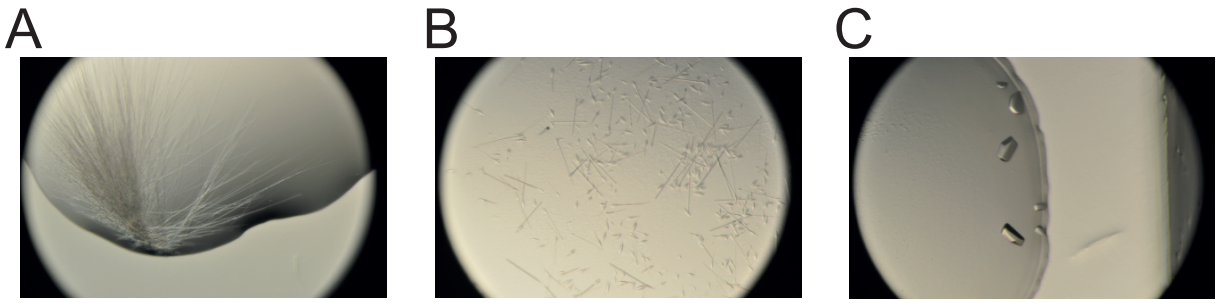

Figure 4.6 Protein crystals of Liprin-α3 • mDia1 complexes.
Shown are examples of the crystals that grew after 1–2 days under the listed condition of the respective screens. A: Protein crystals of $Lip_{567–587}$ • $mDia_{DID}$ grown in Pact A5 (0.2 M, lithium chloride 20 % w/v, PEG 6000, 0.1 M HEPES pH 7.0). B: Protein crystals of $Lip_{567–587}$ • $mDia_{79–443}$ grown in clear strategy I G6 (0.8 M sodium formate, 0.1 M Tris pH 8.5, 25 % w/v PEG 2k, monomethyl ether). C: Protein crystals of $Lip_{567–587}$ • $mDia_{DID}$ grown in pact premier C6 (0.2 M sodium chloride, 0.1 M Tris pH 8.0, 20 % w/v PEG 6k).

4.2.2 Data Collection and refinement

The atomic structure of the $mDia_{DID}$ • $Lip_{567–587}$ was solved up to a final resolution of 1.65 Å. The crystal contained two copies of $mDia_{DID}$ • $Lip_{567–587}$ per asymmetric unit and belonged to the space group C121. An overview of the obtained refinement and geometry validation is given in Table 4.3. Additional data concerning the geometry validation are shown in the appendix (Table A.1, Figure A.7).

Table 4.3 Data collection, refinement and structure validation of the $mDia_{DID}$ • $Lip_{567–587}$ structure.
The data collection and refinement statistics for the highest resolution shell are listed within the parenthesis. One single crystal was used for data collection.

	$mDia_{DID}$ • $Lip_{567–587}$
Data Collection	
Space group	C121
Cell dimensions	
α,β,γ (Å)	121.09, 49.38, 106.37
a,b,y	90.0, 97.86, 90.0
Resolution (Å)	32.30−1.65 (1.74−1.65)
R_{sym} or R_{merge}	0.066 (0.730)
$I/\sigma I$	9.4 (1.6)
Completeness (%)	99.7 (99.9)
Redundancy	3.1 (3.2)
Refinement	
Resolution (Å)	32.32 (1.65)
No. of reflections	71,251
R_{work} / R_{free}	17.55/ 21.01
No. of atoms	
Protein	3926
Ligand/ion	16
Water	394
B factors	
Protein	26.56
Ligand/ion	
Ni^{2+}	22.98
Tris	31.94
Water	35.62
Root mean square deviations	
Bond lengths (Å)	0.022
Bond angles (degrees)	2.007
Geometry	
Poor rotamers	0
Ramachandran	
Outliers (%)	0
Favored (%)	99.38 (480/483 aa)
Allowed (%)	100 (483/283 aa)
Cβ deviations > 0.25 Å	0
Clashscore[a]	2.39

[a] Clashscore is the number of serious steric overlaps (>0.4 Å) per 1000 atoms.

4.2.3 Structural analysis

The solved crystal structure of the $mDia_{DID}$ • $Lip_{567–587}$ complex is depicted in Figure 4.7 A. While the data resulted in well defined electron density for $mDia_{DID}$ only the N-terminal part of $Lip_{567–587}$ was visible. An example of the electron density for Liprin-α3 is shown in Figure 4.7 B, as difference omit map countered at 3σ. No electron density could be observed for the amino acids 583–587 of Liprin-α3.
Upon binding to $mDia_{DID}$, Liprin-α3 forms an α-helix spanning the amino acids 567–582. The binding occurs at the region of the armadillo repeat motifs (ARM) ARM3–5. Liprin-α3 contacts the third α-helices (α3) of the three α-helices containing ARMs, which form a concave surface for protein-protein interactions. Interestingly, the third α-helix of ARM5 is part of the interdomain helix (ID, α17, $\alpha3^5$), that connects the $mDia_{DID}$ with the dimerization domain (DD).

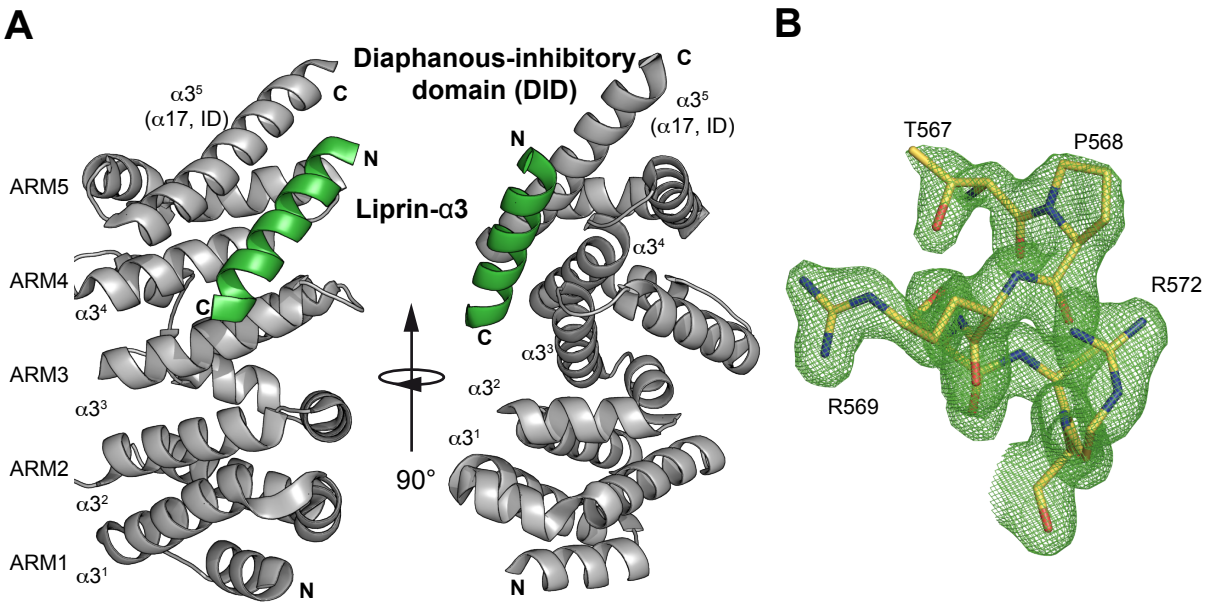

Figure 4.7 Crystal structure of the $mDia_{DID}$ • $Lip_{567–587}$ complex.
A: *Ribbon representation* of $mDia_{DID}$ (aa 135–369, chain A) and $Lip_{567–587}$ (visible aa 567–582, chain B) on the left and a 90 ° clockwise rotated view on the right side. $Lip_{561\text{-}582}$ binds to the armadillo repeats (ARM) 3–5 and interacts with the interdomain helix (ID). B: $F_0 - F_C$ difference omit map of the N-terminal part of $Lip_{567–587}$ covering residues threonine 567 to arginine 572 (chain D) countered at 3σ. The atomic coordinates and structure factors (code 4UWX) have been deposited in the Protein Data Bank (http://www.pdb.org/).

Since the C-terminal amino acids of the $Lip_{567–587}$ fragment were not visible in the crystal structure, additional peptides lacking these amino acids were purified and analyzed by ITC, regarding their capability to interact with $mDia_N$ (Figure 4.8).

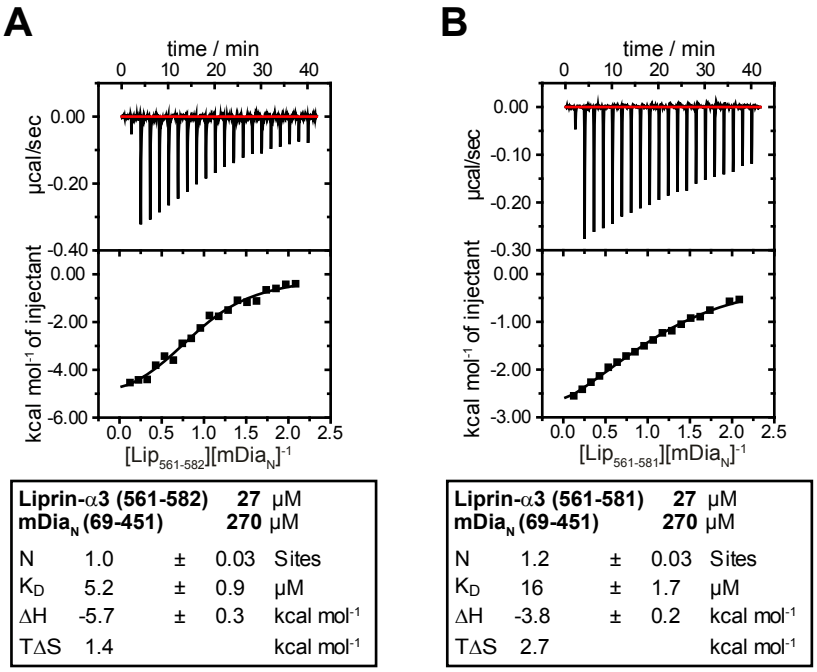

Figure 4.8 ITC measurements with Liprin-α3 fragments visible in the protein structure. ITC measurements of the purified Liprin-α3 fragments $Lip_{561–581}$ and $Lip_{561–582}$ together with $mDia_N$ at 20 ℃ in protein buffer. (K_D: equilibrium dissociation constant; ΔH: change in reaction enthalpy; ΔS: change in reaction entropy; N: stoichiometry of binding; T: temperature in Kelvin)

The fragment $Lip_{561–582}$ is still able to bind to $mDia_N$ with an affinity of 5.2 µM, which is similar to the binding affinity of the fragment $Lip_{567–587}$ (4.4 µM). However, deleting the leucine at position 582 reduces the affinity to 16 µM, indicating that the peptide $Lip_{567–582}$ contains all the essential amino acids needed for the binding of Liprin-α3 to mDia1 *in vitro*. A detailed overview of these interactions is shown in Figure 4.9.

Liprin-α3 binds to the armadillo repeat motifs (ARM) ARM3–5 of $mDia_{DID}$ and aligns in an antiparallel orientation to the interdomain helix (ID, α17, $\alpha3^5$) (Figure 4.9 A,B). Thereby, it makes extensive contacts towards the ID, predominantly forming electrostatic interactions. A salt bridge is formed between the R575 of Liprin-α3 ($R575^L$) and E358 of mDia1 ($E358^D$), that are within a distance of 2.5 Å. Furthermore, $R575^L$ forms a hydrogen bond with $C354^D$ also located on the ID. Additional salt bridges are formed between $R572^L$ and the $E358^D$ and 362^D (2.69 Å, 2.8 Å), thus tightly linking Liprin-α3 to the ID of $mDia_{DID}$. Besides the electrostatic interactions several hydrophobic interactions are involved, including $L573^L$, $M576^L$ and $L580^L$. An overview of all residues participating in the binding is shown in Figure 4.9 B. Based on these data mutational studies were performed.

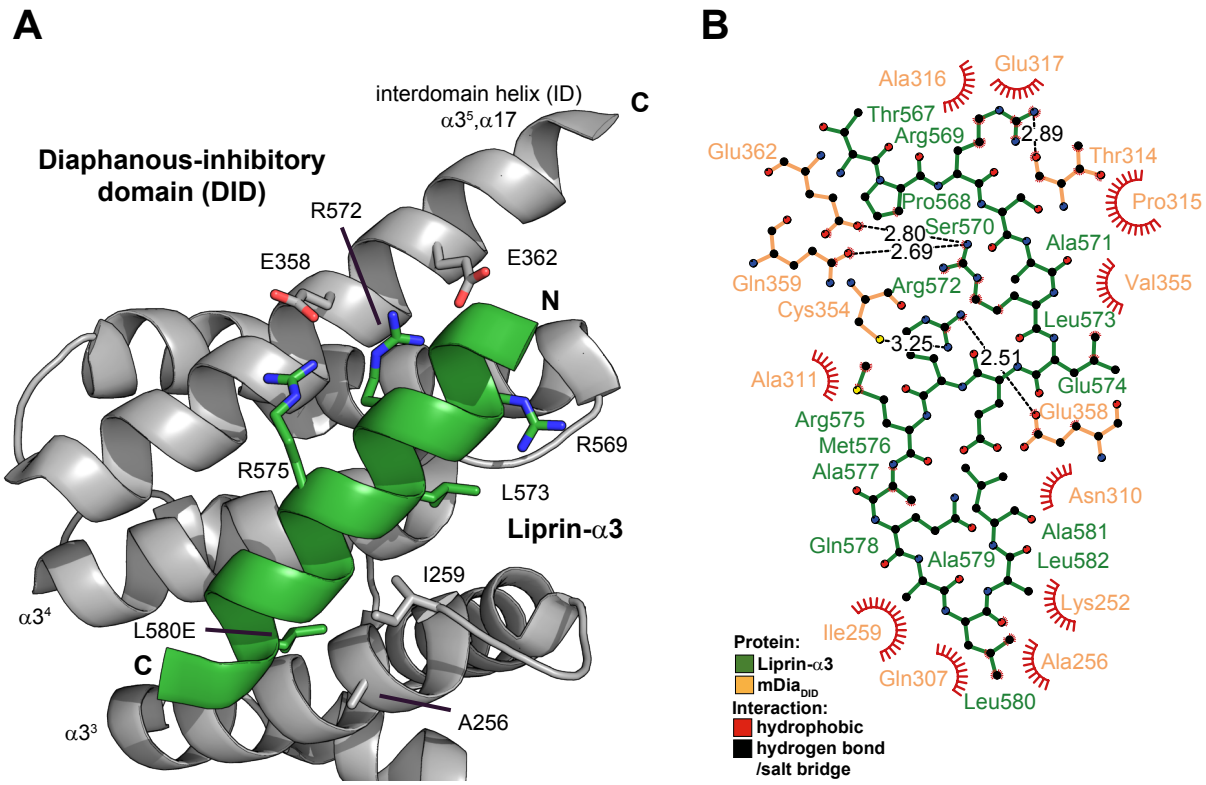

Figure 4.9 Binding interface of $mDia_{DID}$ and $Lip_{567–587}$.
A: Close-up of the mDia1-Liprin-α3 binding site. Shown are the electrostatic interactions between the arginines (R572, R575) of Liprin-α3 and the glutamic acids (E358, E362) of mDia1, as well as hydrophobic interactions (L573, M576 and L580). B: Schematic presentation of the interaction site of the $mDia_{DID}$ • $Lip_{567–587}$ complex, generated with LigPlot$^+$ (version 1.4.5), showing the hydrophobic and electrostatic contacts.

4.2.4 Mutational analysis

Several residues of mDia1 and Liprin-α3 were mutated and measured by ITC in order to characterize the binding and to confirm the structural data. The mutations A256D^D and I259D^D, that have been described in earlier studies to abolish binding of $mDia_{DID}$ to $mDia_{DAD}$, also interfere with Liprin-α3 binding. While $mDia_N$ I259D^D showed no binding to $Lip_{567–587}$ the mutant A256D^D had a nearly tenfold decreased affinity of 42 µM (Table 4.4). These data are in line with the structural data since I259D^D is located directly within the hydrophobic interface with Liprin-α3, whereas A256D^D is located at the edge of the binding interface (Figure 4.9 A,B). Furthermore, the mutant N165D^D, which has been shown to have an impact on mDia1-RhoA • GTP-binding, and no impact on $mDia_{DAD}$-binding, does also not interfere with Liprin-α3 binding (Table 4.4).

Table 4.4 ITC data of the mutational characterization of the mDia1-Liprin-α3 binding interface. The fragments with the indicated mutations were purified and measured via ITC in protein buffer at 20 °C. Superscript S,C indicate whether the protein fragment was loaded into the cell or syringe of the ITC_{200}. (K_D: equilibrium dissociation constant; ΔH: change in reaction enthalpy; ΔS: change in reaction entropy; N: stoichiometry of binding; T: temperature in Kelvin)

	interaction	K_D	ΔH	TΔS	N
		μM	*kcal mol^{-1}*	*kcal mol^{-1}*	
Liprin 567–587	$^{C}Lip_{567–587}$-$^{S}mDia_{N}$ I259D		no binding		
	$^{C}Lip_{567–587}$-$^{S}mDia_{N}$ N165D	5.0 ±0.3	−6.7 ±0.1	0.4	0.9
	$^{C}Lip_{567-587}$-$^{S}mDia_{N}$ A256D	42.0 ±6.0	−11.7 ±1.4	−5.8	0.8
	$^{S}Lip_{567–587}$-$^{C}mDia_{DID}$ E358R		no binding		
	$^{S}Lip_{567–587}$-$^{C}mDia_{DID}$ E362R		no binding		
	$^{S}Lip_{567–587}$-$^{C}mDia_{DID}$ E317R	14.6 ±1.1	−10.1 ±0.4	−3.6	0.8
Liprin 561–587	$^{S}Lip_{561–587}$ R569E-$^{C}mDia_{N}$		no binding		
	$^{S}Lip_{561-587}$ R572E-$^{C}mDia_{N}$		no binding		
	$^{S}Lip_{561-587}$ L573E-$^{C}mDia_{N}$		no binding		
	$^{S}Lip_{561-587}$ R575E-$^{C}mDia_{N}$		no binding		
	$^{S}Lip_{561-587}$ M576E-$^{C}mDia_{N}$		no binding		
	$^{S}Lip_{561-587}$ L580E-$^{C}mDia_{N}$		no binding		

Based on the structural data different residues on the $Lip_{561–587}$ fragment within the hydrophobic core were mutated, including $L573E^{L}$, $M576E^{L}$ and $L580E^{L}$. None of these mutated fragments showed any binding to $mDia_N$. In addition mutations of the salt bridge forming residues $R572E^{L}$ and $R575E^{L}$, as well as, $R569E^{L}$ did completely abolish the binding. Likewise, opposite charge mutations of the counterparts on mDia1 $E358R^{D}$ and $E362R^{D}$ did prevent any binding. Mutation of the residue $E317R^{D}$, which is not involved in any salt bridge formation reduced the affinity approximately threefold to 14.6 µM (Table 4.4). The integrity of the mutated fragments was tested and confirmed via size exclusion chromatography. They showed the same elution profiles and peak symmetries as the wildtype samples (Figure A.6).

4.2.5 Binding specificity of mDia

In order to test the binding specificity of mDia1 to Liprin-α3, an mDia2 fragment, similar to the $mDia_N$ fragment in mDia1 was cloned and purified. This fragment spanned the residues 87–467. Using this fragment, no binding to $Lip_{457–587}$ could be observed in ITC measurements under the same conditions used for the determination of the mDia1-Liprin-α3 binding (Figure 4.10 C).

The alignment of $mDia_{DID}$ of mDia1, mDia2 and mDia3 reveals the high conservation of this region. However, especially in the case of charged residues some differences can

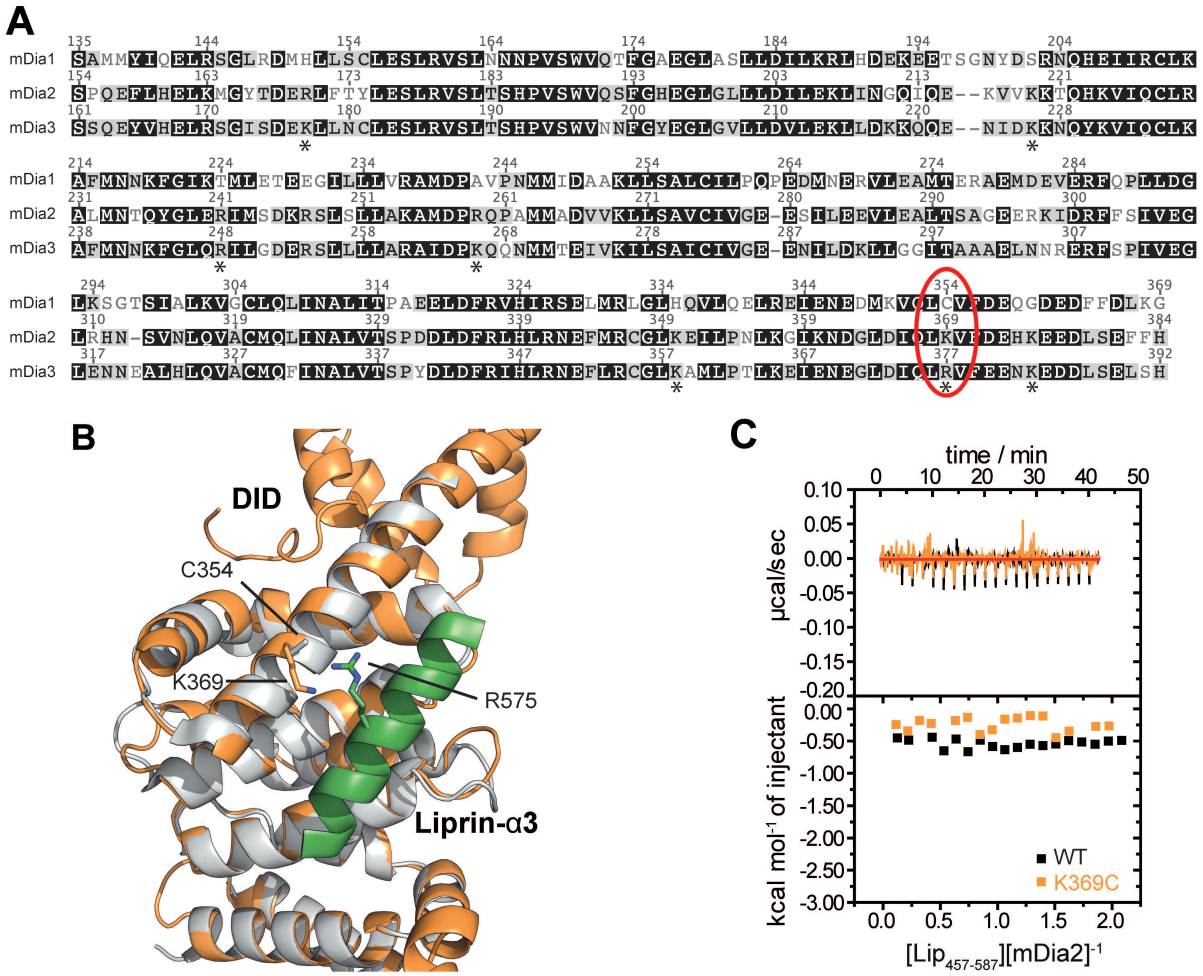

Figure 4.10 Binding specificity of mDia to Liprin-α3.
A: Alignment of the Diaphanous inhibitory domain (DID) of mDia1, mDia2 and mDia. B: Structural differences between mDia1 and mDia2. Shown is the superposition of the solved mDia1 • Liprin-α3 structure (PDB: 4UWX) in gray and green and the modeled mDia2 structure (SWISS-Model CITE). C: ITCs of $mDia2_{87–467}$ with $Lip_{457–587}$. The measurements performed with mDia2 WT and mDia2 K369C are shown in black and orange, respectively.

be spotted. While the majority of negatively charged amino acids is conserved, there are same additional positively charged amino acids present in mDia2 and mDia3, in comparison to mDia1 (Figure 4.10 A). Superposition of the solved mDia1 • Liprin-α3 structure with an mDia2 model indicates that especially K369 of mDia2 (C354 in mDia1) seems to be of importance, since it is facing towards the binding interface. Thereby, it would be in close contact to R575 of Liprin-α3, leading to an electrostatic repulsion (Figure 4.10 B). A K369C mutation was introduced into the mDia2 fragment and the binding towards $Lip_{561–587}$ was measured again by ITC. Introducing this mutation did not result in detectable binding, indicating that additional specificity determinants must exit. (Figure 4.10 C).

4.2.6 Liprin-α3 specificity and regulation by posttranslational phosphorylation

The Liprin-α3 region that has been shown to be essential for mDia1 binding is highly conserved throughout different species. Especially, the arginines 569 and 572 in Liprin-α3, that are responsible for the formation of salt bridges, seem to be present in most organisms. The same holds true for the hydrophobic residues L573, M576 and L580 (Figure 4.11 A). Alignments of human and mouse Liprin-α1 to Liprin-α4 reveal that the different Liprins are highly conserved in the N-terminal half (aa 563–576) of

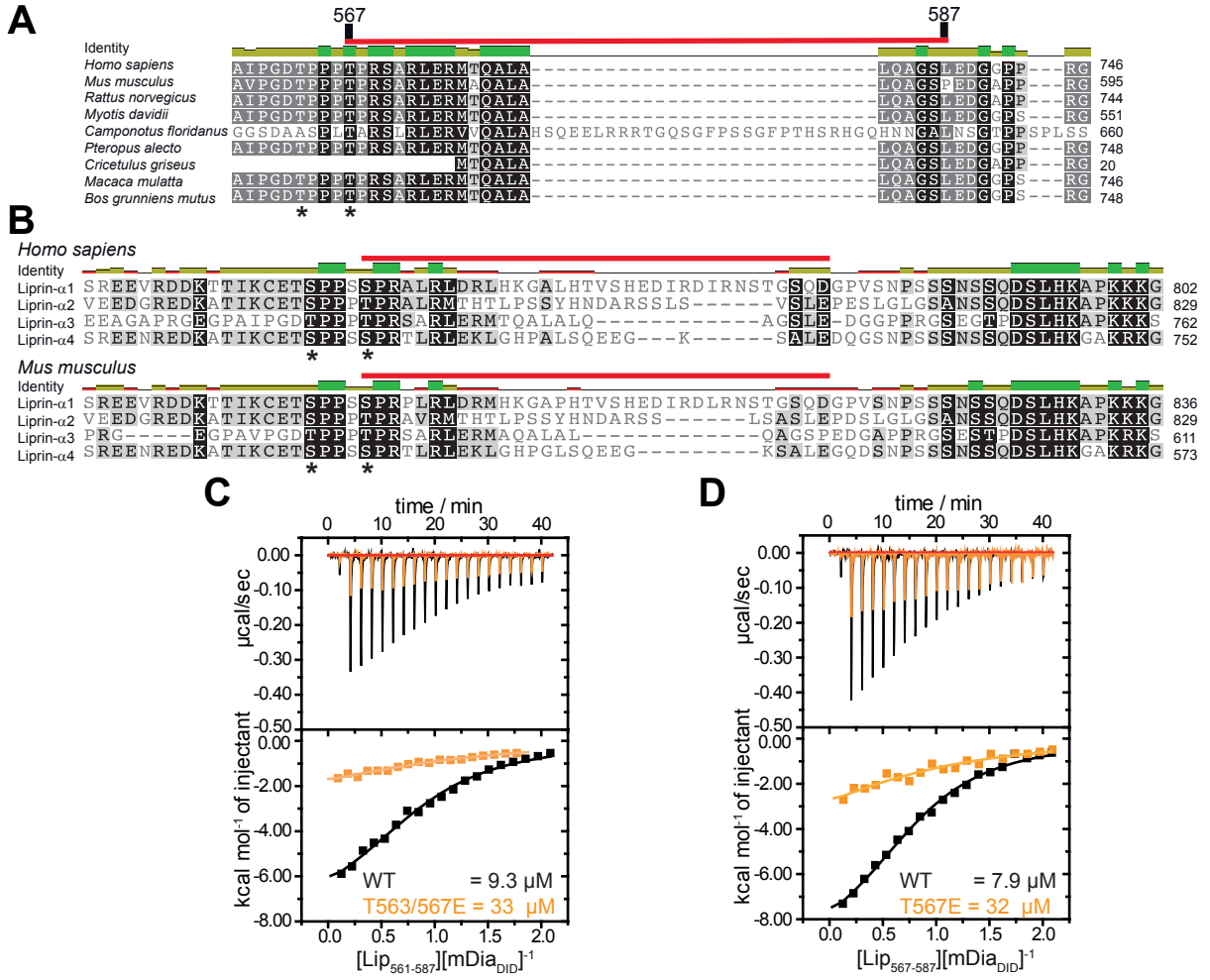

Figure 4.11 Regulation of Liprin-α3 • mDia1 binding by posttranslational phosphorylation. A: Alignment of the mDia1 binding region of Liprin-α3 in different species. B: Alignment of the binding region of different Liprins in *Homo sapiens* and *Mus musculus*. A,B: The red bar spans the residues which were visible within the crystal structure. The asterisks indicate the possible phosphorylation sites found in *Homo sapiens* Liprin-α3 (T563/567 in mouse Liprin-α3). C: ITC measurements of $mDia_{DID}$ with a double phosphomimetic mutant (T563/567E) in $Lip_{561–587}$ and a single phosphomimetic mutant (T567E) in $Lip_{567–587}$ in orange with the corresponding wildtype measurements in black.

the mDia1 binding region. Although R569 and R575 are present in all Liprins several hydrophobic residues, known to be important for the mDia1-Liprin-α3 interaction, are not completely conserved. This makes it unlikely that other Liprins next to Liprin-α3 can bind with this region to mDia1 (Figure 4.11 B). Interestingly, it has been shown that human Liprin-α3 can be phosphorylated at the threonines 563 and 567 (Mayya *et al.*, 2009). These positions seem to be of functional importance, since all Liprin isoforms of each species carry a serine/threonine at those positions (Figure 4.11 A,B). Based on this the phosphomimetic mutants T563/567E were introduced into the $Lip_{561–587}$ fragment to test the effect on mDia1 binding. Indeed, the binding towards $mDia_{DID}$ was reduced to 33 µM as determined by ITC (Figure 4.11 C, Table 4.5). Additionally, the binding enthalpy increased to -3.2 kcal mol^{-1}, which was partially compensated by an increase in favorable entropy (2.8 kcal mol^{-1}). This indicates an altered binding mechanism due to electrostatic interactions. Since of both threonines only T567 showed a defined electron density in the crystal structure the fragment $Lip_{567–587}$ with the single mutant T567E was measured as well (Figure 4.11 D). Again the binding affinity was reduced to 32 µM, associated with an increase in binding enthalpy and entropy. These data show that the single T567 mutant is sufficient to mediate the loss of affinity and support that T563 is not directly involved in the interaction with mDia1.

Table 4.5 Phosphomimetic Liprin-α3 ITC measurements. Data of the measurements shown in Figure 4.11 C,D. (K_D: equilibrium dissociation constant; ΔH: change in reaction enthalpy; ΔS: change in reaction entropy; N: stoichiometry of binding; T: temperature in Kelvin)

	interaction	**K_D**	**ΔH**	**TΔS**	**N**
		µM	*kcal mol^{-1}*	*kcal mol^{-1}*	
Liprin 561-587	$mDia_{DID}$-$Lip_{561-587}$ WT	9.3 ± 1.3	−8.2 ± 0.5	−1.4	0.9
	$mDia_{DID}$-$Lip_{561-587}$ T563/567E	33.0 ± 14	−3.2 ± 0.9	2.8	1.3
Liprin 567-587	$mDia_{DID}$-$Lip_{567-587}$ WT	7.9 ± 0.9	−9.9 ± 0.5	−3.1	0.8
	$mDia_{DID}$-$Lip_{567-587}$ T567E	32.0 ± 19	−6.1 ± 3.6	−0.02	0.9

4.3. Binding Mechanism

Once the the binding of Liprin-α3 to mDia1 and particularly the binding region had been characterized functionally and structurally, the next aim was to elucidate how Liprin-α3 interferes with RhoA and $mDia_{DAD}$ binding towards $mDia_N$

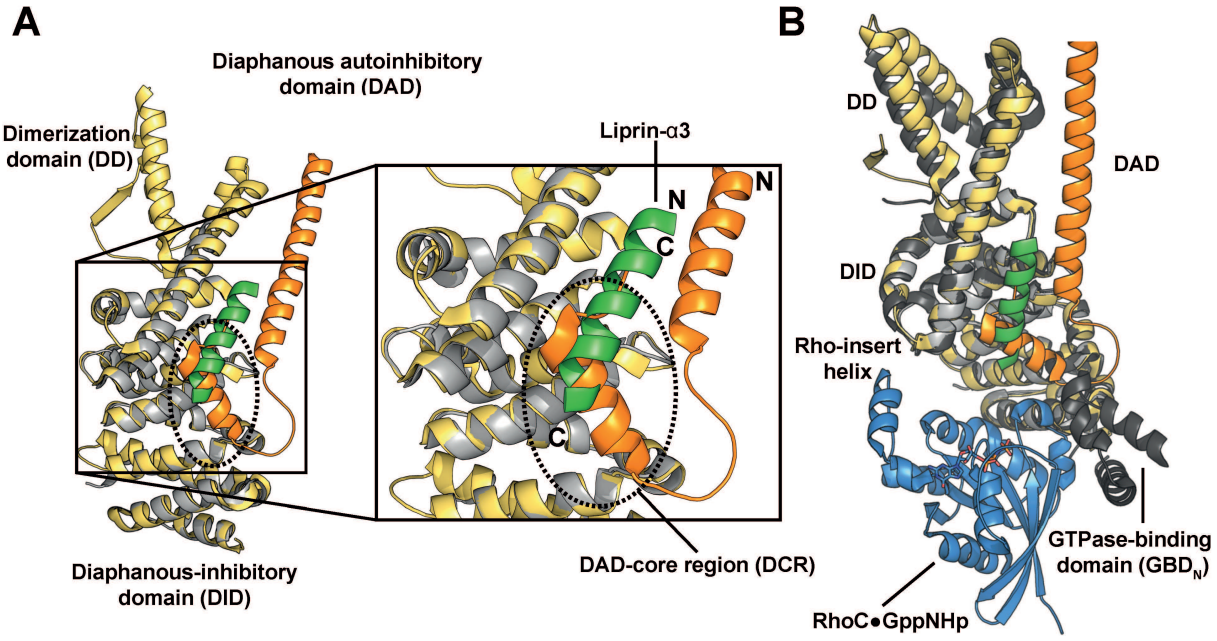

Figure 4.12 Superposition of putative Liprin-α3 • $mDia_{DAD}$/RhoA complex.
A: *Left* Superposition of the $mDia_{DID}$ • $Lip_{567–587}$ structure (PDB: 4UWX, grey: $mDia_{DID}$, green: $Lip_{567–587}$ and a selected section of the $mDia_N\Delta G$ • $mDia_{DAD}$ structure (PDB: 3OBV, yellow: $mDia_N\Delta G$, orange: $mDia_{DAD}$). *Right* detailed view of the overlapping binding regions of Liprin-α3 and $mDia_{DAD}$. B: Same superposition as shown in A with the additional complex $mDia_N$ • RhoC • GppNHp (PDB: 1Z2C, darkgrey: $mDia_N$, blue: RhoC).

Interplay of Liprin-α3 and $mDia_{DAD}$

Sakamoto *et al.* showed that $mDia_{DAD}$ (aa 1145–1196) can be displaced from mDia1 by $Lip_{457–737}$. Indeed, the binding sites of Liprin-α3 and $mDia_{DAD}$ for mDia1 are highly overlapping as shown by the superposition of the $mDia_N\Delta G$ • $mDia_{DAD}$ complex (PDB: 3OBV) and the solved structure of the $mDia_{DID}$ • $Lip_{567–687}$ structure (PDB: 4UWX) (Figure 4.12 A). Particularly, the C-terminal region of the Liprin-α3 fragment covers the same area as the DAD-core-region (DCR, aa 1175–1195). The adjacent DAD-basic-region (DBR, aa 1196–1209), which is not visible in the structure has been shown to align with the ID α-helix and thereby taking a similar path as the N-terminal part of $Lip_{567–587}$ (Figure 4.12 A *right*). The presence of these additional amino acids of the DBR increase the affinity of $mDia_{DAD}$ towards $mDia_{DID}$ 70 fold (Lammers *et al.*,

2005). This makes it unlikely that Liprin-α3 can displace $mDia_{DAD}$ including the DAD-basic-region from $mDia_{DID}$. In contrast to Liprin-α3 the binding of $mDia_{DAD}$ to $mDia_{DID}$ mainly induced by hydrophobic interactions and is not creating salt bridges.

Interplay of Liprin-α3 and RhoA

The autoinhibitory state of mDia1, in which $mDia_{DAD}$ binds to $mDia_{DID}$, is released upon binding of RhoA to $mDia_N$. Sakamoto *et al.* could show that RhoA also displaces Liprin-α3 from mDia1. Since the binding sites of $mDia_{DAD}$ and Liprin-α3 closely match, a similar RhoA induced displacement mechanism can be assumed. However, in consideration of the structure presented here RhoC and $Lip_{567–587}$ occupy completely distinct and non-overlapping binding sites on mDia1 (Figure 4.12 B).

To gain further insights into the interactions of mDia1, Liprin-α3, RhoA and $mDia_{DAD}$ and into possible displacement mechanisms, the impact of Liprin-α3 for RhoA (4.3.1) and $mDia_{DAD}$ binding (4.3.2) to $mDia_N$ was analyzed by ITC and stopped-flow experiments.

4.3.1 Effect of Liprin-α3 on the RhoA • mDia1 interaction

ITC competition analysis of the RhoA-mDia1 interaction

As shown qualitatively by Sakamoto *et al.* RhoA was used successfully to displace $Lip_{457–737}$ from mDia1. In this study ITC measurements were used to quantitatively analyze the interplay and the interference of shorter Liprin-α3 fragments on RhoA binding to $mDia_N$. For this purpose complexes of Liprin-α3 fragments, containing only the essential amino acids (aa 561–576, 561–582, 567–587) needed for mDia1 binding, and $mDia_N$ were preformed before the addition of constitutively active RhoA (RhoA Q63L).
RhoA Q63L binds to $mDia_N$ with an affinity (K_D) of 4 nM as determined by ITC (Figure 4.13 A). The stoichiometry for this interaction is 1:1, with a change in enthalpy of -4.0 kcal mol^{-1}. Additionally, the reaction was entropically driven ($T\Delta S = 7.3$ kcal mol^{-1}), resulting in a Gibbs free energy change of $\Delta G = -11.3$ kcal mol^{-1} (Table 4.6). In presence of $Lip_{561–587}$ the binding affinity was reduced to 58 nM and the favorable enthalpy change increased to -0.7 kcal mol^{-1}, which can be explained by the release of the Liprin-α3 fragment from $mDia_N$ (Figure 4.13 B, Table 4.6). In addition the entropy change increased to $T\Delta S = 9.0$ kcal mol^{-1}, resulting in a Gibbs free energy change of $\Delta G = -9.9$ kcal mol^{-1}.

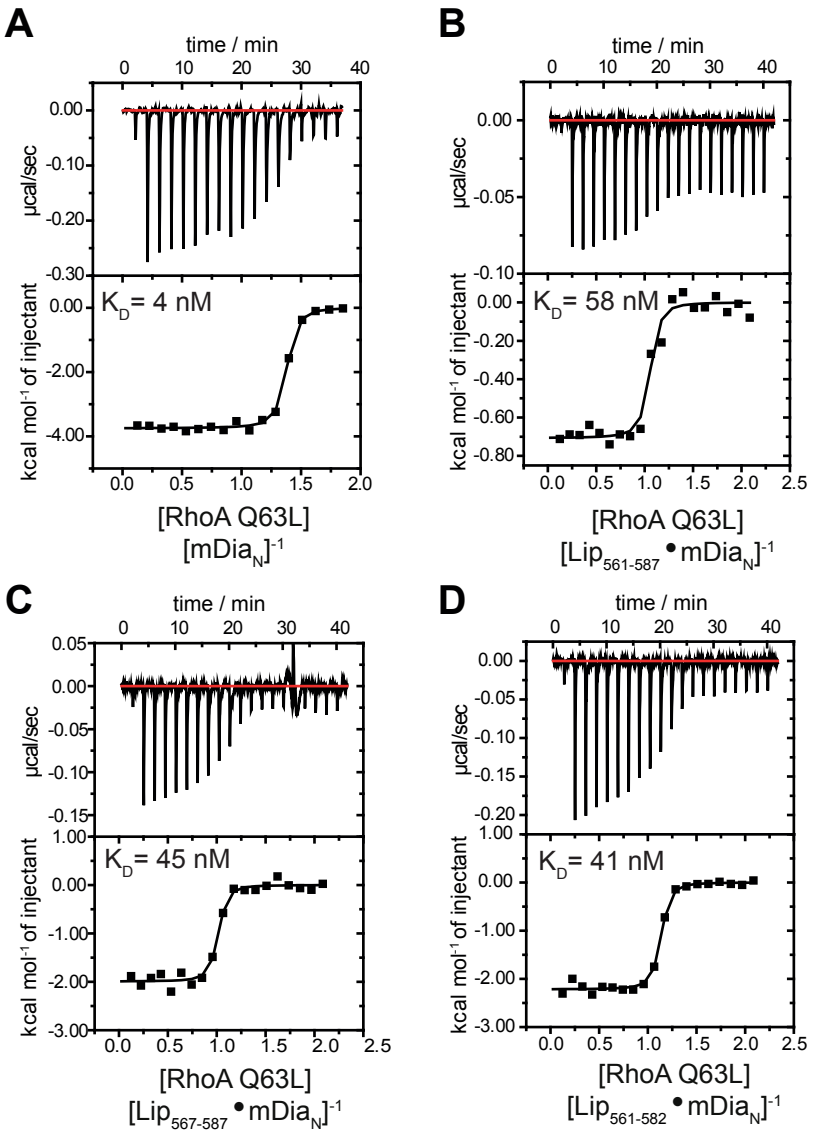

Figure 4.13 ITC analysis of the influence of Liprin-α3 on the mDia$_N$-RhoA binding thermodynamics.
All ITCs were performed at 20 °C in protein buffer. Active RhoA (RhoA Q63L) was titrated to saturated complexes of mDia$_N$ and Lip$_{567–587}$ (B), Lip$_{561–587}$ (C), Lip$_{561–582}$ (D) or in the absence of Liprin-α3 (A). The tested Liprin-α3-fragments reduced the binding affinity of RhoA to mDia$_N$ up to 10–15 fold.

As a control and to exclude an effect of the C- and N-terminal regions of the Liprin-α3 fragment the experiment was repeated with Lip$_{567–587}$ and the structurally visible fragment Lip$_{561–582}$. Again the presence of Liprin-α3 reduced the binding affinity of RhoA to mDia$_N$ to 45 nM and 41 nM for Lip$_{567–587}$ and Lip$_{561–582}$, respectively. Moreover, ΔH increased, albeit to a lesser extend compared to Lip$_{561–587}$ (Lip$_{567–587}$: ΔH = -2.0 kcal mol^{-1}; Lip$_{561–582}$: ΔH = -2.2 kcal mol^{-1}) (Figure 4.13 C,D, Table 4.6). The positive entropic contribution of the RhoA binding towards mDia$_N$, however, was not influ-

enced by $Lip_{567–587}$ ($T\Delta S = 7.9\,kcal\,mol^{-1}$) and $Lip_{561–582}$ ($T\Delta S = 7.7\,kcal\,mol^{-1}$). Resulting from that the Gibbs free energy change was similar for all tested Liprin-α3-fragments (ΔG = -9.7 to -9.9 $kcal\,mol^{-1}$). Taken together, the presence of Liprin-α3 decreased the binding affinity of RhoA to $mDia_N$ by 10-15 fold with an increase of the negative ΔG of approximately 1.5 $kcal\,mol^{-1}$.

Table 4.6 Rho-Liprin-α3 ITC competition measurements. Data of the measurements shown in Figure 4.13. K_D: equilibrium dissociation constant; ΔH: change in reaction enthalpy; ΔS: change in reaction entropy; N: stoichiometry of binding; T: temperature in Kelvin)

interaction		K_D	ΔH	$T\Delta S$	N
		nM	*kcal mol^{-1}*	*kcal mol^{-1}*	
without Liprin-α3	RhoA Q63L-$mDia_N$	4 ± 4	−4.0 ± 0.04	7.3	1.3
Liprin 567–587	RhoA Q63L-$mDia_N$ • Liprin	45 ±21	−2.0 ± 0.04	7.9	1.0
Liprin 561–582	RhoA Q63L-$mDia_N$ • Liprin	41 ±11	−2.2 ± 0.03	7.7	1.1
Liprin 561–587	RhoA Q63L-$mDia_N$ • Liprin	58 ±37	−0.7 ± 0.02	9.0	1.0

Although RhoA and Liprin-α3 use distinct binding sites on mDia1, these data show that the presence of Liprin-α3 alters and weakens the interaction of RhoA and mDia1. However, these ITC experiments do not exclude the possibility of a ternary complex formed by mDia1, RhoA and Liprin-α3. Therefore additional fluorescence polarization assays were performed.

Fluorescence polarization assays of the putative ternary mDia1 • RhoA • Liprin-α3 complex

Fluorescence polarization assays were performed to exclude a possible ternary complex formation of $mDia_N$ • RhoA • Liprin-α3. Therefore, the fragments $Lip_{567–587}$ and $Lip_{567–582}$ were synthesized with an N-terminal fluorescein label and titrated together with $mDia_N$ and RhoA (Figure 4.14). Upon addition of $mDia_N$ to the labeled $Lip_{567–587}$ fragment the polarization signal increased, indicating a complex formation of $mDia_N$ and Liprin-α3. Addition of active RhoA Q63L to the complex led to a decrease of the fluorescence polarization signal. This drop of signal, to a level comparable to the baseline, reflects the dissociation of the mDia1 • Liprin-α3 complex. The residues 583–587 of Liprin-α3, that were not visible in the crystal structure, seem to be orientated towards RhoA in a putative ternary mDia1 • Liprin-α3 • RhoA complex (Figure 4.12). In order to exclude that these residues might contribute to the RhoA induced dissociation of $Lip_{567–587}$ from $mDia_N$, the experiment was repeated using the C-terminally truncated $Lip_{567–582}$ fragment. As indicated by the changes in the polarization signal, $Lip_{567–582}$ still bound to $mDia_N$ and was also dissociated from it by RhoA.

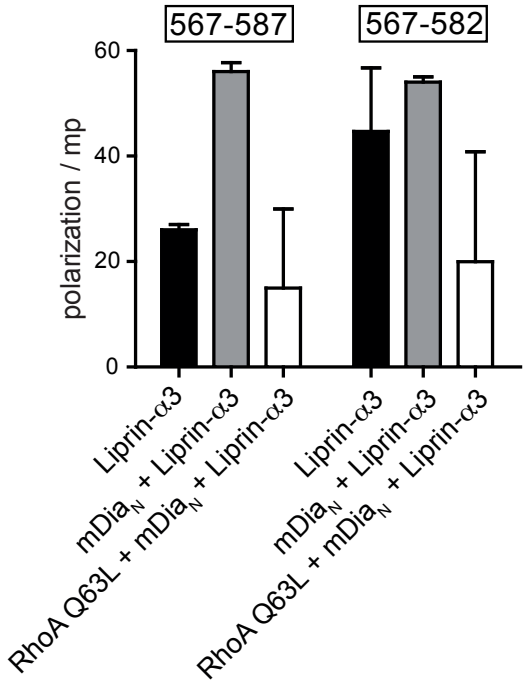

Figure 4.14 Polarization assays of putative ternary mDia1 • RhoA • Liprin-α3 complexes.
The polarization signals of $Lip_{567–587}$ and $Lip_{567–582}$ peptides were measured alone, in complex with $mDia_N$ and after titration of RhoA Q63L to the complex. Addition of RhoA reduced the polarization signal, thus indicating the dissociation of both Liprin-α3 fragments from $mDia_N$. The assay was performed in protein buffer at 20 ℃. Data are presented as mean ± S.D. of triplicate measurements.

These data confirm that active RhoA can displace Liprin-α3 from $mDia_N$, despite the distinct binding region of Liprin-α3 on mDia1. In combination with the ITC competition experiments (Figure 4.13) and the protein structure these data rather support an allosteric displacement mechanism of Liprin-α3 by RhoA, than a competition for an overlapping binding-site.

Stopped-flow kinetics of the RhoA-mDia1 interaction

Besides thermodynamic data obtained from ITC measurements, stopped-flow analyses can be performed to investigate the binding kinetics. Using this method the interaction dynamics of mDia1 and RhoA were analyzed in presence and absence of Liprin-α3 fragments.

Influence of Liprin-α3 on the association rates of RhoA and $mDia_N$
Prior to the pre-equilibrium stopped-flow experiment RhoA was loaded with mant-GppNHp (non-hydrolyzable GTP analogue). The fluorescently labeled RhoA was then titrated with increasing concentration of $mDia_N$, under pseudo-first order conditions. In order to analyze the effect of Liprin-α3 on RhoA binding a twofold molar excess of different Liprin-α3 fragments was added to the titrated $mDia_N$. For this purpose the N-terminally most extended fragment $Lip_{217–587}$, as well as the fragments $Lip_{561–587}$ $Lip_{567–587}$ and $Lip_{561–582}$, that were also measured in the ITC competition assays, were used in this study. Single exponential fits of the primary data yielded the observed association rate constants (k_{obs}) (Figure A.9). These rates were plotted against the

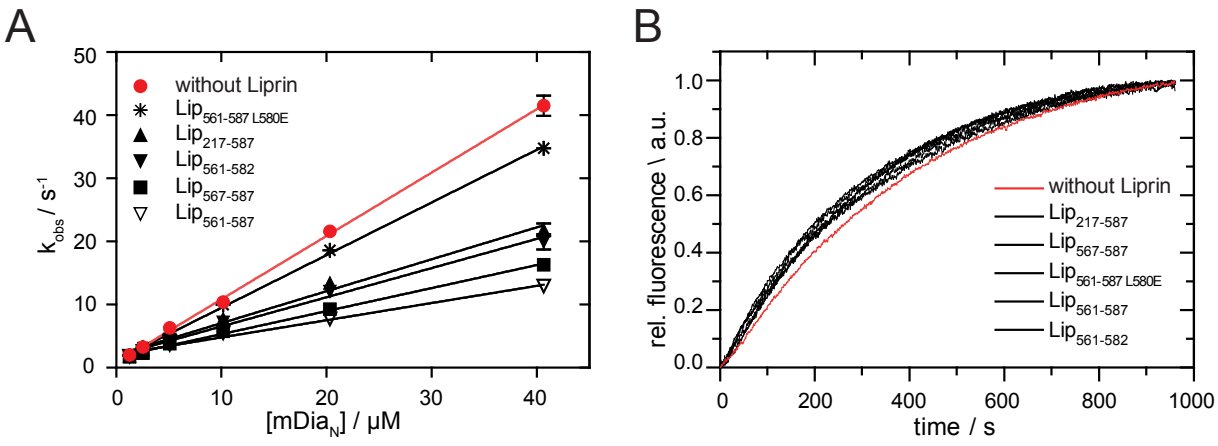

Figure 4.15 Stopped-flow analysis of the influence of Liprin-α3 on the mDia1 • RhoA interaction dynamics.
A: *association rate constant*. Mant-GppNHp loaded RhoA was titrated with increasing $mDia_N$ concentrations in presence/absence of different Liprin-α3-fragments. The slope of the linear fit represents the association rate constant (k_{ass}). Data are shown as mean ± S.D. of three independent experiments. B: *dissociation rate constant*. Complexes of mDia1 • RhoA • mant-GppNHp were titrated with a 100-fold excess of active RhoA Q63L in the presence/absence of Liprin-α3-fragments, as indicated. Data were fitted to a single exponential curve.

$mDia_N$ concentration and finally a linear fit was applied resulting in the second order association rate constant (k_{ass}) (Figure 4.15 A, Table 4.7). In the case of RhoA binding to $mDia_N$ in absence of Liprin-α3 the calculated association rate was $k_{ass} = 1.00\,\mu M^{-1}\,s^{-1}$ (Table 4.7). A distinguishable reduction in association can be detected, due to the presence of Liprin-α3. All tested Liprin-α3-fragments nearly had the same reducing effect, albeit the longest fragment $Lip_{217–587}$ displayed the smallest effect with an association rate constant of $k_{ass} = 0.51\,\mu M^{-1}\,s^{-1}$. The shorter fragments induced slightly more severe effects ($Lip_{561–587}$: $k_{ass} = 0.27\,\mu M^{-1}\,s^{-1}$; $Lip_{567–587}$: $k_{ass} = 0.37\,\mu M^{-1}\,s^{-1}$; $Lip_{561–582}$: $k_{ass} = 0.46\,\mu M^{-1}\,s^{-1}$) (Figure 4.15 A, Table 4.7). To exclude the possibility that the reduced association rates of RhoA to $mDia_N$, are based on some artificial effect induced by the addition of a third protein to the solution, the Liprin-α3 mutant L580E was used as a control. Previous ITC data showed that the fragment $Lip_{561–587}$ containing the L580E mutant is not able to bind mDia1. Indeed, using this mutant in the stopped-flow experiment nearly restored the association rate of RhoA to $mDia_N$ ($k_{ass} = 0.83\,M^{-1}\,s^{-1}$). In accordance with the ITC competition data these data elucidate the importance of the Liprin-α3 residues 567–582, that were visible in the crystal structure. Although, Liprin-α3 and RhoA exhibit no overlapping binding region on mDia1, the association rate of RhoA to mDia1 is clearly affected by Liprin-α3.

Influence of Liprin-α3 on the dissociation rates of RhoA and mDia$_N$

Comparable to the association rates the influence of different Liprin-α3 fragments on the dissociation rate constant (k_{diss}) of RhoA and mDia$_N$ were tested. Therefore, a complex of mDia$_N$ • RhoA • mant-GppNHp was preformed and mixed with a 100 fold molar excess of unlabeled and active RhoA Q63L. This approach makes it possible to analyze the release of fluorescently loaded RhoA from the complex over a period of time. Equimolar ratios of the same Liprin-α3 fragments used for the association rate determination were mixed with RhoA Q63L in order to determine their impact on the dissociation rate (Figure 4.15 B). As reported earlier the dissociation kinetics showed a single exponential behavior. The obtained dissociation rate for the RhoA-mDia$_N$ interaction in absence of Liprin-α3 ($k_{diss} = 2.35\,m\,s^{-1}$) is in agreement with the published data (Lammers *et al.*, 2008). Addition of the fragments Lip$_{217–587}$ ($k_{diss} = 2.82\,m\,s^{-1}$), Lip$_{561–587}$ ($k_{diss} = 2.84\,m\,s^{-1}$), Lip$_{567–587}$ ($k_{diss} = 3.22\,m\,s^{-1}$) and Lip$_{561–582}$ ($k_{diss} = 3.22\,m\,s^{-1}$) did only slightly increase the dissociation rate (Table 4.7).

Table 4.7 Effect of different Liprin-α3-fragments on the RhoA-mDia1 interaction dynamics as determined by stopped-flow measurements. k_{ass} is the association rate constant, and k_{diss} is the dissociation rate constant

Liprin-α3-fragment	$\mathbf{k_{ass}}$	$\mathbf{k_{diss}}$	$\mathbf{K_D}$
	$\mu M^{-1}s^{-1}$	ms^{-1}	nM
Without fragment	1.00 ± 0.01	2.35 ± 0.09	2.4
217–587	0.51 ± 0.01	2.82 ± 0.07	5.5
567–587	0.37 ± 0.01	3.22 ± 0.04	8.7
561–582	0.46 ± 0.01	3.22 ± 0.07	7.0
561–587	0.27 ± 0.01	2.84 ± 0.11	10.5
561–587 L580E	0.83 ± 0.01	3.04 ± 0.05	3.7

Taken together, Liprin-α3 influences the binding dynamics of the RhoA • mDia1 interaction. The association rate of RhoA is reduced, while the dissociation rate is only marginally affected. Interestingly, all tested fragments showed a comparable impact on the RhoA • mDia1 interaction emphasizing again the importance of Liprin-α3 residues 567–582.

4.3.2 Effect of Liprin-α3 on the $mDia_{DAD}$ • $mDia_N$ interaction

Similar to the isothermal titration calorimetry (ITC) competition assays regarding the influence of Liprin-α3 on the RhoA-$mDia_N$ interaction, the effect for the $mDia_{DAD}$-$mDia_{DID}$ interaction was analyzed. In their study Sakamoto *et al.* used fluorescence polarization assays to show that $Lip_{457–737}$ is able to displace $mDia_{DAD}$ from $mDia_N$. However, in their experiments they used the DAD-core-region (DCR, aa 1075–1195), which binds to $mDia_{DID}$ with approximately 15 µM (Lammers *et al.*, 2005). In comparison, the elongated fragment $DAD_{1145–1200}$ displays a three orders of magnitude enhanced binding affinity of 29 nM. Including the complete DAD-basic region (DBR, 1196–1209) even further increases the binding affinity of $mDia_{DAD}$ to $mDia_{DID}$ to 14 nM (Table 4.8). This makes it actually unlikely, that Liprin-α3 is able to displace $mDia_{DAD}$ from mDia1.

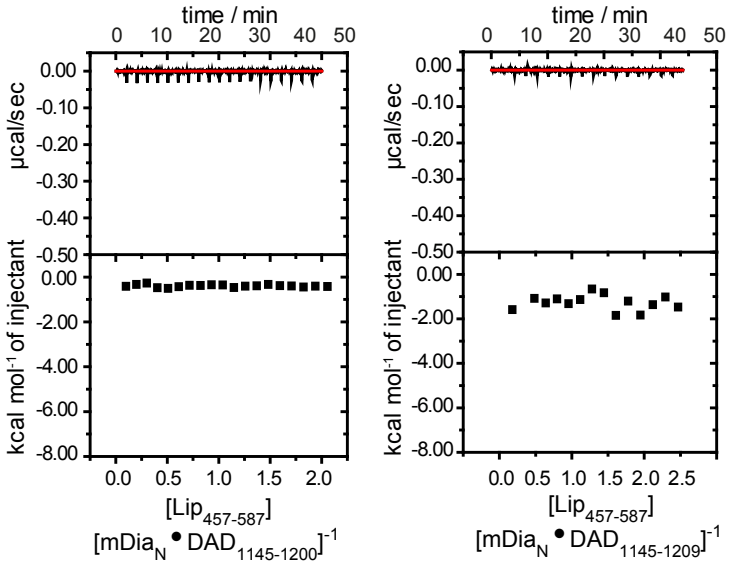

Figure 4.16 ITC analysis of the influence of $mDia_{DAD}$ on the $mDia_N$ - Liprin-α3 binding thermodynamics.
Liprin-α3 was titrated to preformed complexes of $mDia_N$ • $DAD_{1145–1200}$ and $mDia_N$ • $DAD_{1145–1209}$ at 25 °C in protein buffer. No heat signals could be detected, indicating that Liprin-α3 was not able to displace $mDia_{DAD}$ from the complex or bind to $mDia_N$.

Indeed, titrating Liprin-α3 to the $mDia_N$ • $DAD_{1145–1200}$ and $mDia_N$ • $DAD_{1145–1209}$ complexes did not result in detectable changes in the heat signals (Figure 4.16). This indicates that Liprin-α3 is not capable to displace $mDia_{DAD}$ from $mDia_N$ or to bind $mDia_N$ in presence of $mDia_{DAD}$.
Notably, when $DAD_{1145–1200}$ was titrated to an $mDia_{DID}$ • Liprin-α3 complex, the complex dissociated and Liprin-α3 was released from $mDia_{DID}$, as shown by ITC (Figure 4.17) and analytical size exclusion chromatography (Figure 4.18). In the initial ITC experiment a saturated $mDia_{DID}$ • $Lip_{561–587}$ complex was preformed, with a twofold molar excess of Liprin-α3. Subsequently, $DAD_{1145–1200}$ was titrated to this complex and the occurring heat signals deriving from the $DAD_{1145–1200}$-$mDia_{DID}$ binding and simultaneously release of $Lip_{561–587}$ were recorded (Figure 4.17 B). Since the structural data showed a highly overlapping binding region for $mDia_{DAD}$ and

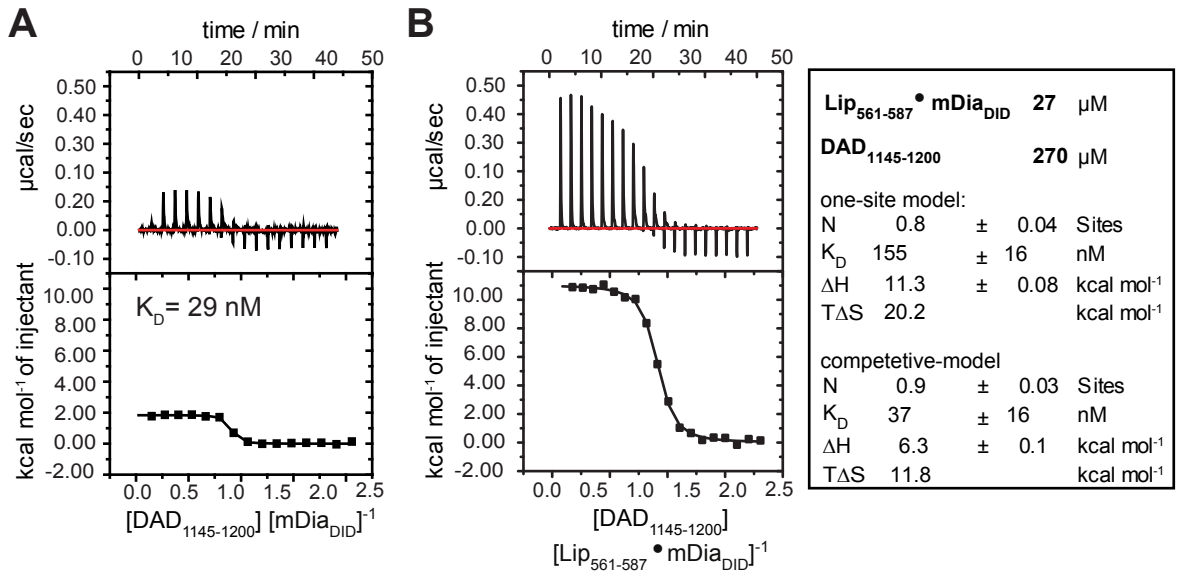

Figure 4.17 ITC experiments to analyze the influence of Liprin-α3 on the $mDia_{DID}$ • $mDia_{DAD}$ binding thermodynamics.
A: ITC measurement of the $DAD_{1145–1200}$-$mDia_N$ interaction. B: $DAD_{1145–1200}$ was titrated to a preformed complex of $mDia_{DID}$ • $Lip_{561–587}$. The obtained binding curve was fitted with the one-site and the competitive model. A,B: The experiment was performed at 25 ℃ in protein buffer. (K_D: equilibrium dissociation constant; ΔH: change in reaction enthalpy; ΔS: change in reaction entropy; N: stoichiometry of binding; T: temperature in Kelvin)

$Lip_{567–582}$ the formation of a ternary complex seems to be unlikely. Even though, the binding sites are only highly overlapping and not identical, a competitive fit model was applied to approximately determine the initial binding of $Lip_{561–587}$ to $mDia_{DID}$. The resulting binding affinity ($K_D = 37$ nM) is in agreement with the direct measurement ($K_D = 29$ nM, Table 4.8, Figure 4.17 A). In comparison, the one-site model fit showed a reduced affinity of 155 nM in the presence of Liprin-α3. The binding displayed an unfavorable enthalpic contribution (11.3 kcal mol^{-1}), as opposed to $Lip_{561–587}$ alone (-10.4 kcal mol^{-1}, Table 4.2) and is mainly entropically driven ($T\Delta S = 20.2$ kcal mol^{-1}). The same experiment was repeated with the N-terminally elongated fragment $Lip_{457–587}$ and the C-terminally elongated $DAD_{1145–1209}$ (appendix Figure A.8). Similar to the previous results $Lip_{457–587}$ reduced the binding affinity of $DAD_{1145–1209}$ to $mDia_N$ΔGCC from 14 nM (direct measurement), respectively 3 nM (competitive model) to 23 nM (Table 4.8).

Although, the binding regions of $mDia_{DAD}$ and Liprin-α3 on $mDia_{DID}$ are highly overlapping and the ITC data confirm the influence of Liprin-α3 for the $mDia_{DAD}$ binding, the formation of a putative ternary complex needs to be investigated. Therefore, the content of the ITC sample cell was used for an analytical size exclusion chromatography (SEC) run and further SDS-PAGE analysis (Figure 4.18).

Table 4.8 $mDia_{DAD}$-Liprin-α3 competition ITC measurements. Summary of the ITC competition experiment. (K_D: equilibrium dissociation constant; ΔH: change in reaction enthalpy; ΔS: change in reaction entropy; N: stoichiometry of binding; T: temperature in Kelvin)

interaction		K_D	ΔH	TΔS	N
		nM	*kcal mol^{-1}*	*kcal mol^{-1}*	
without Liprin-α3	$DAD_{1145–1200}$-$mDia_{DID}$	29 ±38	1.8 ± 0.01	11.8	0.8
Liprin 561–587 (one-site model)	$DAD_{1145–1200}$-$mDia_{DID}$ • $Liprin_{561–587}$	155 ±16	11.3 ± 0.1	20.2	0.8
Liprin 561–587 (competitive model)	$DAD_{1145–1200}$-$mDia_{DID}$ • $Liprin_{561–587}$	37 ± 5	6.3 ± 0.1	11.8	0.9
without Liprin-α3	$DAD_{1145–1209}$-$mDia_N$	14 ± 7	5.1 ± 0.1	15.5	0.8
Liprin 457–587 (one-site model)	$DAD_{1145–1209}$-$mDia_N$ΔGCC • $Liprin_{457–587}$	23 ±13	5.6 ± 0.1	15.9	1.0
Liprin 457–587 (competitive model)	$DAD_{1145–1209}$-$mDia_N$ΔGCC • $Liprin_{457–587}$	3 ± 1.6	3.9 ± 0.1	no data	1.0

The loaded sample showed three distinct elution peaks, as visualized by the absorption at 220 and 280 nm. While $mDia_{DAD}$ co-eluted with $mDia_{DID}$ in the first peak, $Lip_{561–587}$ eluted in the second peak. An excess of titrated $mDia_{DAD}$ was visible within the third peak. The same result was observed with the sample of the second ITC competition assay using the fragments $Lip_{457–587}$, $DAD_{1145–1209}$ and $mDia_N$ΔGCC (Figure A.8).

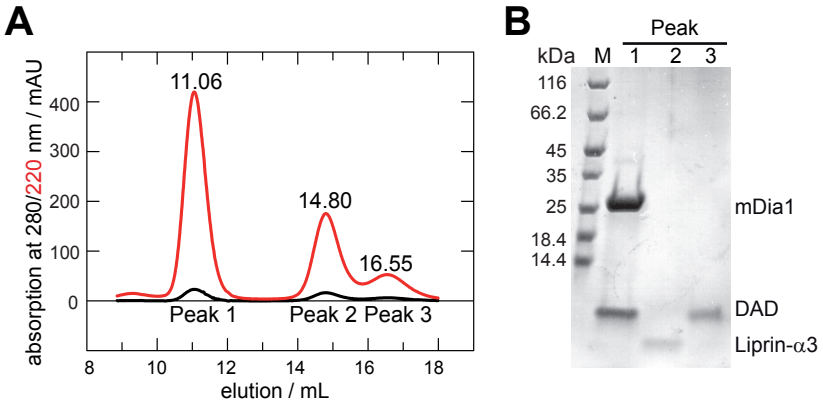

Figure 4.18 Size exclusion chromatography and SDS-PAGE analysis of the putative ternary $mDia_{DID}$ • $Lip_{561–587}$ • $mDia_{DAD}$ complex.
A: The cell content of the ITC measurement from Figure 4.17 B was used for an analytical size exclusion chromatography (SEC) run (S75 10/300). B: The resulting peaks from the SEC were analyzed by SDS-PAGE.

Taken all together, the ITC and SEC data clearly show that $mDia_{DAD}$ can displace Liprin-α3 from mDia1 and not *vice versa*. Liprin-α3 is only able to bind to the open form of mDia1 and is not capable to effectively compete with $mDia_{DAD}$ using these conditions

4.4. Effect of Liprin-α3 on F-actin formation in different cell types

Besides the extensive biochemical and structural characterization of the interactions between Liprin-α3, RhoA and the autoinhibitory regulation of mDia1, the influence of Liprin-α3 on cellular level was of great interest. The functionality of the minimal Liprin-α3 fragments was analyzed by their effect on F-actin formation in mammalian cells. Presence of $Lip_{1–817}$ reduces the cellular Rho-induced F-actin content, as it has been shown by Sakamoto *et al.*.

4.4.1 Transiently transfected HeLa cells

The cellular effect of the different Liprin-α3 fragments was determined by co-expression with active RhoA (RhoA G14V) in HeLa cells (Figure 4.19 A). For the quantification the phalloidin stained filamentous actin (F-actin) of transfected cells was compared to non-transfected cells of the same sample (Figure 4.19 B). As expected the transfection of empty vectors (mock) had no effect on the F-actin content, while overexpressed active RhoA significantly enhanced stress-fiber formation. Additional transfection of full-length Liprin-α3 (Lip_{fl}) had no effect on the increased amount of F-actin. However, co-expression of the fragments Lip_{1-817}, $Lip_{561–587}$ and $Lip_{561–582}$ lead to a significant decrease in the cellular F-actin content compared to the level in RhoA G14V expressing cells. This effect was not observed for $Lip_{567–587}$. To exclude the possibility that the N-terminally truncated $Lip_{567–587}$ fragment is not able to bind mDia1 due to steric interference with the N-terminal mCherry-tag, a polypetide linker (GSGSGS) was added ($Lip_{(3GS)567–587}$). Indeed, the fragment $Lip_{(3GS)567–587}$ exhibited the same actin reducing effect as $Lip_{561-582}$, elucidating the importance of the Liprin-α3 N-terminus for mDia1 binding. In addition to $Lip_{561–587}$ the same construct containing a L580E mutation ($Lip_{561–587}$ L580E) was co-expressed with active RhoA. In accordance with the ITC analysis (Table 4.4) the fragment had no effect on the F-actin content presumably due to its abolished binding to mDia1.

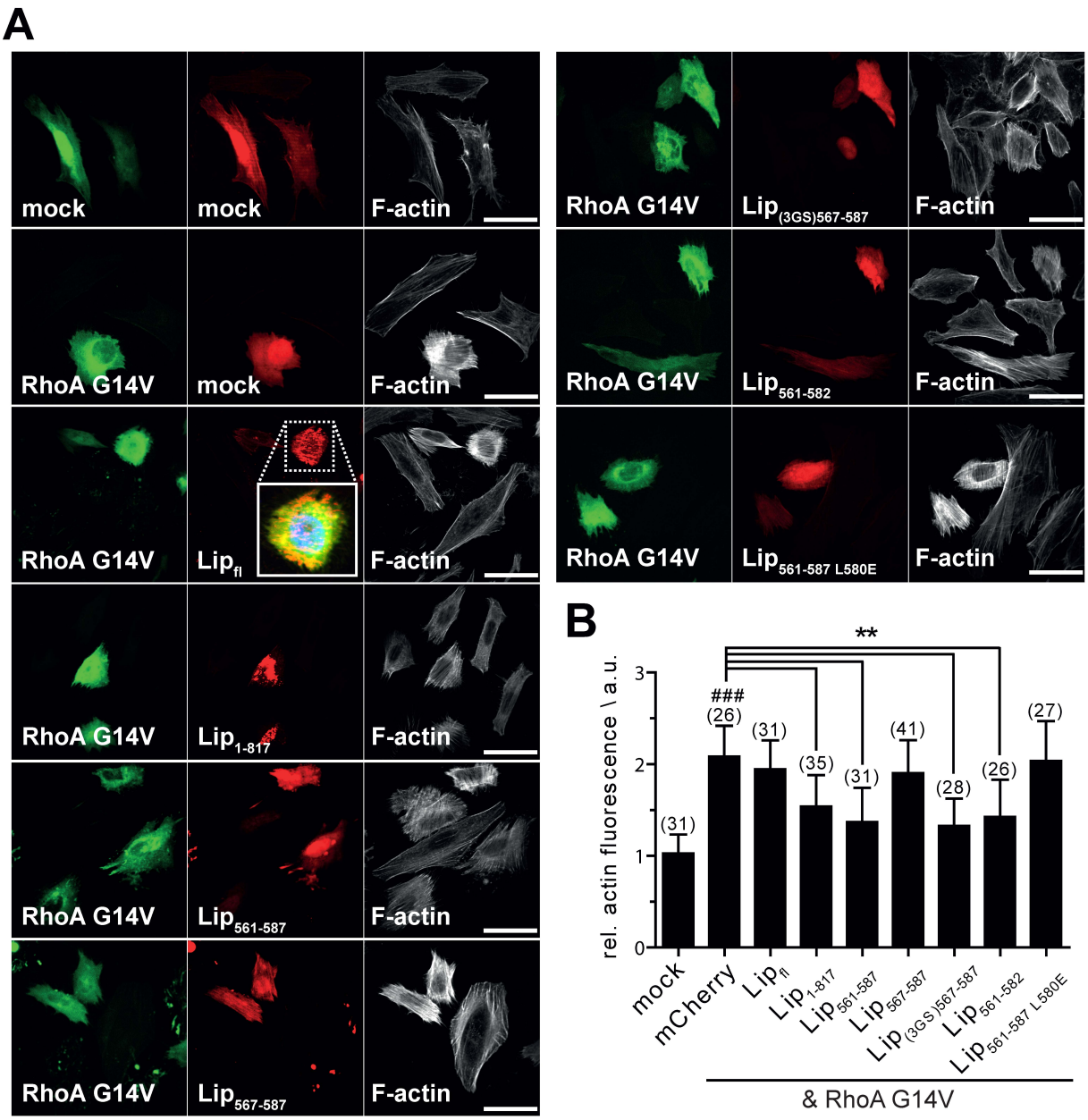

Figure 4.19 The effect of different Liprin-α3 fragments on the amount of F-actin in RhoA overexpressing HeLa cells.
A: HeLa cells were transiently transfected with pEGFP-N3-RhoA (G14V mutant) and mCherry-C1-Liprin-α3 fragments. CF647-phalloidin was used for the staining of filamentous actin and its quantification. The images are shown as single 0.2 µm thick optical sections at the cell bottom. In addition a close up of a single cell transfected with RhoA and full-length Liprin-α3 (Lip_{fl}) is shown as merge image of the DAPI, pEGFP-N3-RhoA and mCherry-C1-Lip_{fl} fluorescence. Scale bars: 50 µm. B: Quantification of the filamentous actin in Hela cells presented as the ratio of transfected to non-transfected cells. Data are shown as mean ± S.D. with the number of counted cells depicted in brackets. The experiment was repeated independently three times. Depicted here is one representative experiment. $^{**}p < 0.01$ for indicated comparison. $^{###}p < 0.001$ compared to mock transfection (one-way ANOVA).

In this experiment overexpressed full-length Liprin-α3 had no visible effect on the F-actin content in HeLa cells. However, Sakamoto *et al.* observed an increase of F-actin, by siRNA induced knock-down of Liprin-α3 in HeLa cells. Therefore, the experiment was repeated with murine neuroblastoma N2a cells, to investigate possible cell-type dependent effects (4.4.2).

4.4.2 Transiently transfected N2a cells

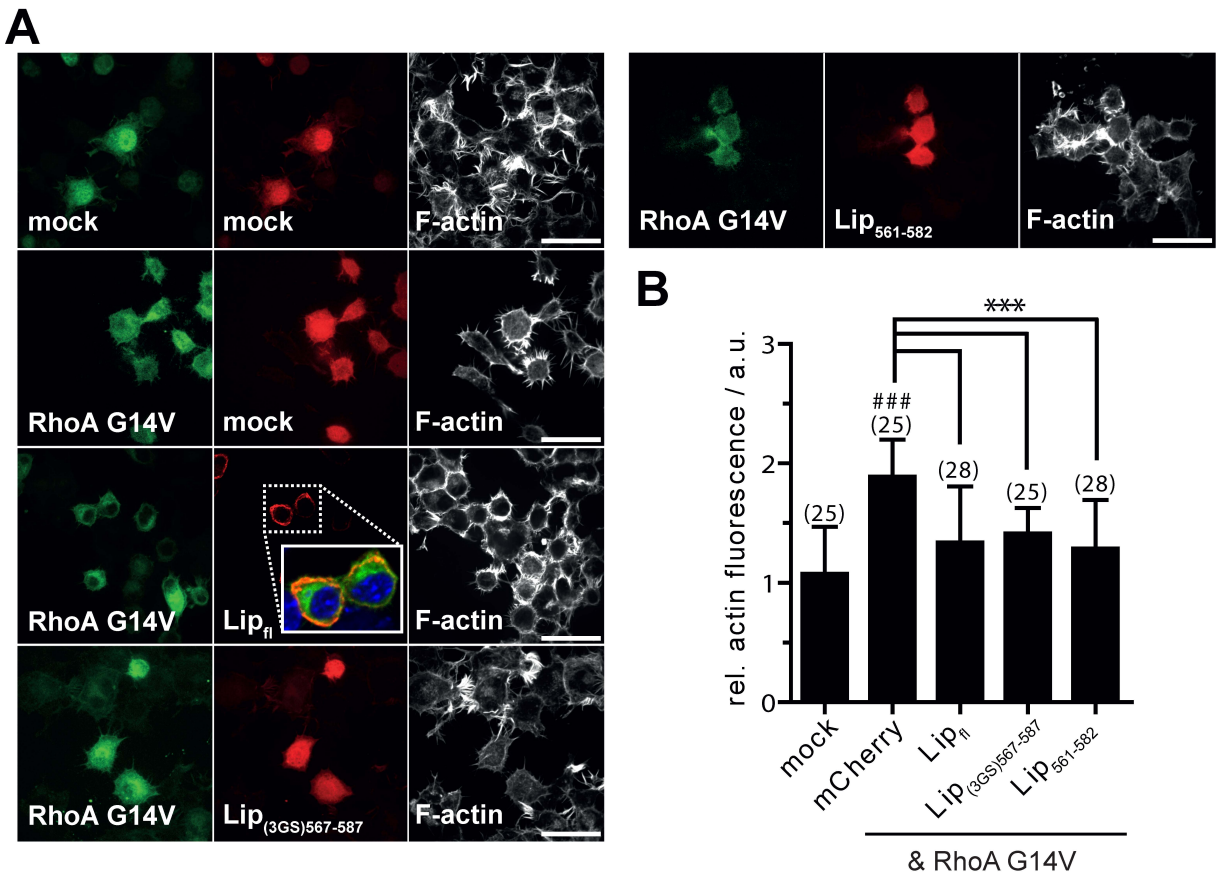

Figure 4.20 The effect of different Liprin-α3 fragments on the amount of F-actin in RhoA overexpressing N2a cells.
A: N2a cells were transiently transfected with pEGFP-N3-RhoA (G14V mutant) and mCherry-C1-Liprin-α3 fragments. CF647-phalloidin was used for the staining of filamentous actin and quantification. The images are shown as a single 0.2 µm thick optical section of the cell bottom. In addition a close up of a cell transfected with RhoA and full-length Liprin-α3 (Lip_{fl}) is shown as merge image of the DAPI, pEGFP-N3-RhoA and mCherry-C1-Lip_{fl} fluorescence. Scale bars: 50 µm. B: Quantification of the filamentous actin in N2a cells presented as the ratio of transfected to non-transfected cells. Data are shown as mean ± S.D. with the number of counted cells depicted in brackets. The experiment was repeated independently three times. Depicted here is one representative experiment. $^{***}p < 0.001$ for indicated comparison. $^{###}p < 0.001$ compared to mock transfection (one-way ANOVA).

Since Liprin-α3 is known to be expressed mainly in neuronal tissues, the effect of different Liprin-α3 fragments on the amount of F-actin in RhoA overexpressing cells was also tested in murine neuroblastoma N2a cells (Figure 4.20). For this reason the Liprin-α3 fragments $Lip_{561–582}$ and $Lip_{(3GS)567–587}$ that showed a reducing effect on F-actin in Hela cells were again co-transfected with active RhoA G14V. Additionally, full-length Liprin-α3 was used, since it displayed no effect on the F-actin content in HeLa cells. Overexpression of active RhoA (RhoA G14V) led to a significant increase of filamentous actin (F-actin) in N2a cells, similar to what have been observed in HeLa cells. Furthermore, co-expression of $Lip_{561–582}$ and $Lip_{(3GS)567–587}$ resulted in a significant reduction of this effect. However, in contrast to the HeLa cells full-length Liprin-α3 had the same reducing effect on the amount of F-actin in N2a cells, as the smaller fragments. This indicates that indeed some cell type depended mechanisms must exist, that bring full-length Liprin-α3 in a state capable of leading to this reduction in the cellular F-actin content. (Figure 4.20).

As a control, the transfection efficiencies and protein expressions for both cell types were analyzed to exclude that the observed effects are induced by differences in protein abundance (Figure 4.21). Both cell types showed a nearly identical transfection efficiency. More than 65 % of the HeLa and N2a cells were transfected with pEGFP-N3-RhoA, while slightly less than 60 % of the cells were additionally transfected with mCherry-C1-Liprin-α3 (Figure 4.21 A). The protein expression levels were controlled by immunoblotting. Transfected cells were blotted and stained against pEGFP or mCherry.

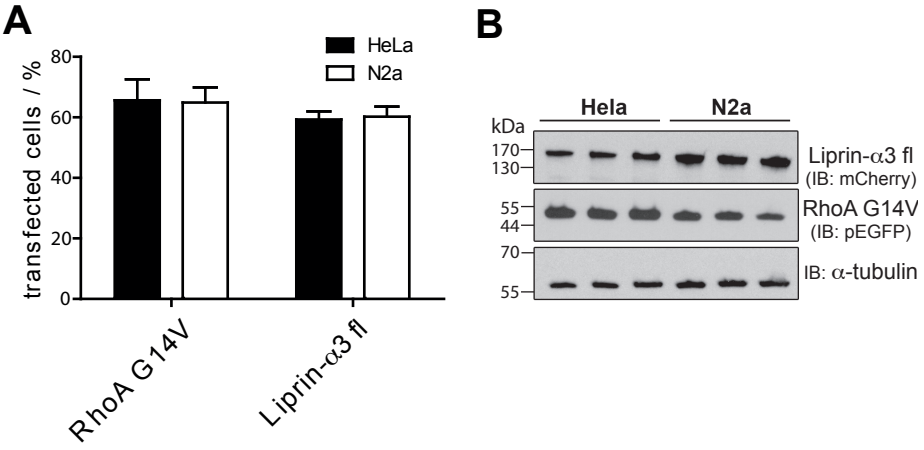

Figure 4.21 Comparison of the transfection efficiency and protein expression levels in HeLa and N2a cells.
A: Transfection efficiency of pEGFP-N3-RhoA and mCherry-C1-Liprin-α3 of three independent experiments. Depicted as mean ± S.D. B: Protein expression levels were analyzed by immunoblotting. Liprin-α3 expression was detected with an anti mCherry antibody, RhoA expression with an anti pEGFP antibody and an antibody against α-tubulin served as loading control.

Equal loading was controlled by SDS-PAGE (data not shown) and by staining against α-tubulin, which has a similar expression in these two cell types (Figure 4.21 B). In both cell types RhoA G14V, as well as Liprin-α3 were expressed substantially and showed only slight differences in their expression level. While RhoA G14V was expressed to a comparable extent, the amount of Liprin-α3 seemed to be marginally higher in N2a cells. Overall, both cell types were equally transfected and displayed a similar amount of expressed Liprin-α3 and RhoA, excluding a systematic influence on the actin cytoskeleton regulation.

4.4.3 Localization of Liprin-α3 fragments in different cell types

Besides the differences in the regulation of the RhoA induced F-actin formation, some variations in the cellular localization of the overexpressed Liprin-α3 fragments could be observed. The N-terminally truncated fragments $Lip_{(3GS)567–587}$ and $Lip_{561–582}$ showed a comparable diffuse cytosolic distribution in N2a and HeLa cells. However, $Lip_{1–817}$ and full-length Liprin-α3 (Lip_{fl}) were evenly clustered throughout the HeLa cells (Figure 4.19 A inset). In contrast, Lip_{fl} displayed an accumulation at the cell periphery in N2a cells (Figure 4.20 inset).

5. Discussion

5.1. Summary of Results

Definition of the binding site

In the first part of this work the binding of mDia1 and Liprin-α3 was characterized using recombinantly expressed proteins and isothermal titration calorimetry (ITC) analyses. Different constructs of mDia1 and Liprin-α3 were cloned, purified and their binding affinities were determined by ITC. Finally, $mDia_{DID}$ and $Lip_{567–587}$ were identified to contain the essential residues needed for the binding. Using these fragments the protein structure of the $mDia_{DID} \bullet Lip_{567–587}$ complex was solved up to a final resolution of 1.65 Å. Based on the structural data the Liprin-α3-core region (LCR), encompassing the amino acids 567–582 was defined. A closer look at the Liprin-α3 fragments used in the ITC studies, revealed that the N-terminally longest fragment $Lip_{217–587}$, forms higher oligomers in solution and binds mDia1 with a stoichiometry of 0.5.

Crystal structure of the $mDia_{DID} \bullet Lip_{567–587}$ complex

The solved crystal structure showed, that Liprin-α3 binds to mDia1 via an α-helix spanning the amino acids 567–582. The binding of the α-helix occurs at the armadillo repeat motifs 3–5. It mainly contacts the third α-helix of ARM5, which is part of the interdomain helix (ID, α17, $\alpha 3^5$), that connects the $mDia_{DID}$ with the dimerization domain (DD). Additionally, superpositions with published mDia1 structures showed, that the binding sites on $mDia_N$ for Liprin-α3 and $mDia_{DAD}$ are highly overlapping, whereas the binding of RhoA to mDia1 occurs at a distinct non-overlapping region.

Interplay of Liprin-α3, RhoA and $mDia_{DAD}$

ITC competition assays were used to study, whether the presence of Liprin-α3 interferes with the binding of $mDia_{DAD}$ and RhoA to $mDia_N$. Liprin-α3 decreased the binding of RhoA to $mDia_N$ by 10–15 fold, whereas the binding of $mDia_{DAD}$ was only reduced by 3–4 fold. The reduced binding affinity of RhoA in presence of Liprin-α3 is mainly mediated by the slower RhoA-$mDia_N$ association rate, as determined by stopped-flow

measurements. Formation of possible ternary complexes were analyzed by analytical size exclusion chromatography for $mDia_{DAD}$ and by fluorescence polarization assays for RhoA. The data clearly showed, that RhoA and $mDia_{DAD}$ are able to dissociate Liprin-α3 from $mDia_N$.

Effect of the different Liprin-α3 fragments on F-actin formation in cells.

Different fragments of Liprin-α3, including Lip_{fl} and $Lip_{567–587}$ were co-transfected with active RhoA in HeLa cells and the mouse neuroblastoma cell line N2a. Except for full-length Liprin-α3, all tested fragments showed a significant reduction of the F-actin content in HeLa and N2a cells. Lip_{fl} had no effect on the amount of F-actin in HeLa cells, but reduced the amount of F-actin in N2a cells. In N2a cells overexpressed full-length Liprin-α3 accumulated near the plasma membrane, whereas in HeLa cells it was clustered throughout the cells.

5.2. Binding specificity of the mDia1-Liprin-α3 interaction

Sakamoto *et al.* used pull-down assays to identify all three isoforms of mDia as potential binding partners of Liprin-α1 and Liprin-α3. Using ITC analysis the binding of mDia1 to Liprin-α3 could be confirmed in this study, whereas no binding was detected for mDia2. The crystal structure of the $mDia_{DID} \bullet Lip_{567–587}$ complex presented here, allows a detailed comparison of the interaction regions, resulting in the identification of possible binding determinants within the mDia and Liprin isoforms. The $mDia_{DID}$ of the isoforms is highly conserved, though some differences of mDia1 towards mDia2 and mDia3 can be detected (Figure 4.10). Several positively charged amino acids of mDia2 and mDia3 are substituted by neutral amino acids in mDia1. The single mutation of K369 in mDia2 to the corresponding cysteine in mDia1 did not to lead to an alteration of the Liprin-α3 binding specificity and as a consequence to binding of Liprin-α3 to mDia2. This lysine is facing towards the binding interface, but it does not seem to be the only specificity determinant. Distinct differences in the electrostatic surface potential at the Liprin-α3 interacting site of mDia1 might be the reason why Liprin-α3 binding is specific for mDia1, whereas it is not binding to mDia2 or presumably mDia3.

The sequences of the different Liprin-α isoforms are highly conserved in the N-terminal half of the Liprin-α3-mDia1 interacting region (aa 567–576). This also includes some of the amino acids involved in the binding of Liprin-α3 to mDia1, *e.g.* R572. Overall, the Liprin-α1 fragment displays the most conserved N-terminal consensus sequence

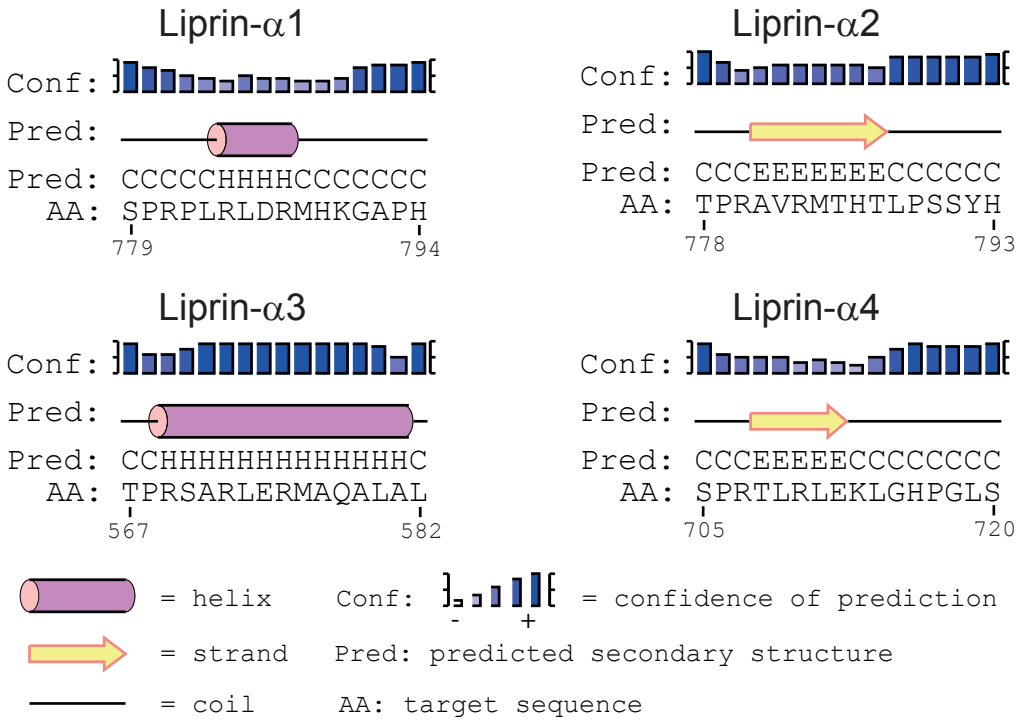

Figure 5.1 Secondary structure predictions of the mDia1-binding region of Liprin-α isoforms.
Fragments of the mouse Liprin-α isoforms (aa 567–582 in Liprin-α3) were analyzed concerning their potential to form secondary structures. Predictions were performed using the PSIPRED server (Buchan *et al.*, 2013).

with Liprin-α3. However, the C-terminal residues of the mDia1 interaction region are quite diverse in the different Liprin-α isoforms. Especially, L580 which has been shown to mediate important hydrophobic interactions with A256 and Q307 of mDia1 is exclusively present in Liprin-α3. Additionally, secondary structure predictions using the PSIPRED server (Buchan *et al.*, 2013) of the corresponding $Lip_{567–582}$ regions of all Liprin-α isoforms, display striking differences in the formation of secondary structures (Figure 5.1). The fragments of Liprin-α2 and -α4 are predicted to form short β-helices, while Liprin-α1 and -α3 fragments most likely form α-helical structures. Interestingly, the predicted α-helix of Liprin-α1 spans only four amino acids, while the predicted and structurally confirmed α-helix of Liprin-α3 consists of more than 12 amino acids. Based on the differences of the Liprin-α isoforms, regarding their sequence and predicted secondary structures, binding of Liprin-α2 and -α4 to mDia1 can be excluded. In the case of Liprin-α1 the binding to mDia1 seems to be unlikely. Either way, it can be assumed that the interaction of Liprin-α1 with mDia1 is at least distinctly weaker compared to the Liprin-α3, making a physiological relevance less likely. Since Liprins can form hetero- and homooligomers the detected binding of Liprin-α1 to mDia1 in pull-down experiments (Sakamoto *et al.*, 2012a) could also reflect indirect interactions.

Moreover, these data provide no information about possible mDia1 binding sites on Liprin-α1, or -α2 and α4, that are distinct from the region identified for Liprin-α3. Therefore, the binding of Liprin-α1 and mDia1 needs to be confirmed by more direct *in vitro* assays, such as ITC.

5.3. Liprin-α3 interferes with $mDia_{DAD}$ and RhoA binding

5.3.1 Interplay of $mDia_{DAD}$ and Liprin-α3

The crystal structure of $mDia_{DID}$ • $Lip_{567–587}$ presented here, reveals that the binding site of $Lip_{567–587}$ on mDia1 is highly overlapping with the binding region of the DAD-core-region (DCR, aa 1175–1195). Both peptides bind to mDia1 along the negatively charged ID, which has also been confirmed by mutational ITC studies. The opposite charge mutations of E358R and E362R at the ID, that abolished the binding towards Liprin-α3, have also been shown to decrease the binding to $mDia_{DAD}$ (Lammers *et al.*, 2008).

In their study Sakamoto *et al.* postulated that $Lip_{457–747}$ can displace the DAD-core region (DCR, aa 1175–1195) from $mDia_N$. As judged by ITC studies, the DCR binds to $mDia_N$ with an affinity of 15 µM (Lammers *et al.*, 2005). However, the importance of the adjacent DAD-basic-region (DBR, aa 1196–1209) has been shown by previous ITC and cell culture experiments. ITCs with $mDia_{DAD}$ including the complete DBR resulted in three orders of magnitude increased binding affinities towards $mDia_{DID}$. Additionally, deletion and mutation studies of the DBR emphasized its importance for actin filament formation and indicated the requirement of the DBR for the autoinhibitory regulation of mDia1 (Wallar *et al.*, 2006). In this study the physiological more relevant $mDia_{DAD}$ constructs $DAD_{1145–1200}$ and $DAD_{1145–1209}$ were used to analyze their impact on the autoregulatory interactions of mDia1. The performed ITC competition assays show, that Liprin-α3 is not able to dissociate $DAD_{1145–1200}$ or $DAD_{1145–1209}$ from $mDia_{DID}$. In contrast, $DAD_{1145–1200}$ and $DAD_{1145–1209}$ were successfully used to displace Liprin-α3 from $mDia_{DID}$. Furthermore, the binding affinity of $mDia_{DAD}$ to $mDia_{DID}$ was only slightly decreased in presence of Liprin-α3. In this work the interactions between $mDia_{DID}$ and $mDia_{DAD}$ were investigated *in vitro* with intermolecular fragments. Considering the intramolecular interactions occurring *in vivo*, the actual autoinhibitory potential of mDia1 might be even more efficient. This further emphasizes a rather low capacity of Liprin-α3 to compete with $mDia_{DAD}$ for $mDia_{DID}$ binding and indicates, that Liprin-α3 preferentially binds to the open conformation of mDia1.

Interestingly, the residues 583–587 of Lip$_{567–587}$, that were not visible in the crystal structure, N-567-TPRSARLERMAQALA**LQAGSP**-587-C, are a perfect match for the C-terminus of the consensus sequence defined for the DCR (aa: 1175–1196) N-(G/A)(V/A)MDXLLEX**L(K/R/Q)X(G/A)(S/G/A)(A/P)**-C. However, these fragments of Liprin-α3 and mDia$_{DAD}$ align to mDia$_N$ in the opposite direction (Figure 4.12 A). As shown by ITC analysis the residues 583–587 of Liprin-α3 do not contribute to the binding of mDia1 and might therefore fulfill a different function, *e.g.* acting as a recognition site for other proteins. Whether this is of any physiological relevance, needs further investigations.

5.3.2 Possible mechanisms leading to the displacement of Liprin-α3 from mDia1 by RhoA

The data presented in this work show that the binding affinity of RhoA to mDia$_N$ is decreased by 10–15 fold in the presence of Liprin-α3, and that RhoA is able to displace Liprin-α3 from mDia$_N$, *i.e.* no ternary mDia$_N$-RhoA-Liprin-α3 complex can be formed. Based on the structure of the mDia$_{DID}$ • Lip$_{567–587}$ complex presented here, it is not obvious how Lip$_{567–582}$ interferes with RhoA binding and how it is displaced from mDia$_{DID}$, since both use completely distinct binding sites. Additionally, it remains unclear how Liprin-α3 is able to weaken the binding affinity of RhoA by 10–15 fold, despite the three orders of magnitude higher binding affinity of RhoA to mDia1. These data suggest an allosteric displacement mechanism of Liprin-α3 from mDia1 by RhoA. Two different mechanisms, that are not mutually exclusive, how RhoA displaces Liprin-α3 from mDia1 seem to be possible.

The first mechanism involves the conformational flexibility within the C-terminal half of the mDia1 interdomain helix (ID) and the dimerization domain (DD). Superpositions of mDia$_{DID}$ derived from several mDia$_N$ crystal structures, either in the uncomplexed form (PDB: 2BNX), or in complex with RhoC (PDB: 1Z2C), mDia$_{DAD}$ (PDB: 2BAP) or Lip$_{567–587}$ (PDB: 4UWX), display conformational differences (Figure 5.2). The different structures are highly similar regarding mDia$_{DID}$. However, structural differences upon binding of mDia$_{DAD}$ and RhoA to mDia1 are visible in the ID and the following DD. Although, the C-terminal half of the ID and the DD are not existent in the mDia$_{DID}$ • Lip$_{567–587}$ structure presented here, the data show that Liprin-α3 aligns along the ID forming salt bridges to acidic residues in the ID. Binding of RhoA to mDia1 might lead to alterations in the conformation of the ID/DD, which subsequently could interfere with Liprin-α3 binding and thereby support the allosteric dissociation of Liprin-α3 from mDia1.

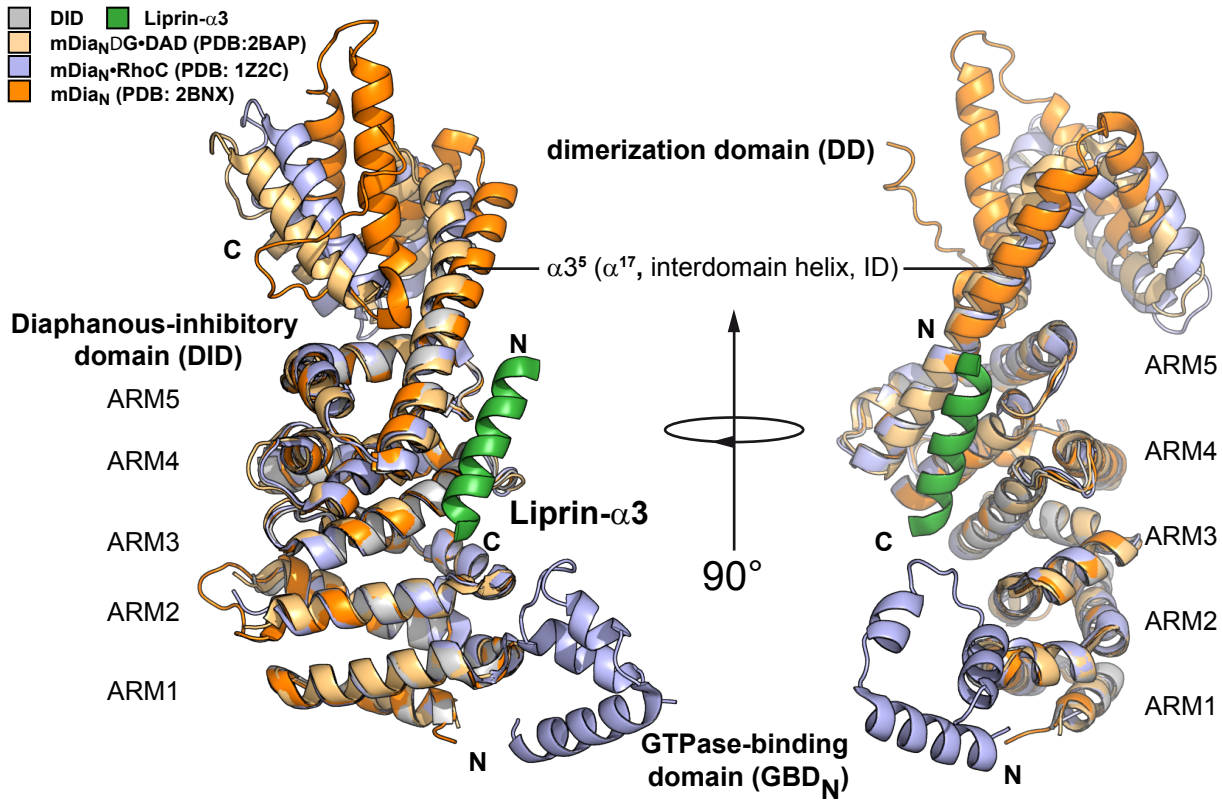

Figure 5.2 Structural comparison of the mDia$_N$ in complex with different interaction partners.
The depicted mDia domains of mDia$_N$ • RhoC (PDB: 1Z2C), mDia$_N$ΔG • mDia$_{DAD}$ (PDB: 2BAP), mDia$_N$ (PDB: 2BNX) and mDia$_{DID}$ • Lip$_{567–587}$ (PDB: 4UWX) were superposed on mDia$_{DID}$ (aa 135–369). The root mean square deviations were within a range of 0.401–0.583 Å for the peptide backbone and 0.367–0.541 Å for the Cα-atoms, displaying the high similarities in the mDia$_{DID}$. Structural differences can be observed in the interdomain helix (ID) and the following dimerization domain (DD, aa 370–451).

The second possible mechanism that could explain the displacement of Liprin-α3 from mDia1 by RhoA is based on the electrostatic interactions between RhoA and mDia$_N$. In presence of Liprin-α3 the association rates of RhoA and mDia1 were reduced, whereas the dissociation rates were nearly unaffected, under the conditions tested. Earlier studies implicated the importance of electrostatics for the association rates in protein complex formation, *e.g.* for the interaction of Raf-RBD and Ras (Sydor *et al.*, 1998; Vijayakumar *et al.*, 1998). A similar effect was also observed with the opposite charge mutation K133E in the Rho-insert helix, which reduced the association rate of RhoA to mDia$_N$ (Lammers *et al.*, 2008). Liprin-α3 binds to mDia$_{DID}$ at a highly negatively charged patch along the ID. In complex with mDia$_N$ the positively charged insert helix of RhoA is in close proximity to this patch (Figure 5.3). Taken together, presence of Liprin-α3 could lead to a reduced electrostatic attraction of RhoA by mDia1, resulting in a slower association.

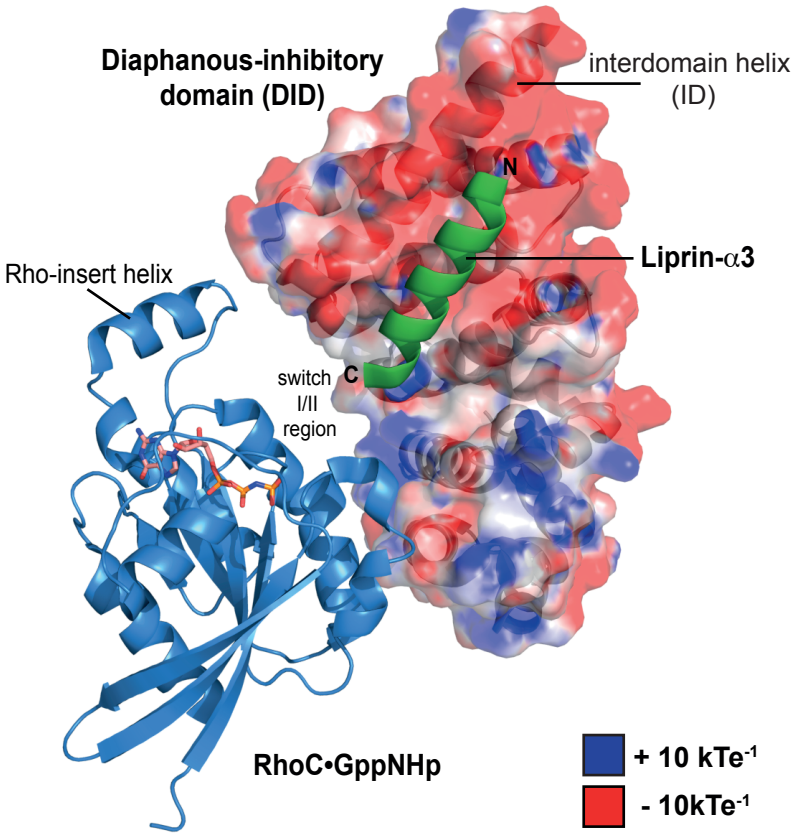

Figure 5.3 Electrostatic surface potential of mDia$_{DID}$ in a putative ternary complex with RhoC and Liprin-α3.
The mDia$_{DID}$ • Lip$_{567–587}$ structure (PDB: 4UWX) is shown together with RhoC from the mDia$_N$ • RhoC complex (PDB: 1Z2C). In addition the electrostatic surface potential of mDia$_{DID}$ is plotted onto the surface. Liprin-α3 interacts with the negatively charged groove on the mDia$_N$ surface, which is also in interaction distance of the Rho-insert helix. The shown electrostatic surface potential of mDia$_{DID}$ was generated using the Adaptive Poisson-Boltzmann Solver (APBS). Blue represents a positive and red a negative charge. Scaled from -8 to +8 kTe^{-1}.

RhoA has a bipartite binding site on mDia1 and the measured association rates were 2–3 orders of magnitude lower than expected for a diffusion controlled reaction. Based on this at least a two-step binding mechanism can be assumed (5.1). Similar mechanisms have also been postulated for the dissociation of mDia$_{DAD}$ from mDia$_{DID}$ by RhoA (Rose *et al.*, 2005) and the nucleotide exchange of Ras-like proteins by guanine-nucleotide exchange factors (Vetter & Wittinghofer, 2001).

$$mDia_N \bullet Liprin_T + RhoA \underset{k_{-1}}{\overset{k_{+1}}{\rightleftharpoons}} mDia_N \bullet Liprin_T \bullet RhoA_L \underset{k_{-2}}{\overset{k_{+2}}{\rightleftharpoons}} mDia_N \bullet RhoA_T + Liprin \tag{5.1}$$

with T = tight and L = loose

In accordance to a two-step binding mechanism, Liprin-α3 forms tight complex with $mDia_N$. During the initial binding step active RhoA forms a loose contact with the GTPase-binding domain of $mDia_N$ (GBD_N), which is not influenced by the presence of Liprin-α3. Subsequently, RhoA binds to the armadillo repeat region of $mDia_N$ ($mDia_{DID}$) with residues from switch I/II and the Rho-insert helix. This would result in a tight association of RhoA to $mDia_N$ and finally to the dissociation of Liprin-α3 from $mDia_{DID}$.

5.4. Regulation of the inhibitory potency of Liprin-α3

While the overexpression of the smallest Liprin-α3 fragments reduced the amount of F-actin in HeLa and N2a cells, full-length Liprin-α3 exclusively displayed this actin reducing effect in neuroblastoma cells (N2a). This indicates that cell-type dependent mechanisms must exist to bring full-length Liprin-α3 into a state capable of mDia1 binding and inactivation. Furthermore, overexpressed full-length Liprin-α3 was localized at the plasma membrane of N2a cells, whereas it was clustered in the cytosol of HeLa cells. A similar distribution was also detectable for the C-terminally truncated fragment $Lip_{1–817}$ in HeLa cells. In contrast, all N-terminally truncated Liprin-α3 fragments tested, showed a diffuse cytosolic distribution. Taken together these data point out the importance of the Liprin-α3 N-terminus for its regulation and that additional events must occur *in vivo*, localizing Liprin-α3 at the cell periphery. This assumption is further supported by the *in vitro* characterization of the different Liprin-α3 fragments. In comparison to the shorter fragments, the N-terminally longest fragment, $Lip_{217–587}$, bound mDia1 with a 2–3 fold reduced affinity, as determined by ITC. Additionally, the stoichiometry for this reaction was 0.5 (N = 1.0 for N-terminally truncated fragments), indicating that one mDia1 molecule bound two Liprin-α3 fragments. The effect was independent of the oligomeric state of the mDia1 fragments, since it was observed using the $mDia_{DID}$ monomer ,as well as the dimeric $mDia_NCC$ fragment. In accordance to this, the size exclusion chromatography analysis indicate a higher oligomeric state of $Lip_{217–587}$ compared to the shorter fragment analyzed. Furthermore, $Lip_{217–587}$ induced the lowest reduction of the RhoA-$mDia_N$ association rate in the stopped-flow experiments. Hence, it can be assumed that the N-terminus of Liprin-α3 mediates the homooligomerization, which leads to the masking of one mDia1 binding site. The functional importance of the N-terminus for Liprin-α3 oligomerization and the corresponding physiological influence has also been investigated for the role of Liprin-α3 during the presynaptic assembly in *C. elegans* (Taru & Jin, 2011).
Besides the oligomeric state of Liprin-α3, additional events that regulate the localization seem to be important for its functionality. The recruitment of Liprin-α3 to the

plasma membrane in N2a cells is most likely induced by proteins of the leukocyte common antigen-related (LAR) family of transmembrane protein tyrosine phosphatases. These proteins, which also led to the discovery of Liprins, are an integral component of the plasma membrane and are mainly expressed in neuronal tissues. The binding of Liprins to the cytoplasmic phosphatase domain of the transmembrane tyrosine phosphatase occurs via the C-terminus of Liprins (Pulido *et al.*, 1995), which was missing in the shorter Liprin-α3 fragments tested. One possible result of the receptor binding could be the dissociation of Liprin-α3 oligomers, which might unmask binding sites for mDia1. Another consequence of the recruitment of Liprin-α3 to the plasma membrane is the increase in its local subcellular concentration. Thereby, Liprin-α3 would be able to compete more efficiently with other proteins for mDia1 binding.

Another regulatory mechanism of Liprin-α3 that has been investigated for the first time in this work is its phosphorylation at the conserved T567. This site has been identified by mass spectrometry to be phosphorylated in human Liprin-α3. ITC studies with the phosphomimetic mutant $Lip_{567–587}$ T567E showed an approximately sixfold reduced affinity to $mDia_{DID}$. This effect might be even stronger *in vivo* using the phosphorylated tyrosine, instead of the mimetic mutant. Since, this site is conserved throughout many organisms it is most likely that phosphorylation events at this site play an important role in the regulation of Liprin-α3. Further studies are needed to show how this phosphorylation is spatially and temporally regulated *in vivo* and to find out which kinases and phosphatases are involved.

5.5. Mechanisms explaining the inhibition of F-actin formation by Liprin-α3

The recruitment of further regulatory proteins by Liprin-α3, such as RhoGAPs has been postulated as a possible mechanism, that explains the inhibitory effect of Liprin-α3 on the F-actin formation (Sakamoto *et al.*, 2012b). It has been reported, that the *Xenopus* Liprin xKazrinA binds to RhoGAP p190B (Cho *et al.*, 2010). A similar interaction has also been identified between the *C. elegans* Liprin Syd-2 and Syd-1, a protein containing a Rho-GTPase-like activating domain (Hallam *et al.*, 2002). Admittedly, interactions between Liprins and RhoGAPs have not been shown in mammals so far. The recruitment of RhoGAPs by Liprin-α3 could lead to an enhanced hydrolysis of the bound nucleotide and thereby inactivation of the Rho protein and its subsequent displacement from mDia1. In the experiments conducted in this work even the shortest Liprin-α3 fragments, containing only the essential amino acids needed for the binding of mDia1, had the same effect on the amount of cellular F-actin as longer

fragments. Based on their small size it is unlikely that these fragments are able to recruit further regulatory proteins to mDia1. Therefore, the observed reduction in the amount of cellular F-actin induced by short Liprin-α3 fragments must be regulated by other mechanisms. However, it is still likely and not excluded from these data, that full-length Liprin-α3 recruits other proteins to mDia1 *in vivo*.

The shortest Liprin-α3 fragment, that displayed an F-actin reducing effect in cells was $Lip_{576–582}$ (LCR). This fragment is not capable to sterically interfere with the catalytic FH1 and FH2 domains of mDia1, when it is bound to $mDia_{DID}$. Therefore, the F-actin reducing effect of the short Liprin-α3 fragments in HeLa and N2a cells must be directly connected to the $mDia_{DID}$ binding. Different mechanisms how the presence of Liprin-α3 downregulates the function of mDia1 and constrains the activation by RhoA are highlighted hereafter and are also summarized in Figure 5.4.

Firstly, the presence of Liprin-α3 alters the autoinhibitory regulation of mDia1 by shifting the equilibrium of RhoA and $mDia_{DAD}$ for $mDia_N$ binding into the direction of $mDia_{DAD}$. RhoA binds to $mDia_N$ with a slightly higher affinity ($K_D = 4$ nM), compared to $DAD_{1145–1209}$ ($K_D = 3–14$ nM). In presence of Liprin-α3 the binding affinity of RhoA to $mDia_N$ is more strongly reduced (10–15 fold to 40–60 nM), compared to $DAD_{1145–1209}$ (3–4 fold to 23 nM). As a result, $mDia_{DAD}$ has a higher potential than RhoA to bind to $mDia_N$, supporting the re-establishment of the autoinhibited state.

Secondly, it has been shown, that RhoGAPs bind to GTP loaded RhoA with an affinity in the low nanomolar range (Graham *et al.*, 1999). The 10–15 fold reduced binding affinity of RhoA to mDia1, in presence of Liprin-α3 might lead to a more sufficient competition of regulatory proteins such as RhoGAPs. Presence of Liprin-α3 could support the inactivation of RhoA and subsequently lead to the inactivation of mDia1. A similar effect might occur for $mDia_{DAD}$. The interaction of the C-terminal region of mDia1 with PIP_2 at the plasma membrane has been shown to inhibit the mDia1 mediated F-actin formation (Ramalingam *et al.*, 2010). It has been postulated that the inhibition of mDia1 is mediated by blocking the interaction of the FH2 domain with actin subunits, leading to decreased actin nucleation and polymerization. In the Liprin-α3 bound state the competitive binding potency of $mDia_{DID}$ for $mDia_{DAD}$ decreases, which could support the interaction of $mDia_{DAD}$ with PIP_2. This would lead to an altered inhibition mechanism of mDia1 due to an enhanced insertion of its C-terminus into the plasma membrane.

Thirdly, Liprin-α3 can interfere with other proteins that have been reported to bind to the $mDia_{DID}$. Sakamoto *et al.* showed, that the binding of Liprin-α3 to $mDia_N$ leads to the translocation of mDia1 from the plasma membrane. For example, IQGAP1 has been reported to recruit mDia1 to the plasma membrane in phagocytic cups, by binding to $mDia_{DID}$ (Brandt *et al.*, 2007). Additional proteins that are identified to bind to $mDia_{DID}$-DD and are reported to be involved in the localization of mDia1 are

Neurochondrin, Abi, Anillin and the recently identified F-Bar protein CIP4/Toca-1 (Ryu *et al.*, 2009; Schwaibold & Brandt, 2008; Watanabe *et al.*, 2010; Yan *et al.*, 2013). These proteins might also recruit further regulatory proteins to mDia1. In the case of Anillin it has been shown, that it interacts with RhoA (Piekny & Glotzer, 2008). Thus, binding of Liprin-α3 to $mDia_{DID}$ might interfere with a range of mDia1 regulating events, possibly enhancing the inhibitory potential of Liprin-α3.

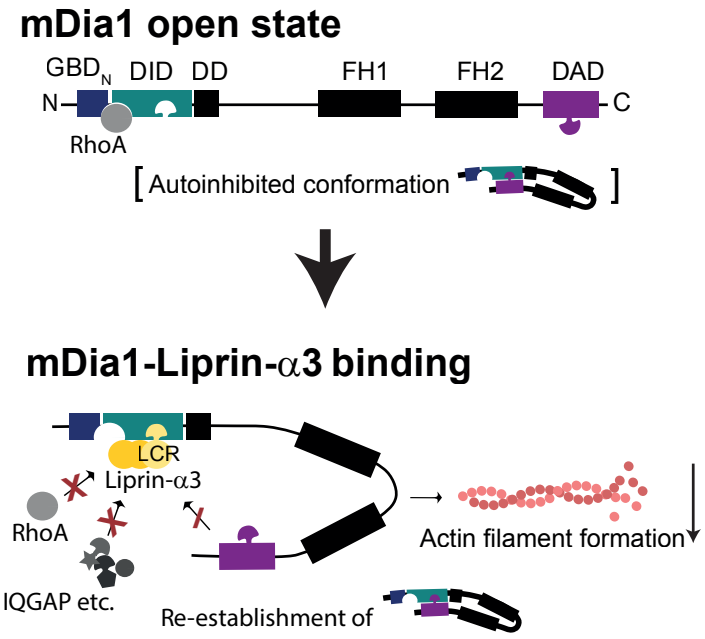

Figure 5.4 Model for the inhibition of mDia1 function by Liprin-α3. The Liprin-core-region (LCR, aa 567–582) binds to $mDia_{DID}$ only in the open state of the formin. In presence of Liprin-α3 the binding affinity of $mDia_{DAD}$ to $mDia_N$ is more efficiently reduced than RhoA binding. Thereby, the re-establishment of the autoinhibited conformation is supported. Furthermore, blocking of the $mDia_{DID}$ binding interface for other proteins, such as IQGAPs could interfere with the membrane localization of mDia1. Additionally, other Rho regulatory proteins, such as RhoGAPS could be recruited by Liprin-α3, leading to RhoA inactivation and dissociation from $mDia_N$ (not shown in the model). The simplified model does not include the dimeric state of mDia1 and oligomeric states (homo- and heterooligomers) of Liprin-α3.

5.6. Physiological relevance of the mDia1-Liprin-α3 interaction

The regulation of synapse morphogenesis by Liprins (Dliprin-α) and the receptor protein tyrosine phosphatase (Dlar) has been firstly described in *Drosophila* (Kaufmann *et al.*, 2002). Further studies showed that the Dlar induced modulation of synaptic actin is linked to Diaphanous-related formins (DRFs) (Pawson *et al.*, 2008). As shown in this study and by Sakamoto *et al.*, Liprin-α3 is able to directly regulate the activity of mDia1 and thereby the formation of cellular F-actin. Hitherto, the interactions of Liprins and DRFs have been exclusively described in neuronal cells. Primarily mDia1 has been described for the formin induced regulation of actin in a neuronal context

(Arakawa *et al.*, 2003). Taken together, the inhibition of formins by Liprin-α3 seems to display an exclusive mechanism for mDia1 regulation, that is specific for neuronal cells and tissues. This is further supported by the already highlighted binding specificity of mDia1 and Liprin-α3, which is mainly expressed in neuronal cells.
Although the postulated models (5.5) explain how Liprin-α3 might exert the inhibitory effect on F-actin formation, some general questions remain unanswered. Taken the much higher affinities of $mDia_{DAD}$ and RhoA for $mDia_N$ it is not obvious how Liprin-α3 can bind to mDia1 in the first place. The ITC competition analyses performed in this study support the postulated idea, that Liprin-α3 preferentially binds to mDia1 in the open conformation (Sakamoto *et al.*, 2012a). This indicates, that additional cellular mechanisms must exist holding the formin in an open conformation even if RhoA is released. In line with this, *in vitro* actin polymerization assays showed, that mDia1 is only partially activated by RhoA (Maiti *et al.*, 2012). Current models postulate an interaction of the mDia1 N-terminus with the negatively charged PIP_2, following the RhoA mediated recruitment of mDia1 to the plasma membrane. Subsequently, binding of scaffold proteins, such as IQGAP, to $mDia_{DID}$ further strengthen the interaction of the N-terminus with the plasma membrane. Finally, the C-terminus of mDia1 also clusters PIP_2, resulting in its insertion into the lipid bilayer and the inhibition of formin induced actin polymerization (Ramalingam *et al.*, 2010). Hitherto, no mechanisms are known, that keep cytosolic mDia1 in an open conformation. Taken together with the periphery localization of full-length Liprin-α3 in N2a cells, this indicates that the binding of Liprin-α3 to mDia1 is spatially restricted to the plasma membrane.
Binding of Liprin-α3 to mDia1 could aid in the establishment of an inactive pool of mDia1, that might either still be bound to the plasma membrane or gets translocated to the cytoplasm. Sakamoto *et al.* showed that Liprin-α3 induces the translocation of $mDia_N\Delta GCC$ (aa 135–570) from the plasma membrane. However, in their experiment Sakamoto *et al.* did not take into account the far N- and C-terminus of mDia1, which also strongly contribute to the localization of mDia1. In further studies it should be investigated whether Liprin-α3 can also interfere with RhoA independent mechanisms that localize full-length mDia1 at the plasma membrane, *e.g.* the interactions of IQGAP, Anillin, Toca-1 or Neurochondrin with mDia1 or the insertion of the N-terminal domain into the lipid bilayer.

5.7. Conclusion and Outlook

In a comprehensive, functional and structural study the interaction of Liprin-α3 with mDia1 and the interplay with RhoA and $mDia_{DAD}$ were analyzed. It was shown that Liprin-α3 is able to reduce the binding of both, $mDia_{DAD}$ and RhoA, to $mDia_{DID}$. Moreover, cell culture experiments showed, that the minimal mDia1-binding Liprin-α3 peptide (Liprin-core region, LCR) is able to reduce the amount of cellular F-actin. Additionally, the presented data highlight the importance of the oligomeric state of Liprin-α3 and indicate a possible regulation by phosphorylation.
Although, the results from this study can explain the fundamental mechanisms of how mDia1 function is inhibited by Liprin-α3, succeeding studies are needed to investigate the regulation under physiological conditions. The local concentration, the regulation via post-translational modifications and the localization of the interaction partners can influence the interplay mechanistically. Further experiments might answer how Liprin-α3 is able to bind to mDia1 in the first place and in which sequential order the activation by RhoA, inhibition by $mDia_{DAD}$ and binding of Liprin-α3 to mDia1 occur. Super-resolution microscopy and FRET assays might aid in answering these questions and could give further insights into the impact of Liprin-α3 on the localization and autoinhibition of mDia1 in cells.
This study elucidates, that besides functioning as a scaffold protein Liprin-α3 is also involved in the regulation of the actin cytoskeleton. The results of this study could be of therapeutic interest, since they might display new possibilities to regulate F-actin formation during processes such as metastasis or tumor invasions, by specific inhibition of formins.

A. Appendix

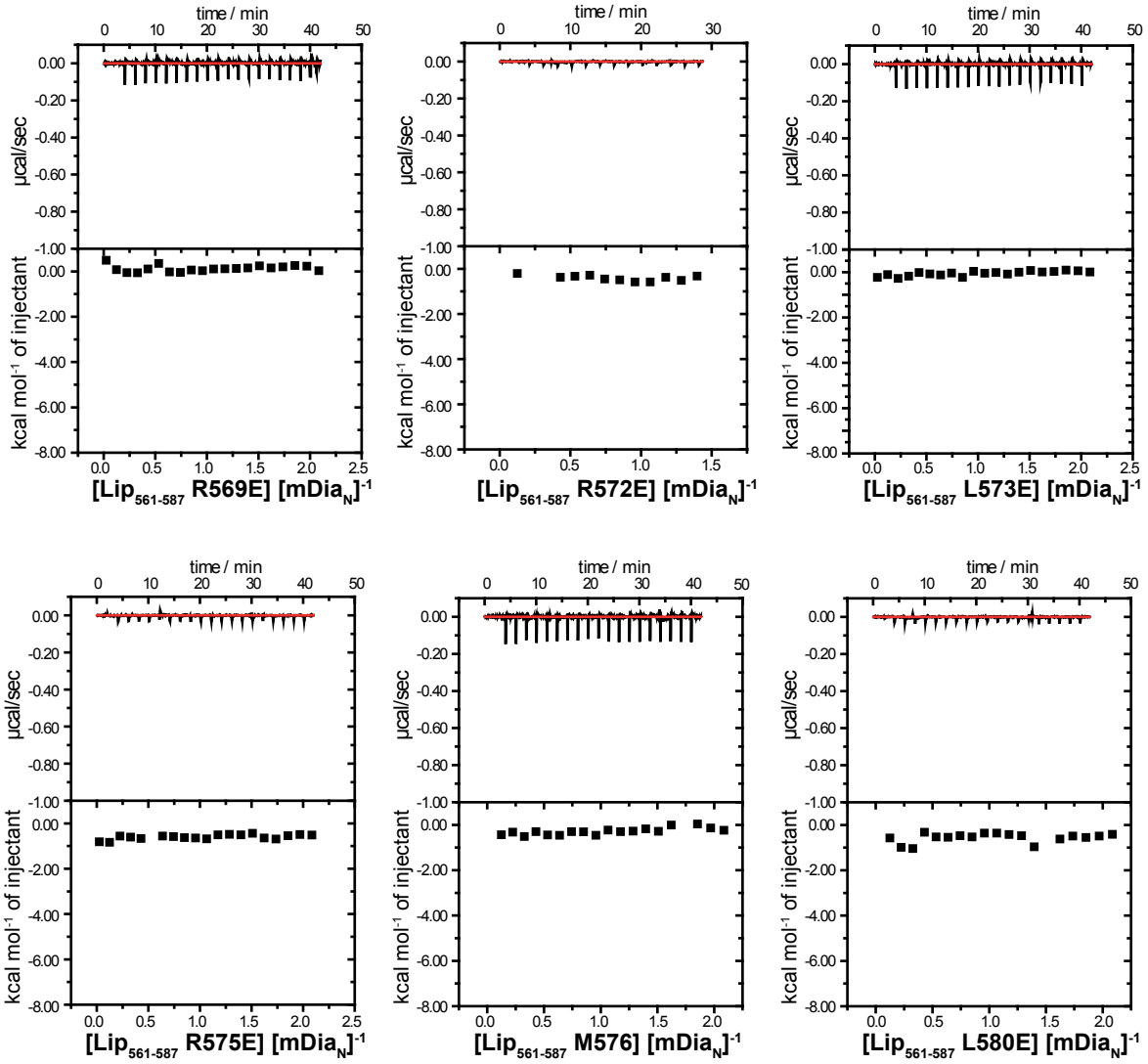

Figure A.1 Mutational analysis of the mDia1-Liprin-α3 interaction I.
ITC measurements of $Lip_{561–587}$ containing the indicated mutations with mDia1 fragments. Experiments were performed at 20 ℃ in protein buffer. No binding could be detected for any of the tested mutations in Liprin-α3.

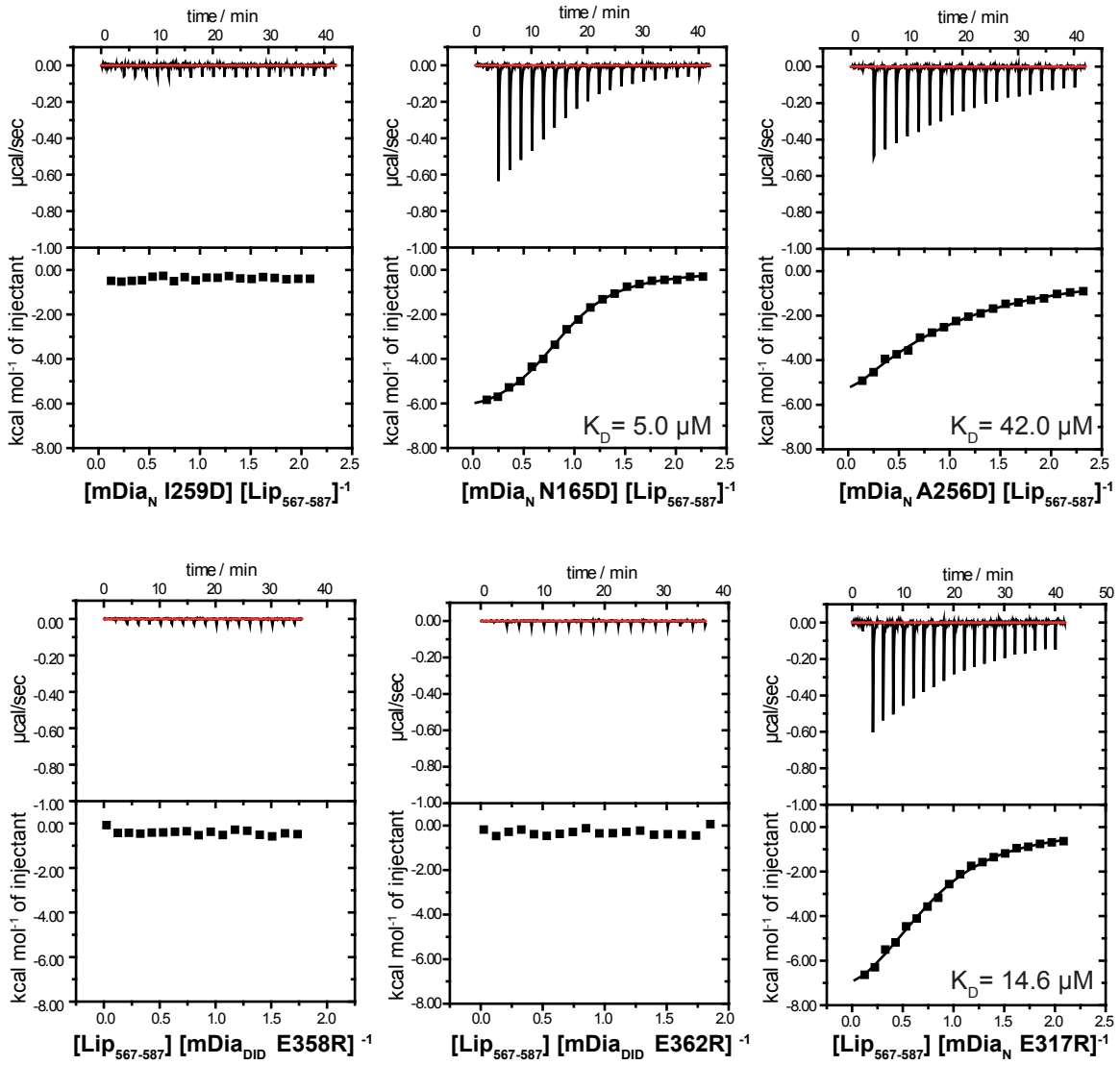

Figure A.2 Mutational analysis of the mDia1-Liprin-α3 interaction II.
ITC measurements of $Lip_{567–587}$ with mDia1 fragments containing the indicated mutations. Experiments were performed at 20 °C in protein buffer. (K_D: equilibrium constant; ΔH: changes in reaction enthalpy; ΔS: change in reaction entropy; N: stoichiometry of binding; T: temperature in Kelvin)

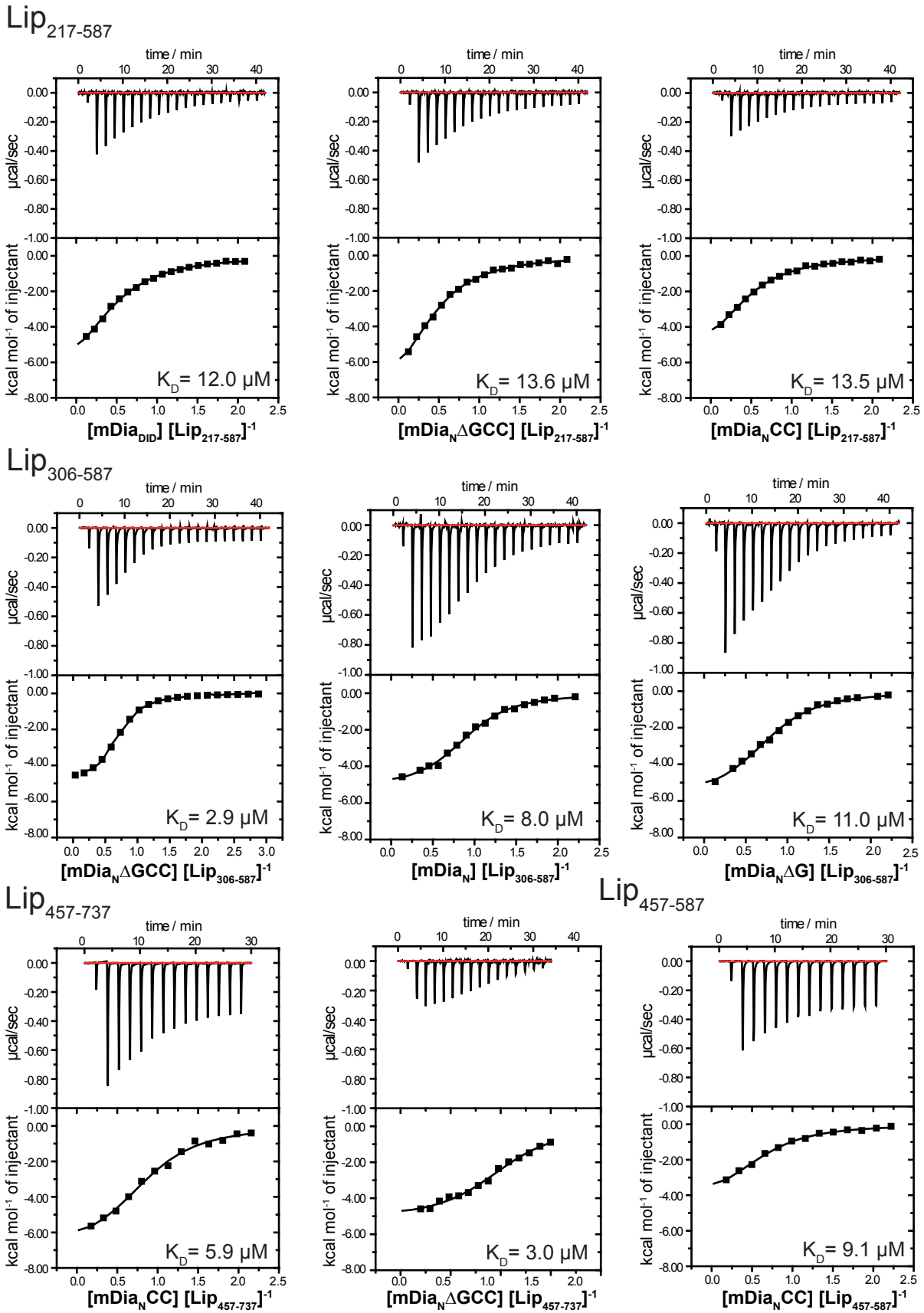

Figure A.3 Interaction of mDia1 and Liprin-α3 as determined by ITC I.
Shown are the ITC measurements of the depicted mDia1 and Liprin-α3 fragments at 20 ℃ in protein buffer. The determined equilibrium constant (K_D) is shown for every interaction. All thermodynamic data are summarized in Table 4.2.

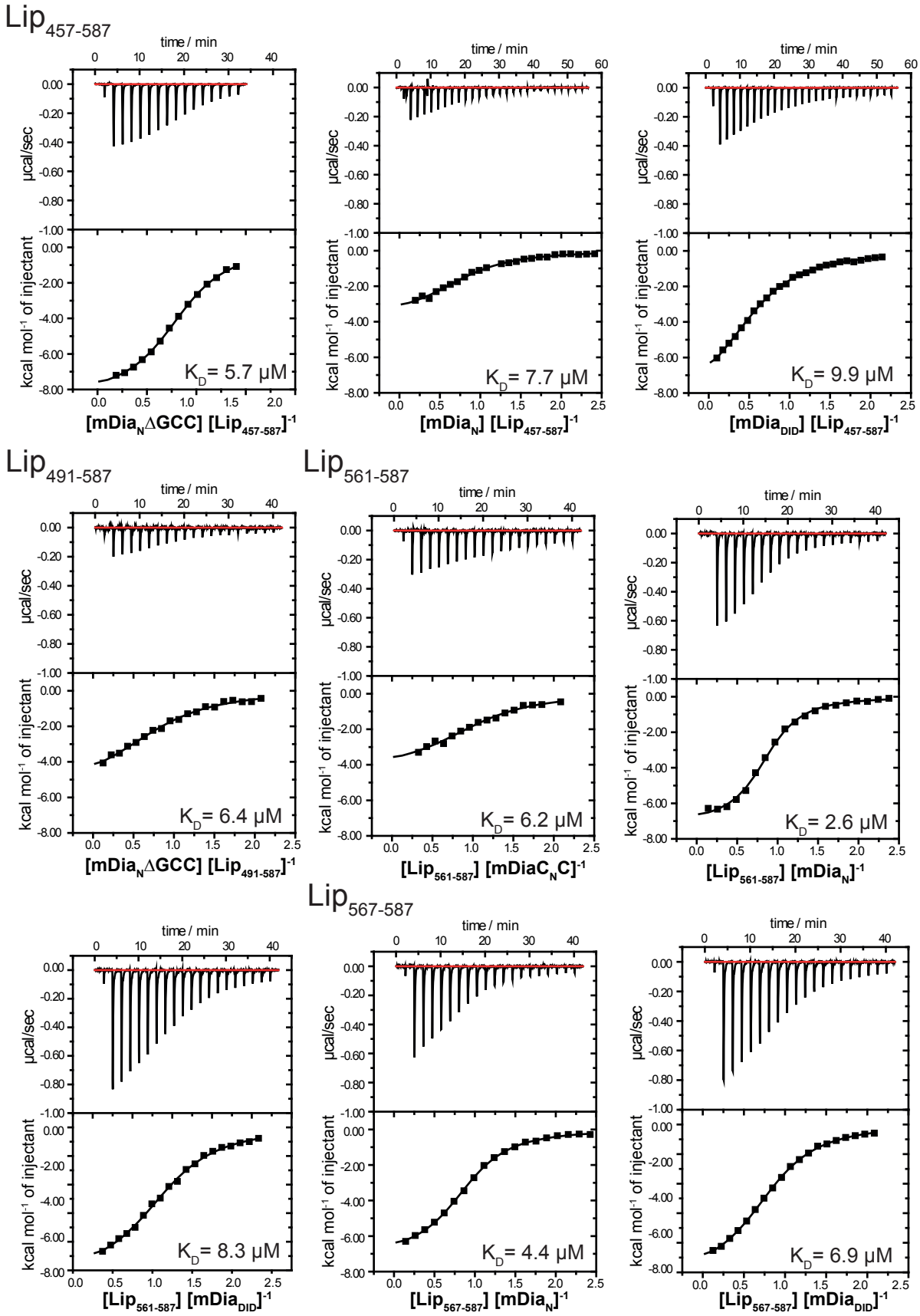

Figure A.4 Interaction of mDia1 and Liprin-α3 as determined by ITC II.
Shown are the ITC measurements of the depicted mDia1 and Liprin-α3 fragments at 20 ℃ in protein buffer. The determined equilibrium constant (K_D) is shown for every interaction. All thermodynamic data are summarized in Table 4.2.

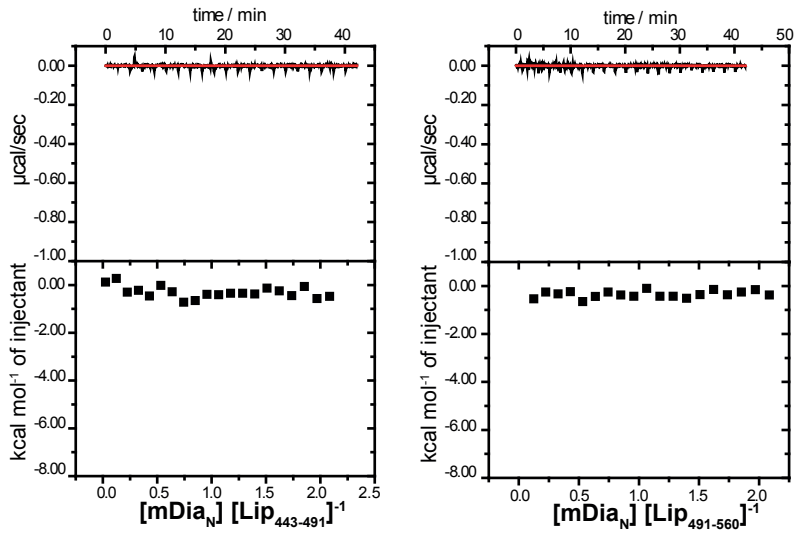

Figure A.5 Interaction of mDia1 and Liprin-α3 as determined by ITC III.
Shown are the ITC measurements of the depicted mDia1 and Liprin-α3 fragments at 20 ℃ in protein buffer. No binding could be detected using these fragments. The thermodynamic data are summarized in Table 4.2.

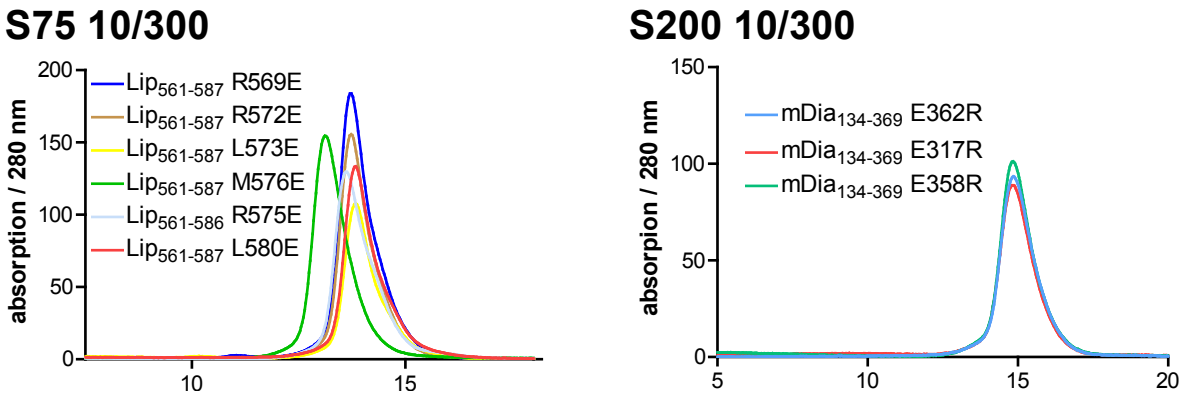

Figure A.6 Analytical size exclusion chromatography of Liprin-α3 and mDia1 mutants.
The purified Liprin561–587 and $mDia_{135–369}$ fragments containing the depicted mutations were analyzed by size exclusion chromatography using S75 10/300 and S200 10/300 columns. Elution was monitored at 280 nm. All fragments showed a similar running behavior.

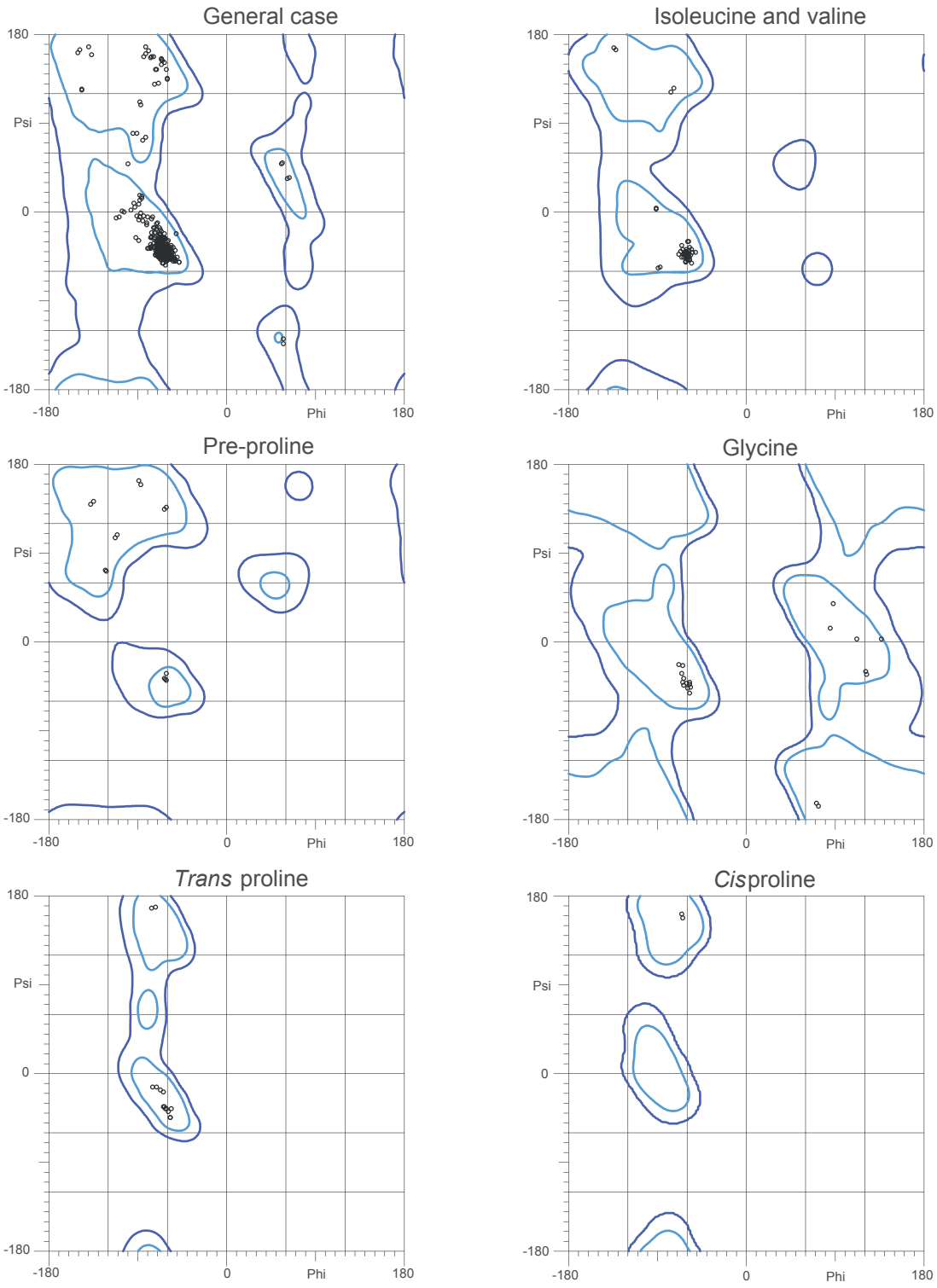

Figure A.7 Ramachandran plots by residue type.
Ramachandran analysis was performed with MolProbity version 4.2 (Chen *et al.*, 2009). 99.4 % (480/483) of all residues were in favored (98 %) regions. 100.0 % (483/483) of all residues were in allowed (>99.8 %) regions. There were no outliers.

Table A.1 Validation of the $Lip_{567–587}$ • $mDia_N$ structure. Validation by MolProbity 4.0 version 4.02 Clashscore is the number of serious steric overlaps (> 0.4 ,Å) per 1000 atoms

	No. of residues (total: 483)	No. of residues in %	Goal in %
Poor rotamers	0	0	<1
Ramachandran outliers	0	0	<0.05
Ramachandran favored	480	99.38	>98
Ramachandran allowed	483	100	>99.8
Cb-deviations >0.25 Å	0	0	0
Clashscore		2.39	

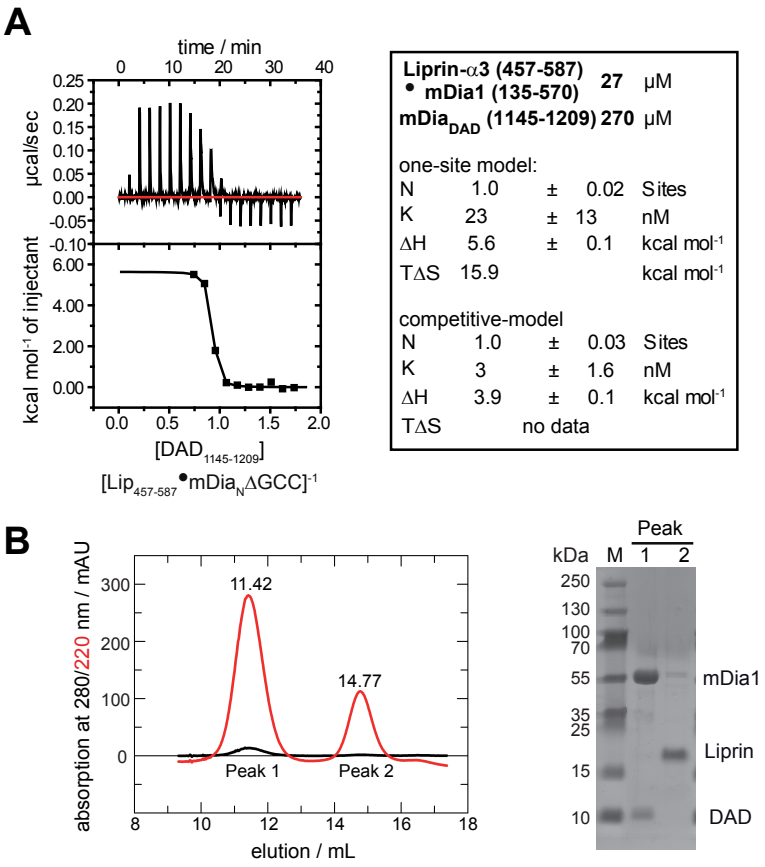

Figure A.8 ITC experiments to analyze the influence of $Lip_{457–587}$ on the $mDia_N\Delta GCC$ • $mDia_{DAD}$ binding thermodynamics.
B: $DAD_{1145–1209}$ was titrated to a preformed complex of $mDia_N\Delta GCC$ • $Lip_{457–587}$. The obtained binding curve was fitted with the one-site and the competitive model (K_D: equilibrium constant; ΔH: changes in reaction enthalpy; ΔS: change in reaction entropy; N: stoichiometry of binding; T: temperature in Kelvin). B: Size exclusion chromatography and SDS-PAGE analysis of the putative ternary $mDia_N\Delta GCC$ • $Lip_{457–587}$ • $mDia_{DAD}$ complex. The cell content of the ITC measurement from (A) was used for an analytical size exclusion chromatography run (S75 10/300) and the resulting peaks from the SEC were analyzed by SDS-PAGE. $Lip_{457–587}$ was dissociated from $mDia_N\Delta GCC$ by $mDia_{DAD}$.

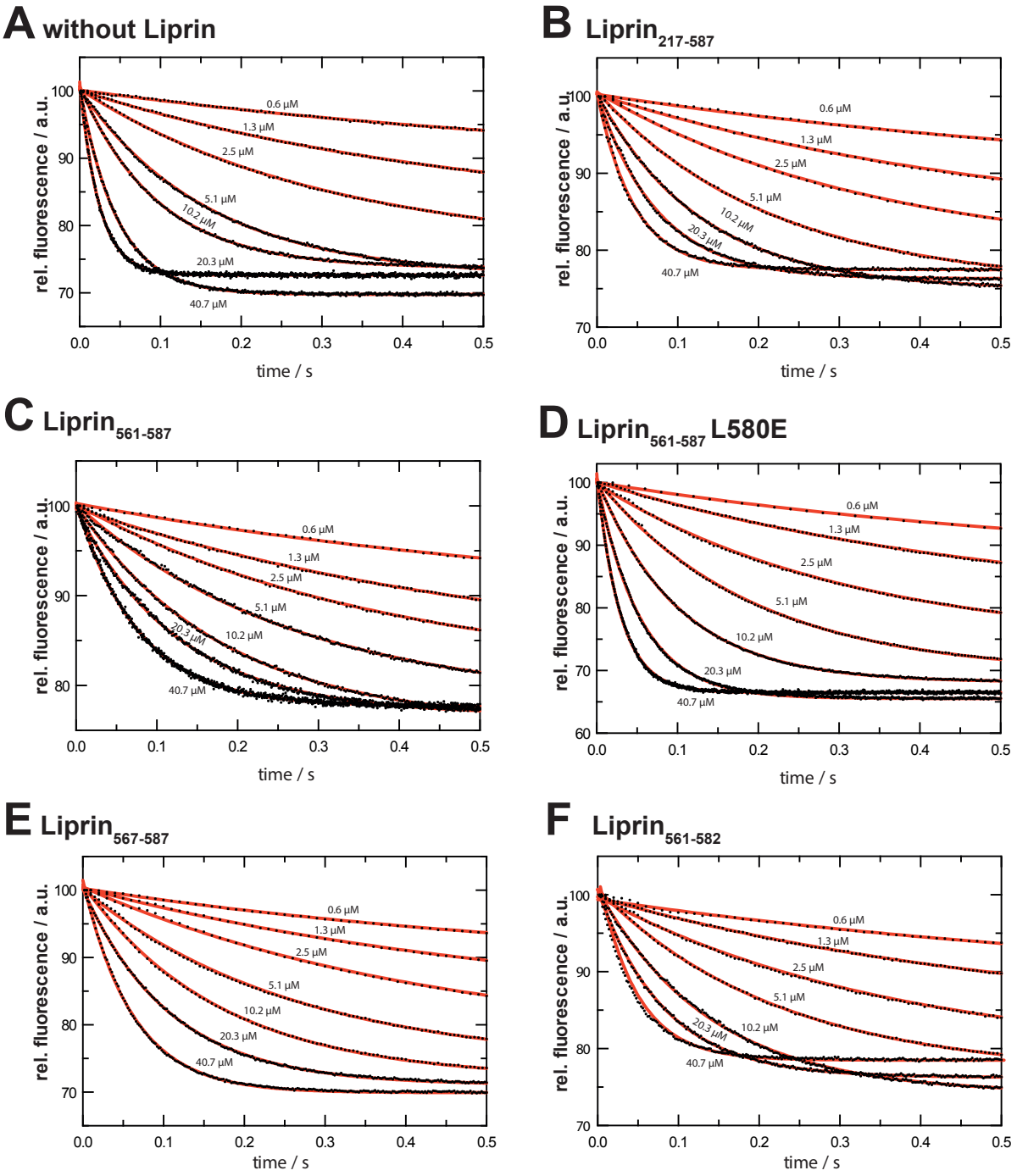

Figure A.9 Primary data of the association-rates determined by stopped-flow kinetics. The fluorescence signal is shown over time for $mDia_N$ without (A) or in presence of Liprin-α3 fragments (B-F). 250 nM (final concentration) of RhoA • mant-GppNHp was titrated with increasing mDia1 concentration (final: 0.6 µM–40.7 µM) establishing pseudo-first order conditions. Single exponential fits to the primary data result in the observed rate-constants, k_{obs} for association of RhoA and $mDia_N$ with and without Liprin-α3.

Literature

Ahuja, Rashmi, Pinyol, Roser, Reichenbach, Nicole, Custer, Laura, Klingensmith, John, Kessels, Michael M & Qualmann, Britta (2007). Cordon-bleu is an actin nucleation factor and controls neuronal morphology. *Cell*, 131(2), 337–350.

Alberts, Arthur S (2001). Identification of a carboxyl-terminal diaphanous-related formin homology protein autoregulatory domain. *Journal of Biological Chemistry*, 276(4), 2824–2830.

Alberts, Arthur S, Bouquin, Nicolas, Johnston, Leland H & Treisman, Richard (1998). Analysis of rhoa-binding proteins reveals an interaction domain conserved in heterotrimeric g protein β subunits and the yeast response regulator protein skn7. *Journal of Biological Chemistry*, 273(15), 8616–8622.

Arakawa, Yoshiki, Bito, Haruhiko, Furuyashiki, Tomoyuki, Tsuji, Takahiro, Takemoto-Kimura, Sayaka, Kimura, Kazuhiro, Nozaki, Kazuhiko, Hashimoto, Nobuo & Narumiya, Shuh (2003). Control of axon elongation via an sdf-1alpha/rho/mdia pathway in cultured cerebellar granule neurons. *J Cell Biol*, 161(2), 381–391.

Aspenström, Pontus, Richnau, Ninna & Johansson, Ann-Sofi (2006). The diaphanous-related formin daam1 collaborates with the rho gtpases rhoa and cdc42, cip4 and src in regulating cell morphogenesis and actin dynamics. *Experimental cell research*, 312(12), 2180–2194.

Astigarraga, Sergio, Hofmeyer, Kerstin, Farajian, Reza & Treisman, Jessica E (2010). Three drosophila liprins interact to control synapse formation. *The Journal of Neuroscience*, 30(46), 15358–15368.

Bailey, S (1994). The ccp4 suite: programs for protein crystallography. *Acta crystallographica. Section D, Biological crystallography*, 50(Pt 5), 760.

Bartolini, Francesca, Moseley, James B, Schmoranzer, Jan, Cassimeris, Lynne, Goode, Bruce L & Gundersen, Gregg G (2008). The formin mdia2 stabilizes microtubules independently of its actin nucleation activity. *The Journal of cell biology*, 181(3), 523–536.

Bedford, Mark T, Chan, David C & Leder, Philip (1997). Fbp ww domains and the abl sh3 domain bind to a specific class of proline-rich ligands. *The EMBO Journal*, 16(9), 2376–2383.

Bernards, André (2003). Gaps galore! a survey of putative ras superfamily gtpase activating proteins in man and drosophila. *Biochimica et Biophysica Acta (BBA)-Reviews on Cancer*, 1603(2), 47–82.

Bishop, ALHA & Hall, Alan (2000). Rho gtpases and their effector proteins. *Biochem. j*, 348, 241–255.

Blanchoin, Laurent, Amann, Kurt J, Higgs, Henry N, Marchand, Jean-Baptiste, Kaiser, Donald A & Pollard, Thomas D (2000). Direct observation of dendritic actin filament net-

works nucleated by arp2/3 complex and wasp/scar proteins. *Nature*, 404(6781), 1007–1011.

Blanchoin, Laurent & Pollard, Thomas D (2002). Hydrolysis of atp by polymerized actin depends on the bound divalent cation but not profilin. *Biochemistry*, 41(2), 597–602.

Block, Jennifer, Breitsprecher, Dennis, Kühn, Sonja, Winterhoff, Moritz, Kage, Frieda, Geffers, Robert, Duwe, Patrick, Rohn, Jennifer L, Baum, Buzz, Brakebusch, Cord *et al.* (2012). Fmnl2 drives actin-based protrusion and migration downstream of cdc42. *Current Biology*, 22(11), 1005–1012.

Block, Johanna, Schroeder, Viktor, Pawelzyk, Paul, Willenbacher, Norbert & Köster, Sarah (2015). Physical properties of cytoplasmic intermediate filaments. *Biochimica et Biophysica Acta (BBA)-Molecular Cell Research*.

Bourne, Henry R, Sanders, David A, McCormick, Frank *et al.* (1991). The gtpase superfamily: conserved structure and molecular mechanism. *Nature*, 349(6305), 117–127.

Brandt, Dominique T, Marion, Sabrina, Griffiths, Gareth, Watanabe, Takashi, Kaibuchi, Kozo & Grosse, Robert (2007). Dia1 and iqgap1 interact in cell migration and phagocytic cup formation. *The Journal of cell biology*, 178(2), 193–200.

Breitsprecher, Dennis & Goode, Bruce L (2013). Formins at a glance. *Journal of cell science*, 126(1), 1–7.

Brenig, Julian, de Boor, Susanne, Knyphausen, Philipp, Kuhlmann, Nora, Wroblowski, Sarah, Baldus, Linda, Scislowski, Lukas, Artz, Oliver, Trauschies, Philip, Baumann, Ulrich, Neundorf, Ines & Lammers, Michael (2015). Structural and biochemical basis for the inhibitory effect of liprin-α-3 on mouse diaphanous 1 (mdia1) function. *J Biol Chem*, 290(23), 14314–14327.

Brucker, Sven, Gerwert, Klaus & Kötting, Carsten (2010). Tyr39 of ran preserves the ran· gtp gradient by inhibiting gtp hydrolysis. *Journal of molecular biology*, 401(1), 1–6.

Brunger, Axel T (1992). Free r value: a novel statistical quantity for assessing the accuracy of crystal structures. *Nature*, 355, 472–475.

Buchan, Daniel WA, Minneci, Federico, Nugent, Tim CO, Bryson, Kevin & Jones, David T (2013). Scalable web services for the psipred protein analysis workbench. *Nucleic acids research*, 41(W1), W349–W357.

Buttery, Shawnna M, Kono, Keiko, Stokasimov, Ema & Pellman, David (2012). Regulation of the formin bnr1 by septins anda mark/par1-family septin-associated kinase. *Molecular biology of the cell*, 23(20), 4041–4053.

Carlier, MF & Pantaloni, Do (1986). Direct evidence for adp-inorganic phosphate-f-actin as the major intermediate in atp-actin polymerization. rate of dissociation of inorganic phosphate from actin filaments. *Biochemistry*, 25(24), 7789–7792.

Carlier, Marie-France, Jean, Catherine, Rieger, Klaus J, Lenfant, Maryse & Pantaloni, Dominique (1993). Modulation of the interaction between g-actin and thymosin beta 4 by the atp/adp ratio: possible implication in the regulation of actin dynamics. *Proceedings of the National Academy of Sciences*, 90(11), 5034–5038.

Carlier, Marie-France, Pantaloni, Dominique, Evans, John A, Lambooy, Peter K, Korn, Edward D & Webb, Martin R (1988). The hydrolysis of atp that accompanies actin polymerization is essentially irreversible. *FEBS letters*, 235(1), 211–214.

Castrillon, Diego H & Wasserman, Steven A (1994). Diaphanous is required for cytokinesis in drosophila and shares domains of similarity with the products of the limb deformity gene. *Development*, 120(12), 3367–3377.

Chen, Vincent B, Arendall, W Bryan, Headd, Jeffrey J, Keedy, Daniel A, Immormino, Robert M, Kapral, Gary J, Murray, Laura W, Richardson, Jane S & Richardson, David C (2009). Molprobity: all-atom structure validation for macromolecular crystallography. *Acta Crystallographica Section D: Biological Crystallography*, 66(1), 12–21.

Cheng, Lina, Zhang, Jiayin, Ahmad, Sana, Rozier, Lorene, Yu, Haiqian, Deng, Haiteng & Mao, Yinghui (2011). Aurora b regulates formin mdia3 in achieving metaphase chromosome alignment. *Developmental cell*, 20(3), 342–352.

Chereau, David, Kerff, Frederic, Graceffa, Philip, Grabarek, Zenon, Langsetmo, Knut & Dominguez, Roberto (2005). Actin-bound structures of wiskott–aldrich syndrome protein (wasp)-homology domain 2 and the implications for filament assembly. *Proceedings of the National Academy of Sciences of the United States of America*, 102(46), 16644–16649.

Chesarone, Melissa A, DuPage, Amy Grace & Goode, Bruce L (2010). Unleashing formins to remodel the actin and microtubule cytoskeletons. *Nature reviews Molecular cell biology*, 11(1), 62–74.

Cheung, Alice Y, Niroomand, Shahriar, Zou, Yanjiao & Wu, Hen-Ming (2010). A transmembrane formin nucleates subapical actin assembly and controls tip-focused growth in pollen tubes. *Proceedings of the National Academy of Sciences*, 107(37), 16390–16395.

Chhabra, Ekta Seth & Higgs, Henry N. (2006). Inf2 is a wasp homology 2 motif-containing formin that severs actin filaments and accelerates both polymerization and depolymerization. *J Biol Chem*, 281(36), 26754–26767.

Chhabra, Ekta Seth, Ramabhadran, Vinay, Gerber, Scott A. & Higgs, Henry N. (2009). Inf2 is an endoplasmic reticulum-associated formin protein. *J Cell Sci*, 122(Pt 9), 1430–1440.

Chien, Yueh-Hsiu, Lai, Michael, Shih, Thomas Y, Verma, Inder M, Scolnick, Edward M, Roy-Burman, Pradip & Davidson, Norman (1979). Heteroduplex analysis of the sequence relationships between the genomes of kirsten and harvey sarcoma viruses, their respective parental murine leukemia viruses, and the rat endogenous 30s rna. *Journal of virology*, 31(3), 752–760.

Chimini, Giovanna & Chavrier, Philippe (2000). Function of rho family proteins in actin dynamics during phagocytosis and engulfment. *Nature Cell Biology*, 2(10), E191–E196.

Cho, Kyucheol, Vaught, Travis G, Ji, Hong, Gu, Dongmin, Papasakelariou-Yared, Catherine, Horstmann, Nicola, Jennings, Jean Marie, Lee, Moonsup, Sevilla, Lisa M, Kloc, Malgorzata *et al.* (2010). Xenopus kazrin interacts with arvcf-catenin, spectrin and p190b rhogap, and modulates rhoa activity and epithelial integrity. *Journal of cell science*, 123(23), 4128–4144.

Clarke, M. & Spudich, J. A. (1977). Nonmuscle contractile proteins: the role of actin and myosin in cell motility and shape determination. *Annu Rev Biochem*, 46, 797–822.

Cooper, John A & Schafer, Dorothy A (2000). Control of actin assembly and disassembly at filament ends. *Current opinion in cell biology*, 12(1), 97–103.

Copeland, John W & Treisman, Richard (2002). The diaphanous-related formin mdia1 controls serum response factor activity through its effects on actin polymerization. *Molecular biology of the cell*, 13(11), 4088–4099.

Dai, Ya, Taru, Hidenori, Deken, Scott L., Grill, Brock, Ackley, Brian, Nonet, Michael L. & Jin, Yishi (2006). Syd-2 liprin-alpha organizes presynaptic active zone formation through elks. *Nat Neurosci*, 9(12), 1479–1487.

Daumke, Oliver, Weyand, Michael, Chakrabarti, Partha P, Vetter, Ingrid R & Wittinghofer, Alfred (2004). The gtpase-activating protein rap1gap uses a catalytic asparagine. *Nature*, 429(6988), 197–201.

Davis, Ian W, Leaver-Fay, Andrew, Chen, Vincent B, Block, Jeremy N, Kapral, Gary J, Wang, Xueyi, Murray, Laura W, Arendall, W Bryan, Snoeyink, Jack, Richardson, Jane S *et al.* (2007). Molprobity: all-atom contacts and structure validation for proteins and nucleic acids. *Nucleic acids research*, 35(suppl 2), W375–W383.

Dean, P, Joan, M Taylor & Christopher, P Mack (2011). Enhancement of mdia2 activity by rho-kinase-dependent phosphorylation of the diaphanous autoregulatory domain. *Biochemical Journal*, 439(1), 57–65.

DeLano, Warren L (2002). The pymol molecular graphics system.

DeMali, Kris A, Barlow, Christy A & Burridge, Keith (2002). Recruitment of the arp2/3 complex to vinculin coupling membrane protrusion to matrix adhesion. *The Journal of cell biology*, 159(5), 881–891.

Dong, Hualing, O'Brien, Richard J, Fung, Eric T, Lanahan, Anthony A, Worley, Paul F & Huganir, Richard L (1997). Grip: a synaptic pdz domain-containing protein that interacts with ampa receptors.

Dunah, Anthone W, Hueske, Emily, Wyszynski, Michael, Hoogenraad, Casper C, Jaworski, Jacek, Pak, Daniel T, Simonetta, Alyson, Liu, Guosong & Sheng, Morgan (2005). Lar receptor protein tyrosine phosphatases in the development and maintenance of excitatory synapses. *Nature neuroscience*, 8(4), 458–467.

Emsley, Paul & Cowtan, Kevin (2004). Coot: model-building tools for molecular graphics. *Acta Crystallographica Section D: Biological Crystallography*, 60(12), 2126–2132.

Etienne-Manneville, Sandrine & Hall, Alan (2002). Rho gtpases in cell biology. *Nature*, 420(6916), 629–635.

Evangelista, Marie, Blundell, Kelly, Longtine, Mark S, Chow, Clinton J, Adames, Neil, Pringle, John R, Peter, Matthias & Boone, Charles (1997). Bni1p, a yeast formin linking cdc42p and the actin cytoskeleton during polarized morphogenesis. *Science*, 276(5309), 118–122.

Evangelista, Marie, Pruyne, David, Amberg, David C, Boone, Charles & Bretscher, Anthony (2002). Formins direct arp2/3-independent actin filament assembly to polarize cell growth in yeast. *Nature cell biology*, 4(1), 32–41.

Evangelista, Marie, Zigmond, Sally & Boone, Charles (2003). Formins: signaling effectors for assembly and polarization of actin filaments. *Journal of cell science*, 116(13), 2603–2611.

Evans, Philip (2006). Scaling and assessment of data quality. *Acta Crystallographica Section D: Biological Crystallography*, 62(1), 72–82.

Favaro, Patricia, Traina, Fabiola, Machado-Neto, João Agostinho, Lazarini, Mariana, Lopes, Matheus Rodrigues, Pereira, João Kleber Novais, Costa, Fernando Ferreira, Infante, Elvira, Ridley, Anne J & Saad, Sara Teresinha Olalla (2013). Fmnl1 promotes proliferation and migration of leukemia cells. *Journal of leukocyte biology*, 94(3), 503–512.

Frost, Adam, Unger, Vinzenz M & De Camilli, Pietro (2009). The bar domain superfamily: membrane-molding macromolecules. *Cell*, 137(2), 191–196.

Fujiwara, Takeshi, Mammoto, Akiko, Kim, Yongman & Takai, Yoshimi (2000). Rho small g-protein-dependent binding of mdia to an src homology 3 domain-containing irsp53/baiap2. *Biochemical and biophysical research communications*, 271(3), 626–629.

Gao, Lina, Liu, Wenyu & Bretscher, Anthony (2010). The yeast formin bnr1p has two localization regions that show spatially and temporally distinct association with septin structures. *Molecular biology of the cell*, 21(7), 1253–1262.

Gasman, Stéphane, Kalaidzidis, Yannis & Zerial, Marino (2003). Rhod regulates endosome dynamics through diaphanous-related formin and src tyrosine kinase. *Nature Cell Biology*, 5(3), 195–204.

Gasmi-Seabrook, Geneviève MC, Marshall, Christopher B, Cheung, Melissa, Kim, Bryan, Wang, Feng, Jang, Ying Ju, Mak, Tak W, Stambolic, Vuk & Ikura, Mitsuhiko (2010). Real-time nmr study of guanine nucleotide exchange and activation of rhoa by pdz-rhogef. *Journal of Biological Chemistry*, 285(8), 5137–5145.

Gasper, Raphael, Thomas, Christoph, Ahmadian, Mohammad Reza & Wittinghofer, Alfred (2008). The role of the conserved switch ii glutamate in guanine nucleotide exchange factor-mediated nucleotide exchange of gtp-binding proteins. *Journal of molecular biology*, 379(1), 51–63.

Gasteier, Judith E, Madrid, Ricardo, Krautkrämer, Ellen, Schröder, Sebastian, Muranyi, Walter, Benichou, Serge & Fackler, Oliver T (2003). Activation of the rac-binding partner fhod1 induces actin stress fibers via a rock-dependent mechanism. *Journal of Biological Chemistry*, 278(40), 38902–38912.

Goh, Wah Ing, Lim, Kim Buay, Sudhaharan, Thankiah, Sem, Kai Ping, Bu, Wenyu, Chou, Ai Mei & Ahmed, Sohail (2012). mdia1 and wave2 proteins interact directly with irsp53 in filopodia and are involved in filopodium formation. *Journal of Biological Chemistry*, 287(7), 4702–4714.

Goley, Erin D & Welch, Matthew D (2006). The arp2/3 complex: an actin nucleator comes of age. *Nature reviews Molecular cell biology*, 7(10), 713–726.

Gomez, Timothy S, Kumar, Karan, Medeiros, Ricardo B, Shimizu, Yoji, Leibson, Paul J & Billadeau, Daniel D (2007). Formins regulate the actin-related protein 2/3 complex-independent polarization of the centrosome to the immunological synapse. *Immunity*, 26(2), 177–190.

Gorelik, Roman, Yang, Changsong, Kameswaran, Vasumathi, Dominguez, Roberto & Svitkina, Tatyana (2011). Mechanisms of plasma membrane targeting of formin mdia2 through its amino terminal domains. *Molecular biology of the cell*, 22(2), 189–201.

Gould, Christopher J, Maiti, Sankar, Michelot, Alphée, Graziano, Brian R, Blanchoin, Laurent & Goode, Bruce L (2011). The formin dad domain plays dual roles in autoinhibition and actin nucleation. *Current biology*, 21(5), 384–390.

Graceffa, Philip & Dominguez, Roberto (2003). Crystal structure of monomeric actin in the atp state. structural basis of nucleotide-dependent actin dynamics. *Journal of Biological Chemistry*, 278(36), 34172–34180.

Graham, Debbie L, Eccleston, John F & Lowe, Peter N (1999). The conserved arginine in rho-gtpase-activating protein is essential for efficient catalysis but not for complex formation with rho gdp and aluminum fluoride. *Biochemistry*, 38(3), 985–991.

Graziano, Brian R, DuPage, Amy Grace, Michelot, Alphee, Breitsprecher, Dennis, Moseley, James B, Sagot, Isabelle, Blanchoin, Laurent & Goode, Bruce L (2011). Mechanism and cellular function of bud6 as an actin nucleation–promoting factor. *Molecular biology of the cell*, 22(21), 4016–4028.

Groot, Karen R, Sevilla, Lisa M, Nishi, Kazunori, DiColandrea, Teresa & Watt, Fiona M (2004). Kazrin, a novel periplakin-interacting protein associated with desmosomes and the keratinocyte plasma membrane. *The Journal of cell biology*, 166(5), 653–659.

Habas, Raymond, Kato, Yoichi & He, Xi (2001). Wnt/frizzled activation of rho regulates vertebrate gastrulation and requires a novel formin homology protein daam1. *Cell*, 107(7), 843–854.

Hall, Alan (1998). Rho gtpases and the actin cytoskeleton. *Science*, 279(5350), 509–514.

Hallam, Steven J, Goncharov, Alexandr, McEwen, Jason, Baran, Renee & Jin, Yishi (2002). Syd-1, a presynaptic protein with pdz, c2 and rhogap-like domains, specifies axon identity in c. elegans. *Nature neuroscience*, 5(11), 1137–1146.

Hannemann, Sebastian, Madrid, Ricardo, Stastna, Jana, Kitzing, Thomas, Gasteier, Judith, Schönichen, André, Bouchet, Jerome, Jimenez, Alberto, Geyer, Matthias, Grosse, Robert *et al.* (2008). The diaphanous-related formin fhod1 associates with rock1 and promotes src-dependent plasma membrane blebbing. *Journal of Biological Chemistry*, 283(41), 27891–27903.

Harris, Elizabeth S, Li, Fang & Higgs, Henry N (2004). The mouse formin, frlα, slows actin filament barbed end elongation, competes with capping protein, accelerates polymerization from monomers, and severs filaments. *Journal of Biological Chemistry*, 279(19), 20076–20087.

Heimsath, Ernest G & Higgs, Henry N (2012). The c terminus of formin fmnl3 accelerates actin polymerization and contains a wh2 domain-like sequence that binds both monomers and filament barbed ends. *Journal of Biological Chemistry*, 287(5), 3087–3098.

Herrmann, Harald, Häner, Markus, Brettel, Monika, Müller, Shirley A, Goldie, Kenneth N, Fedtke, Bettina, Lustig, Ariel, Franke, Werner W & Aebi, Ueli (1996). Structure and assembly properties of the intermediate filament protein vimentin: the role of its head, rod and tail domains. *Journal of molecular biology*, 264(5), 933–953.

Higashi, Tomohito, Ikeda, Tomoyuki, Shirakawa, Ryutaro, Kondo, Hirokazu, Kawato, Mitsunori, Horiguchi, Masahito, Okuda, Tomohiko, Okawa, Katsuya, Fukai, Shuya, Nureki, Osamu *et al.* (2008). Biochemical characterization of the rho gtpase-regulated actin assembly by diaphanous-related formins, mdia1 and daam1, in platelets. *Journal of Biological Chemistry*, 283(13), 8746–8755.

Hill, Caroline S, Wynne, Judy & Treisman, Richard (1995). The rho family gtpases rhoa, racl, and cdc42hsregulate transcriptional activation by srf. *Cell*, 81(7), 1159–1170.

Hoogenraad, Casper C., Feliu-Mojer, Monica I., Spangler, Samantha A., Milstein, Aaron D., Dunah, Anthone W., Hung, Albert Y. & Sheng, Morgan (2007). Liprinalpha1 degradation by calcium/calmodulin-dependent protein kinase ii regulates lar receptor tyrosine phosphatase distribution and dendrite development. *Dev Cell*, 12(4), 587–602.

Hutchinson, Jon P & Eccleston, John F (2000). Mechanism of nucleotide release from rho by the gdp dissociation stimulator protein. *Biochemistry*, 39(37), 11348–11359.

Huxley, HE (1969). The mechanism of muscular contraction. *Science*, 164(3886), 1356–1366.

Imamura, Hiroshi, Tanaka, Kazuma, Hihara, Taro, Umikawa, Masato, Kamei, Takashi, Takahashi, Kazuo, Sasaki, Tomo & Takai, Yoshimi (1997). Bni1p and bnr1p: downstream targets of the rho family small g-proteins which interact with profilin and regulate actin cytoskeleton in saccharomyces cerevisiae. *The EMBO journal*, 16(10), 2745–2755.

Iskratsch, Thomas, Lange, Stephan, Dwyer, Joseph, Kho, Ay Lin, dos Remedios, Cris & Ehler, Elisabeth (2010). Formin follows function: a muscle-specific isoform of fhod3 is regulated by ck2 phosphorylation and promotes myofibril maintenance. *The Journal of cell biology*, 191(6), 1159–1172.

Iskratsch, Thomas, Reijntjes, Susan, Dwyer, Joseph, Toselli, Paul, Dégano, Irene R, Dominguez, Isabel & Ehler, Elisabeth (2013). Two distinct phosphorylation events govern the function of muscle fhod3. *Cellular and Molecular Life Sciences*, 70(5), 893–908.

Ji, Peng, Jayapal, Senthil Raja & Lodish, Harvey F (2008). Enucleation of cultured mouse fetal erythroblasts requires rac gtpases and mdia2. *Nature cell biology*, 10(3), 314–321.

John, Jacob, Sohmen, Roland, Feuerstein, Juergen, Linke, Rosita, Wittinghofer, Alfred & Goody, Roger S (1990). Kinetics of interaction of nucleotides with nucleotide-free h-ras p21. *Biochemistry*, 29(25), 6058–6065.

Kaibuchi, K, Kuroda, S & Amano, M (1999). Regulation of the cytoskeleton and cell adhesion by the rho family gtpases in mammalian cells. *Annual review of biochemistry*, 68(1), 459–486.

Kaufmann, Nancy, DeProto, Jamin, Ranjan, Ravi, Wan, Hong & Van Vactor, David (2002). Drosophila liprin-α and the receptor phosphatase dlar control synapse morphogenesis. *Neuron*, 34(1), 27–38.

Kirschner, Marc W (1980). Implications of treadmilling for the stability and polarity of actin and tubulin polymers in vivo. *The Journal of cell biology*, 86(1), 330–334.

Kitayama, Hitoshi, Sugimoto, Yoshikazu, Matsuzaki, Tomoko, Ikawa, Yoji & Noda, Makoto (1989). A ras-related gene with transformation suppressor activity. *Cell*, 56(1), 77–84.

Kitzing, TM, Wang, Y, Pertz, O, Copeland, JW & Grosse, R (2010). Formin-like 2 drives amoeboid invasive cell motility downstream of rhoc. *Oncogene*, 29(16), 2441–2448.

Klebe, Christian, Prinz, Heino, Wittinghofer, Alfred & Goody, Roger S (1995). The kinetic mechanism of ran-nucleotide exchange catalyzed by rcc1. *Biochemistry*, 34(39), 12543–12552.

Ko, Jaewon, Kim, Seho, Valtschanoff, Juli G, Shin, Hyewon, Lee, Jae-Ran, Sheng, Morgan, Premont, Richard T, Weinberg, Richard J & Kim, Eunjoon (2003). Interaction between liprin-α and git1 is required for ampa receptor targeting. *The Journal of neuroscience*, 23(5), 1667–1677.

Ko, Jaewon, Na, Moonseok, Kim, Seho, Lee, Jae-Ran & Kim, Eunjoon (2003). Interaction of the erc family of rim-binding proteins with the liprin-α family of multidomain proteins. *Journal of Biological Chemistry*, 278(43), 42377–42385.

Kovar, David R, Harris, Elizabeth S, Mahaffy, Rachel, Higgs, Henry N & Pollard, Thomas D (2006). Control of the assembly of atp-and adp-actin by formins and profilin. *Cell*, 124(2), 423–435.

Kovar, David R, Kuhn, Jeffrey R, Tichy, Andrea L & Pollard, Thomas D (2003). The fission yeast cytokinesis formin cdc12p is a barbed end actin filament capping protein gated by profilin. *The Journal of cell biology*, 161(5), 875–887.

Kovar, David R, Wu, Jian-Qiu & Pollard, Thomas D (2005). Profilin-mediated competition between capping protein and formin cdc12p during cytokinesis in fission yeast. *Molecular biology of the cell*, 16(5), 2313–2324.

Kozlov, Michael M & Bershadsky, Alexander D (2004). Processive capping by formin suggests a force-driven mechanism of actin polymerization. *The Journal of cell biology*, 167(6), 1011–1017.

Kühn, Sonja & Geyer, Matthias (2014). Formins as effector proteins of rho gtpases. *Small GTPases*, 5(3), 1–15.

Lammers, Michael, Meyer, Simon, Kühlmann, Dorothee & Wittinghofer, Alfred (2008). Specificity of interactions between mdia isoforms and rho proteins. *Journal of Biological Chemistry*, 283(50), 35236–35246.

Lammers, Michael, Rose, Rolf, Scrima, Andrea & Wittinghofer, Alfred (2005). The regulation of mdia1 by autoinhibition and its release by rho*gtp. *EMBO J*, 24(23), 4176–4187.

Leipe, Detlef D., Wolf, Yuri I., Koonin, Eugene V. & Aravind, L. (2002). Classification and evolution of p-loop gtpases and related atpases. *J Mol Biol*, 317(1), 41–72.

Lenzen, Christian, Cool, Robbert H, Prinz, Heino, Kuhlmann, Jürgen & Wittinghofer, Alfred (1998). Kinetic analysis by fluorescence of the interaction between ras and the catalytic domain of the guanine nucleotide exchange factor cdc25mm. *Biochemistry*, 37(20), 7420–7430.

Leslie, Andrew GW & Powell, Harold R (2007). Processing diffraction data with mosflm. In *Evolving methods for macromolecular crystallography*, S. 41–51. Springer.

Li, Fang & Higgs, Henry N (2003). The mouse formin mdia1 is a potent actin nucleation factor regulated by autoinhibition. *Current biology*, 13(15), 1335–1340.

Lin, Yi-Chia, Yao, Norman Y, Broedersz, Chase P, Herrmann, Harald, MacKintosh, Fred C & Weitz, David A (2010). Origins of elasticity in intermediate filament networks. *Physical review letters*, 104(5), 058101.

Liu, Wei, Sato, Akira, Khadka, Deepak, Bharti, Ritu, Diaz, Hector, Runnels, Loren W. & Habas, Raymond (2008). Mechanism of activation of the formin protein daam1. *Proc Natl Acad Sci U S A*, 105(1), 210–215.

Lodish, Harvey, Berk, Arnold, Zipursky, S Lawrence, Matsudaira, Paul, Baltimore, David, Darnell, James *et al.* (2000). The dynamics of actin assembly.

Lu, Jun, Meng, Wuyi, Poy, Florence, Maiti, Sankar, Goode, Bruce L & Eck, Michael J (2007). Structure of the fh2 domain of daam1: implications for formin regulation of actin assembly. *Journal of molecular biology*, 369(5), 1258–1269.

Lu, Jia & Pollard, Thomas D (2001). Profilin binding to poly-l-proline and actin monomers along with ability to catalyze actin nucleotide exchange is required for viability of fission yeast. *Molecular biology of the cell*, 12(4), 1161–1175.

Maas, Richard L, Zeller, Rolf, Woychik, Richard P, Vogt, Thomas F & Leder, Philip (1990). Disruption of formin-encoding transcripts in two mutant limb deformity alleles.

Machesky, L_m, REEVES, Emer, WIENTJES, Frans, Mattheyse, F, GROGAN, Ann, Totty, N, Burlingame, A, Hsuan, J & Segal, A (1997). Mammalian actin-related protein 2/3 complex localizes to regions of lamellipodial protrusion and is composed of evolutionarily conserved proteins. *Biochem. J*, 328, 105–112.

Machesky, Laura M & Insall, Robert H (1998). Scar1 and the related wiskott–aldrich syndrome protein, wasp, regulate the actin cytoskeleton through the arp2/3 complex. *Current biology*, 8(25), 1347–1356.

Machesky, Laura M, Mullins, R Dyche, Higgs, Henry N, Kaiser, Donald A, Blanchoin, Laurent, May, Robin C, Hall, Margaret E & Pollard, Thomas D (1999). Scar, a wasp-related protein, activates nucleation of actin filaments by the arp2/3 complex. *Proceedings of the National Academy of Sciences*, 96(7), 3739–3744.

Macias, Maria J, Wiesner, Silke & Sudol, Marius (2002). Ww and sh3 domains, two different scaffolds to recognize proline-rich ligands. *FEBS letters*, 513(1), 30–37.

Madaule, Pascal & Axel, Richard (1985). A novel ras-related gene family. *Cell*, 41(1), 31–40.

Madrid, Ricardo, Aranda, Juan F, Rodríguez-Fraticelli, Alejo E, Ventimiglia, Leandro, Andrés-Delgado, Laura, Shehata, Mona, Fanayan, Susan, Shahheydari, Hamideh, Gómez, Sergio, Jiménez, Alberto *et al.* (2010). The formin inf2 regulates basolateral-to-apical transcytosis and lumen formation in association with cdc42 and mal2. *Developmental cell*, 18(5), 814–827.

Maiti, Sankar, Michelot, Alphee, Gould, Christopher, Blanchoin, Laurent, Sokolova, Olga & Goode, Bruce L (2012). Structure and activity of full-length formin mdia1. *Cytoskeleton*, 69(6), 393–405.

Mandel, M. & Higa, A. (1970). Calcium-dependent bacteriophage dna infection. *J Mol Biol*, 53(1), 159–162.

Marchand, Jean-Baptiste, Kaiser, Donald A, Pollard, Thomas D & Higgs, Henry N (2001). Interaction of wasp/scar proteins with actin and vertebrate arp2/3 complex. *Nature cell biology*, 3(1), 76–82.

Martin, Sophie G, Rincón, Sergio A, Basu, Roshni, Pérez, Pilar & Chang, Fred (2007). Regulation of the formin for3p by cdc42p and bud6p. *Molecular biology of the cell*, 18(10), 4155–4167.

Martiniere, Alexandre, Gayral, Philippe, Hawes, Chris & Runions, John (2011). Building bridges: formin1 of arabidopsis forms a connection between the cell wall and the actin cytoskeleton. *The Plant Journal*, 66(2), 354–365.

Maruyma, Koscak & Tsukagoshi, Kiyomi (1984). Effects of kcl, mgcl2 and cacl2 concentrations on the monomer-polymer equilibrium of actin in the presence and absence of cytochalasin d. *Journal of biochemistry*, 96(3), 605–611.

Matsuda, Keiko, Matsuda, Shinji, Gladding, Clare M. & Yuzaki, Michisuke (2006). Characterization of the delta2 glutamate receptor-binding protein delphilin: Splicing variants with differential palmitoylation and an additional pdz domain. *J Biol Chem*, 281(35), 25577–25587.

Matusek, Tamás, Gombos, Rita, Szécsényi, Anita, Sánchez-Soriano, Natalia, Czibula, Ágnes, Pataki, Csilla, Gedai, Anita, Prokop, Andreas, Raskó, István & Mihály, József (2008). Formin proteins of the daam subfamily play a role during axon growth. *The Journal of Neuroscience*, 28(49), 13310–13319.

May, Robin C, Caron, Emmanuelle, Hall, Alan & Machesky, Laura M (2000). Involvement of the arp2/3 complex in phagocytosis mediated by fcγr or cr3. *Nature Cell Biology*, 2(4), 246–248.

Mayya, Viveka, Lundgren, Deborah H, Hwang, Sun-Il, Rezaul, Karim, Wu, Linfeng, Eng, Jimmy K, Rodionov, Vladimir & Han, David K (2009). Quantitative phosphoproteomic analysis of t cell receptor signaling reveals system-wide modulation of protein-protein interactions. *Science signaling*, 2(84), ra46–ra46.

McCoy, Airlie J, Grosse-Kunstleve, Ralf W, Adams, Paul D, Winn, Martyn D, Storoni, Laurent C & Read, Randy J (2007). Phaser crystallographic software. *Journal of applied crystallography*, 40(4), 658–674.

Michelot, Alphée, Guérin, Christophe, Huang, Shanjin, Ingouff, Mathieu, Richard, Stéphane, Rodiuc, Natalia, Staiger, Christopher J & Blanchoin, Laurent (2005). The formin homology 1 domain modulates the actin nucleation and bundling activity of arabidopsis formin1. *The Plant Cell*, 17(8), 2296–2313.

Miller, Kyle E, DeProto, Jamin, Kaufmann, Nancy, Patel, Bharatkumar N, Duckworth, April & Van Vactor, David (2005). Direct observation demonstrates that liprin-α is required for trafficking of synaptic vesicles. *Current Biology*, 15(7), 684–689.

Miyagi, Yohei, Yamashita, Tetsuji, Fukaya, Masahiro, Sonoda, Tomoko, Okuno, Toshiaki, Yamada, Kazuyuki, Watanabe, Masahiko, Nagashima, Yoji, Aoki, Ichiro, Okuda, Kenji *et al.* (2002). Delphilin: a novel pdz and formin homology domain-containing protein that synaptically colocalizes and interacts with glutamate receptor δ2 subunit. *The Journal of neuroscience*, 22(3), 803–814.

Mizuno, Hiroaki, Higashida, Chiharu, Yuan, Yunfeng, Ishizaki, Toshimasa, Narumiya, Shuh & Watanabe, Naoki (2011). Rotational movement of the formin mdia1 along the double helical strand of an actin filament. *Science*, 331(6013), 80–83.

Moseley, James B, Sagot, Isabelle, Manning, Amity L, Xu, Yingwu, Eck, Michael J, Pellman, David & Goode, Bruce L (2004). A conserved mechanism for bni1-and mdia1-induced actin assembly and dual regulation of bni1 by bud6 and profilin. *Molecular biology of the cell*, 15(2), 896–907.

Moss, Joel & Vaughan, Martha (1998). Molecules in the arf orbit. *Journal of Biological Chemistry*, 273(34), 21431–21434.

Mullins, R Dyche, Heuser, John A & Pollard, Thomas D (1998). The interaction of arp2/3 complex with actin: nucleation, high affinity pointed end capping, and formation of branching networks of filaments. *Proceedings of the National Academy of Sciences*, 95(11), 6181–6186.

Murshudov, Garib N, Vagin, Alexei A & Dodson, Eleanor J (1997). Refinement of macromolecular structures by the maximum-likelihood method. *Acta Crystallographica Section D: Biological Crystallography*, 53(3), 240–255.

Neidt, Erin M, Skau, Colleen T & Kovar, David R (2008). The cytokinesis formins from the nematode worm and fission yeast differentially mediate actin filament assembly. *Journal of Biological Chemistry*, 283(35), 23872–23883.

Nezami, Azin, Poy, Florence, Toms, Angela, Zheng, Wei & Eck, Michael J (2010). Crystal structure of a complex between amino and carboxy terminal fragments of mdia1: insights into autoinhibition of diaphanous-related formins. *PloS one*, 5(9), e12992.

Nezami, Azin G, Poy, Florence & Eck, Michael J (2006). Structure of the autoinhibitory switch in formin mdia1. *Structure*, 14(2), 257–263.

Nobes, Catherine D & Hall, Alan (1995). Rho, rac, and cdc42 gtpases regulate the assembly of multimolecular focal complexes associated with actin stress fibers, lamellipodia, and filopodia. *Cell*, 81(1), 53–62.

Oda, Toshiro, Iwasa, Mitsusada, Aihara, Tomoki, Maéda, Yuichiro & Narita, Akihiro (2009). The nature of the globular-to fibrous-actin transition. *Nature*, 457(7228), 441–445.

Okada, Kyoko, Bartolini, Francesca, Deaconescu, Alexandra M, Moseley, James B, Dogic, Zvonimir, Grigorieff, Nikolaus, Gundersen, Gregg G & Goode, Bruce L (2010). Adenomatous polyposis coli protein nucleates actin assembly and synergizes with the formin mdia1. *The Journal of cell biology*, 189(7), 1087–1096.

Olsen, Olav, Moore, Kimberly A, Fukata, Masaki, Kazuta, Toshinari, Trinidad, Jonathan C, Kauer, Fred W, Streuli, Michel, Misawa, Hidemi, Burlingame, Alma L, Nicoll, Roger A *et al.* (2005). Neurotransmitter release regulated by a mals–liprin-α presynaptic complex. *The Journal of cell biology*, 170(7), 1127–1134.

Otomo, Takanori, Otomo, Chinatsu, Tomchick, Diana R., Machius, Mischa & Rosen, Michael K. (2005). Structural basis of rho gtpase-mediated activation of the formin mdia1. *Mol Cell*, 18(3), 273–281.

Otomo, Takanori, Tomchick, Diana R, Otomo, Chinatsu, Machius, Mischa & Rosen, Michael K (2010). Crystal structure of the formin mdia1 in autoinhibited conformation. *PLoS One*, 5(9), e12896.

Otomo, Takanori, Tomchick, Diana R, Otomo, Chinatsu, Panchal, Sanjay C, Machius, Mischa & Rosen, Michael K (2005). Structural basis of actin filament nucleation and processive capping by a formin homology 2 domain. *Nature*, 433(7025), 488–494.

Otterbein, Ludovic R, Graceffa, Philip & Dominguez, Roberto (2001). The crystal structure of uncomplexed actin in the adp state. *Science*, 293(5530), 708–711.

Palazzo, Alexander F, Cook, Tiffani A, Alberts, Arthur S & Gundersen, Gregg G (2001). mdia mediates rho-regulated formation and orientation of stable microtubules. *Nature cell biology*, 3(8), 723–729.

Patel, Maulik R, Lehrman, Emily K, Poon, Vivian Y, Crump, Justin G, Zhen, Mei, Bargmann, Cornelia I & Shen, Kang (2006). Hierarchical assembly of presynaptic components in defined c. elegans synapses. *Nature neuroscience*, 9(12), 1488–1498.

Paul, Aditya & Pollard, Thomas (2008). The role of the fh1 domain and profilin in formin-mediated actin-filament elongation and nucleation. *Current Biology*, 18(1), 9–19.

Paul, Aditya S & Pollard, Thomas D (2009). Energetic requirements for processive elongation of actin filaments by fh1fh2-formins. *Journal of Biological Chemistry*, 284(18), 12533–12540.

Paul, Aditya S & Pollard, Thomas D (2009). Review of the mechanism of processive actin filament elongation by formins. *Cell motility and the cytoskeleton*, 66(8), 606.

Pawelzyk, Paul, Mücke, Norbert, Herrmann, Harald & Willenbacher, Norbert (2014). Attractive interactions among intermediate filaments determine network mechanics in vitro. *PloS one*, 9(4), e93194.

Pawson, Catherine, Eaton, Benjamin A & Davis, Graeme W (2008). Formin-dependent synaptic growth: evidence that dlar signals via diaphanous to modulate synaptic actin and dynamic pioneer microtubules. *The Journal of Neuroscience*, 28(44), 11111–11123.

Peck, Jeremy, Douglas, Gilbert, Wu, Catherine H & Burbelo, Peter D (2002). Human rhogap domain-containing proteins: structure, function and evolutionary relationships. *FEBS letters*, 528(1), 27–34.

Pellegrin, Stéphanie & Mellor, Harry (2005). The rho family gtpase rif induces filopodia through mdia2. *Current Biology*, 15(2), 129–133.

Peng, Jun, Wallar, Bradley J, Flanders, Akiko, Swiatek, Pamela J & Alberts, Arthur S (2003). Disruption of the diaphanous-related formin drf1 gene encoding mdia1 reveals a role for drf3 as an effector for cdc42. *Current Biology*, 13(7), 534–545.

Perrin, Francis (1926). Polarisation de la lumiere de fluorescence. vie moyenne des molécules dans l'etat excité. *J. phys. radium*, 7(12), 390–401.

Petersen, Janni, Nielsen, Olaf, Egel, Richard & Hagan, Iain M (1998). Fh3, a domain found in formins, targets the fission yeast formin fus1 to the projection tip during conjugation. *The Journal of cell biology*, 141(5), 1217–1228.

Petry, Sabine, Groen, Aaron C, Ishihara, Keisuke, Mitchison, Timothy J & Vale, Ronald D (2013). Branching microtubule nucleation in xenopus egg extracts mediated by augmin and tpx2. *Cell*, 152(4), 768–777.

Piekny, Alisa J & Glotzer, Michael (2008). Anillin is a scaffold protein that links rhoa, actin, and myosin during cytokinesis. *Current biology*, 18(1), 30–36.

Pollard, T. D. (1976). Cytoskeletal functions of cytoplasmic contractile proteins. *J Supramol Struct*, 5(3), 317–334.

Pollard, Thomas D (1986). Assembly and dynamics of the actin filament system in nonmuscle cells. *Journal of cellular biochemistry*, 31(2), 87–95.

Pollard, Thomas D & Borisy, Gary G (2003). Cellular motility driven by assembly and disassembly of actin filaments. *Cell*, 112(4), 453–465.

Pring, Martin, Evangelista, Marie, Boone, Charles, Yang, Changsong & Zigmond, Sally H (2003). Mechanism of formin-induced nucleation of actin filaments. *Biochemistry*, 42(2), 486–496.

Prior, Ian A, Lewis, Paul D & Mattos, Carla (2012). A comprehensive survey of ras mutations in cancer. *Cancer research*, 72(10), 2457–2467.

Pruyne, David, Evangelista, Marie, Yang, Changsong, Bi, Erfei, Zigmond, Sally, Bretscher, Anthony & Boone, Charles (2002). Role of formins in actin assembly: nucleation and barbed-end association. *Science*, 297(5581), 612–615.

Pulido, Rafael, Serra-Pages, Carles, Tang, May & Streuli, Michel (1995). The lar/ptp delta/ptp sigma subfamily of transmembrane protein-tyrosine-phosphatases: multiple human lar, ptp delta, and ptp sigma isoforms are expressed in a tissue-specific manner and associate with the lar-interacting protein lip. 1. *Proceedings of the National Academy of Sciences*, 92(25), 11686–11690.

Ramabhadran, Vinay, Gurel, Pinar S & Higgs, Henry N (2012). Mutations to the formin homology 2 domain of inf2 protein have unexpected effects on actin polymerization and severing. *Journal of Biological Chemistry*, 287(41), 34234–34245.

Ramalingam, Nagendran, Zhao, Hongxia, Breitsprecher, Dennis, Lappalainen, Pekka, Faix, Jan & Schleicher, Michael (2010). Phospholipids regulate localization and activity of mdia1 formin. *European journal of cell biology*, 89(10), 723–732.

Rehmann, Holger & Bos, Johannes L (2004). Signal transduction: thumbs up for inactivation. *Nature*, 429(6988), 138–139.

Ridley, Anne J, Paterson, Hugh F, Johnston, Caroline L, Diekmann, Dagmar & Hall, Alan (1992). The small gtp-binding protein rac regulates growth factor-induced membrane ruffling. *Cell*, 70(3), 401–410.

Rojas, Ana Maria, Fuentes, Gloria, Rausell, Antonio & Valencia, Alfonso (2012). The ras protein superfamily: evolutionary tree and role of conserved amino acids. *The Journal of cell biology*, 196(2), 189–201.

Rose, Rolf, Weyand, Michael, Lammers, Michael, Ishizaki, Toshimasa, Ahmadian, Mohammad Reza & Wittinghofer, Alfred (2005). Structural and mechanistic insights into the interaction between rho and mammalian dia. *Nature*, 435(7041), 513–518.

Rouiller, Isabelle, Xu, Xiao-Ping, Amann, Kurt J, Egile, Coumaran, Nickell, Stephan, Nicastro, Daniela, Li, Rong, Pollard, Thomas D, Volkmann, Niels & Hanein, Dorit (2008). The structural basis of actin filament branching by the arp2/3 complex. *The Journal of cell biology*, 180(5), 887–895.

Ryu, Jae Ryun, Echarri, Asier, Li, Ran & Pendergast, Ann Marie (2009). Regulation of cell-cell adhesion by abi/diaphanous complexes. *Molecular and cellular biology*, 29(7), 1735–1748.

Sagot, Isabelle, Rodal, Avital A, Moseley, James, Goode, Bruce L & Pellman, David (2002). An actin nucleation mechanism mediated by bni1 and profilin. *Nature Cell Biology*, 4(8), 626–631.

Sakamoto, Satoko, Ishizaki, Toshimasa, Okawa, Katsuya, Watanabe, Sadanori, Arakawa, Takatoshi, Watanabe, Naoki & Narumiya, Shuh (2012). Liprin-α controls stress fiber formation by binding to mdia and regulating its membrane localization. *J Cell Sci*, 125(Pt 1), 108–120.

Sakamoto, Satoko, Narumiya, Shuh & Ishizaki, Toshimasa (2012). A new role of multi scaffold protein liprin-α: Liprin-α suppresses rho-mdia mediated stress fiber formation. *Bioarchitecture*, 2(2), 43–49.

Samuels, Benjamin Adam, Hsueh, Yi-Ping, Shu, Tianzhi, Liang, Haoya, Tseng, Huang-Chun, Hong, Chen-Jei, Su, Susan C, Volker, Janet, Neve, Rachael L, Yue, David T *et al.* (2007). Cdk5 promotes synaptogenesis by regulating the subcellular distribution of the maguk family member cask. *Neuron*, 56(5), 823–837.

Sander, EE & Collard, JG (1999). Rho-like gtpases: their role in epithelial cell–cell adhesion and invasion. *European Journal of Cancer*, 35(14), 1905–1911.

Saraste, Matti, Sibbald, Peter R & Wittinghofer, Alfred (1990). The p-loop–a common motif in atp-and gtp-binding proteins. *Trends in biochemical sciences*, 15(11), 430–434.

Scheffzek, Klaus, Ahmadian, Mohammad Reza, Kabsch, Wolfgang, Wiesmüller, Lisa, Lautwein, Alfred, Schmitz, Frank & Wittinghofer, Alfred (1997). The ras-rasgap complex: structural basis for gtpase activation and its loss in oncogenic ras mutants. *Science*, 277(5324), 333–339.

Schimmöller, Frauke, Simon, Iris & Pfeffer, Suzanne R (1998). Rab gtpases, directors of vesicle docking. *Journal of Biological Chemistry*, 273(35), 22161–22164.

Schmidt, Gudula, Lenzen, Christian, Simon, Iris, Deuter, Rainer, Cool, Robbert H, Goody, Roger S & Wittinghofer, Alfred (1996). Biochemical and biological consequences of changing the specificity of p21ras from guanosine to xanthosine nucleotides. *Oncogene*, 12(1), 87–96.

Schoch, Susanne, Castillo, Pablo E., Jo, Tobias, Mukherjee, Konark, Geppert, Martin, Wang, Yun, Schmitz, Frank, Malenka, Robert C. & Südhof, Thomas C. (2002). Rim1alpha forms a protein scaffold for regulating neurotransmitter release at the active zone. *Nature*, 415(6869), 321–326.

Schönichen, André & Geyer, Matthias (2010). Fifteen formins for an actin filament: a molecular view on the regulation of human formins. *Biochimica et Biophysica Acta (BBA)-Molecular Cell Research*, 1803(2), 152–163.

Schopferer, Michael, Bär, Harald, Hochstein, Bernhard, Sharma, Sarika, Mücke, Norbert, Herrmann, Harald & Willenbacher, Norbert (2009). Desmin and vimentin intermediate filament networks: their viscoelastic properties investigated by mechanical rheometry. *Journal of molecular biology*, 388(1), 133–143.

Schwaibold, Eva MC & Brandt, Dominique T (2008). Identification of neurochondrin as a new interaction partner of the fh3 domain of the diaphanous-related formin dia1. *Biochemical and biophysical research communications*, 373(3), 366–372.

Scrima, Andrea, Thomas, Christoph, Deaconescu, Delia & Wittinghofer, Alfred (2008). The rap–rapgap complex: Gtp hydrolysis without catalytic glutamine and arginine residues. *The EMBO journal*, 27(7), 1145–1153.

Seewald, Michael J, Körner, Carolin, Wittinghofer, Alfred & Vetter, Ingrid R (2002). Rangap mediates gtp hydrolysis without an arginine finger. *Nature*, 415(6872), 662–666.

Selden, Lynn A, Estes, James E & Gershman, Lewis C (1983). The tightly bound divalent cation regulates actin polymerization. *Biochemical and biophysical research communications*, 116(2), 478–485.

Serra-Pages, C, Kedersha, NL, Fazikas, L, Medley, Q, Debant, A & Streuli, M (1995). The lar transmembrane protein tyrosine phosphatase and a coiled-coil lar-interacting protein co-localize at focal adhesions. *The EMBO Journal*, 14(12), 2827.

Serra-Pages, C., Medley, Q. G., Tang, M., Hart, A. & Streuli, M. (1998). Liprins, a family of lar transmembrane protein-tyrosine phosphatase-interacting proteins. *J Biol Chem*, 273(25), 15611–15620.

Serra-Pagès, Carles, Streuli, Michel & Medley, Quintus G (2005). Liprin phosphorylation regulates binding to lar: evidence for liprin autophosphorylation. *Biochemistry*, 44(48), 15715–15724.

Seth, Abhinav, Otomo, Chinatsu & Rosen, Michael K (2006). Autoinhibition regulates cellular localization and actin assembly activity of the diaphanous-related formins frlα and mdia1. *The Journal of cell biology*, 174(5), 701–713.

Shemesh, Tom, Otomo, Takanori, Rosen, Michael K, Bershadsky, Alexander D & Kozlov, Michael M (2005). A novel mechanism of actin filament processive capping by formin solution of the rotation paradox. *The Journal of cell biology*, 170(6), 889–893.

Shin, Hyewon, Wyszynski, Michael, Huh, Kyung-Hye, Valtschanoff, Juli G., Lee, Jae-Ran, Ko, Jaewon, Streuli, Michel, Weinberg, Richard J., Sheng, Morgan & Kim, Eunjoon (2003). Association of the kinesin motor kif1a with the multimodular protein liprin-alpha. *J Biol Chem*, 278(13), 11393–11401.

Small, JV, Isenberg, G & Celis, JE (1978). Polarity of actin at the leading edge of cultured cells.

Spangler, SA & Hoogenraad, CC (2007). Liprin-alpha proteins: scaffold molecules for synapse maturation. *Biochemical Society Transactions*, 35(Pt 5), 1278–1282.

Spangler, Samantha A, Jaarsma, Dick, De Graaff, Esther, Wulf, Phebe S, Akhmanova, Anna & Hoogenraad, Casper C (2011). Differential expression of liprin-α family proteins in the brain suggests functional diversification. *Journal of Comparative Neurology*, 519(15), 3040–3060.

Spoerner, Michael, Herrmann, Christian, Vetter, Ingrid R, Kalbitzer, Hans Robert & Wittinghofer, Alfred (2001). Dynamic properties of the ras switch i region and its importance for binding to effectors. *Proceedings of the National Academy of Sciences*, 98(9), 4944–4949.

Stamnes, Mark (2002). Regulating the actin cytoskeleton during vesicular transport. *Current opinion in cell biology*, 14(4), 428–433.

Steller, Ingo, Bolotovsky, Robert & Rossmann, Michael G (1997). An algorithm for automatic indexing of oscillation images using fourier analysis. *Journal of applied crystallography*, 30(6), 1036–1040.

Sydor, Jens R, Engelhard, Martin, Wittinghofer, Alfred, Goody, Roger S & Herrmann, Christian (1998). Transient kinetic studies on the interaction of ras and the ras-binding domain of c-raf-1 reveal rapid equilibration of the complex. *Biochemistry*, 37(40), 14292–14299.

Takeya, Ryu, Taniguchi, Kenichiro, Narumiya, Shuh & Sumimoto, Hideki (2008). The mammalian formin fhod1 is activated through phosphorylation by rock and mediates thrombin-induced stress fibre formation in endothelial cells. *The EMBO journal*, 27(4), 618–628.

Taru, Hidenori & Jin, Yishi (2011). The liprin homology domain is essential for the homomeric interaction of syd-2/liprin-α protein in presynaptic assembly. *The Journal of Neuroscience*, 31(45), 16261–16268.

Tolliday, Nicola, VerPlank, Lynn & Li, Rong (2002). Rho1 directs formin-mediated actin ring assembly during budding yeast cytokinesis. *Current biology*, 12(21), 1864–1870.

Trahey, Meg & McCormick, Frank (1987). A cytoplasmic protein stimulates normal n-ras p21 gtpase, but does not affect oncogenic mutants. *Science*, 238(4826), 542–545.

Vaillant, Dominique C, Copeland, Sarah J, Davis, Chris, Thurston, Susan F, Abdennur, Nezar & Copeland, John W (2008). Interaction of the n-and c-terminal autoregulatory domains of frl2 does not inhibit frl2 activity. *Journal of Biological Chemistry*, 283(48), 33750–33762.

Vale, Ronald & Kreis, Thomas (1999). *Guidebook to the cytoskeletal and motor proteins*. Oxford University Press.

Vale, Ronald D (2003). The molecular motor toolbox for intracellular transport. *Cell*, 112(4), 467–480.

Van Aelst, Linda & DSouza-Schorey, Crislyn (1997). Rho gtpases and signaling networks. *Genes & development*, 11(18), 2295–2322.

van Gisbergen, Peter AC, Li, Ming, Wu, Shu-Zon & Bezanilla, Magdalena (2012). Class ii formin targeting to the cell cortex by binding pi (3, 5) p2 is essential for polarized growth. *The Journal of cell biology*, 198(2), 235–250.

van Horck, Francis PG, Ahmadian, M Reza, Haeusler, Lars C, Moolenaar, Wouter H & Kranenburg, Onno (2001). Characterization of p190rhogef, a rhoa-specific guanine nucleotide exchange factor that interacts with microtubules. *Journal of Biological Chemistry*, 276(7), 4948–4956.

Vavylonis, Dimitrios, Kovar, David R, O'Shaughnessy, Ben & Pollard, Thomas D (2006). Model of formin-associated actin filament elongation. *Molecular cell*, 21(4), 455–466.

Vega, Francisco M, Fruhwirth, Gilbert, Ng, Tony & Ridley, Anne J (2011). Rhoa and rhoc have distinct roles in migration and invasion by acting through different targets. *The Journal of cell biology*, 193(4), 655–665.

Vetter, Ingrid R, Arndt, Andreas, Kutay, Ulrike, Görlich, Dirk & Wittinghofer, Alfred (1999). Structural view of the ran–importin β interaction at 2.3 å resolution. *Cell*, 97(5), 635–646.

Vetter, Ingrid R & Wittinghofer, Alfred (2001). The guanine nucleotide-binding switch in three dimensions. *Science*, 294(5545), 1299–1304.

Via, Allegra, Ferrè, Fabrizio, Brannetti, Barbara, Valencia, Alfonso & Helmer-Citterich, Manuela (2000). Three-dimensional view of the surface motif associated with the p-loop structure: cis and trans cases of convergent evolution. *Journal of molecular biology*, 303(4), 455–465.

Vijayakumar, M, Wong, Kwan-Yin, Schreiber, Gideon, Fersht, Alan R, Szabo, Attila & Zhou, Huan-Xiang (1998). Electrostatic enhancement of diffusion-controlled protein-protein association: comparison of theory and experiment on barnase and barstar. *Journal of molecular biology*, 278(5), 1015–1024.

Vojtek, Anne B & Der, Channing J (1998). Increasing complexity of the ras signaling pathway. *Journal of Biological Chemistry*, 273(32), 19925–19928.

Walker, RA, O'brien, ET, Pryer, NK, Soboeiro, MF, Voter, WA, Erickson, HP & Salmon, ED (1988). Dynamic instability of individual microtubules analyzed by video light microscopy: rate constants and transition frequencies. *The Journal of cell biology*, 107(4), 1437–1448.

Wallar, Bradley J & Alberts, Arthur S (2003). The formins: active scaffolds that remodel the cytoskeleton. *Trends in cell biology*, 13(8), 435–446.

Wallar, Bradley J, DeWard, Aaron D, Resau, James H & Alberts, Arthur S (2007). Rhob and the mammalian diaphanous-related formin mdia2 in endosome trafficking. *Experimental cell research*, 313(3), 560–571.

Wallar, Bradley J, Stropich, Brittany N, Schoenherr, Jessica A, Holman, Holly A, Kitchen, Susan M & Alberts, Arthur S (2006). The basic region of the diaphanous-autoregulatory domain (dad) is required for autoregulatory interactions with the diaphanous-related formin inhibitory domain. *Journal of Biological Chemistry*, 281(7), 4300–4307.

Wang, Junxia, Neo, Suat Peng & Cai, Mingjie (2009). Regulation of the yeast formin bni1p by the actin-regulating kinase prk1p. *Traffic*, 10(5), 528–535.

Watanabe, Naoki, Kato, Takayuki, Fujita, Akiko, Ishizaki, Toshimasa & Narumiya, Shuh (1999). Cooperation between mdia1 and rock in rho-induced actin reorganization. *Nature cell biology*, 1(3), 136–143.

Watanabe, Naoki, Madaule, Pascal, Reid, Tim, Ishizaki, Toshimasa, Watanabe, Go, Kakizuka, Akira, Saito, Yuji, Nakao, Kazuwa, Jockusch, Brigitte M & Narumiya, Shuh (1997). p140mdia, a mammalian homolog of drosophila diaphanous, is a target protein for rho small gtpase and is a ligand for profilin. *The EMBO journal*, 16(11), 3044–3056.

Watanabe, Sadanori, Okawa, Katsuya, Miki, Takashi, Sakamoto, Satoko, Morinaga, Tomoko, Segawa, Kohei, Arakawa, Takatoshi, Kinoshita, Makoto, Ishizaki, Toshimasa & Narumiya, Shuh (2010). Rho and anillin-dependent control of mdia2 localization and function in cytokinesis. *Molecular biology of the cell*, 21(18), 3193–3204.

Weaver, Alissa M, Karginov, Andrei V, Kinley, Andrew W, Weed, Scott A, Li, Yan, Parsons, J Thomas & Cooper, John A (2001). Cortactin promotes and stabilizes arp2/3-induced actin filament network formation. *Current Biology*, 11(5), 370–374.

Wegner, Albrecht (1976). Head to tail polymerization of actin. *Journal of molecular biology*, 108(1), 139–150.

Wegner, Albrecht & Engel, Juergen (1975). Kinetics of the cooperative association of actin to actin filament. *Biophysical chemistry*, 3(3), 215–225.

Weis, Karsten (2003). Regulating access to the genome: nucleocytoplasmic transport throughout the cell cycle. *Cell*, 112(4), 441–451.

Wennerberg, Krister & Der, Channing J (2004). Rho-family gtpases: it's not only rac and rho (and i like it). *Journal of cell science*, 117(8), 1301–1312.

Wennerberg, Krister, Rossman, Kent L & Der, Channing J (2005). The ras superfamily at a glance. *Journal of cell science*, 118(5), 843–846.

Westendorf, Jennifer J (2001). The formin/diaphanous-related protein, fhos, interacts with rac1 and activates transcription from the serum response element. *Journal of Biological Chemistry*, 276(49), 46453–46459.

Wittinghofer, Alfred & Pal, Emil F (1991). The structure of ras protein: a model for a universal molecular switch. *Trends in biochemical sciences*, 16, 382–387.

Woodrum, Diane T, Rich, Steven A & Pollard, Thomas D (1975). Evidence for biased bidirectional polymerization of actin filaments using heavy meromyosin prepared by an improved method. *The Journal of cell biology*, 67(1), 231–237.

Wyszynski, Michael, Kim, Eunjoon, Dunah, Anthone W, Passafaro, Maria, Valtschanoff, Juli G, Serra-Pagès, Carles, Streuli, Michel, Weinberg, Richard J & Sheng, Morgan (2002). Interaction between grip and liprin-α/syd2 is required for ampa receptor targeting. *Neuron*, 34(1), 39–52.

Xu, Yingwu, Moseley, James B, Sagot, Isabelle, Poy, Florence, Pellman, David, Goode, Bruce L & Eck, Michael J (2004). Crystal structures of a formin homology-2 domain reveal a tethered dimer architecture. *Cell*, 116(5), 711–723.

Yan, Shuling, Lv, Zhiyi, Winterhoff, Moritz, Wenzl, Christian, Zobel, Thomas, Faix, Jan, Bogdan, Sven & Grosshans, Jörg (2013). The f-bar protein cip4/toca-1 antagonizes the formin diaphanous in membrane stabilization and compartmentalization. *Journal of cell science*, 126(8), 1796–1805.

Yasuda, Shingo, Oceguera-Yanez, Fabian, Kato, Takayuki, Okamoto, Muneo, Yonemura, Shigenobu, Terada, Yasuhiko, Ishizaki, Toshimasa & Narumiya, Shuh (2004). Cdc42 and mdia3 regulate microtubule attachment to kinetochores. *Nature*, 428(6984), 767–771.

Yayoshi-Yamamoto, Shinri, Taniuchi, Ichiro & Watanabe, Takeshi (2000). Frl, a novel formin-related protein, binds to rac and regulates cell motility and survival of macrophages. *Molecular and cellular biology*, 20(18), 6872–6881.

Young, Kevin G., Thurston, Susan F., Copeland, Sarah, Smallwood, Chelsea & Copeland, John W. (2008). Inf1 is a novel microtubule-associated formin. *Mol Biol Cell*, 19(12), 5168–5180.

Zhang, Baolin & Zheng, Yi (1998). Regulation of rhoa gtp hydrolysis by the gtpase-activating proteins p190, p50rhogap, bcr, and 3bp-1. *Biochemistry*, 37(15), 5249–5257.

Zhen, Mei & Jin, Yishi (1999). The liprin protein syd-2 regulates the differentiation of presynaptic termini in c. elegans. *Nature*, 401(6751), 371–375.

Zhong, Jie-Ming, Chen-Hwang, Mo-Chou & Hwang, Yu-Wen (1995). Switching nucleotide specificity of ha-ras p21 by a single amino acid substitution at aspartate 119. *Journal of Biological Chemistry*, 270(17), 10002–10007.

Zigmond, Sally H (1996). Signal transduction and actin filament organization. *Current opinion in cell biology*, 8(1), 66–73.

Zigmond, Sally H (2004). Formin-induced nucleation of actin filaments. *Current opinion in cell biology*, 16(1), 99–105.

Zigmond, Sally H, Evangelista, Marie, Boone, Charles, Yang, Changsong, Dar, Arvin C, Sicheri, Frank, Forkey, Joe & Pring, Martin (2003). Formin leaky cap allows elongation in the presence of tight capping proteins. *Current biology*, 13(20), 1820–1823.

Zong, Hui, Kaibuchi, Kozo & Quilliam, Lawrence A (2001). The insert region of rhoa is essential for rho kinase activation and cellular transformation. *Molecular and cellular biology*, 21(16), 5287–5298.

Zuniga, Aimée, Michos, Odyssé, Spitz, François, Haramis, Anna-Pavlina G, Panman, Lia, Galli, Antonella, Vintersten, Kristina, Klasen, Christian, Mansfield, William, Kuc, Sylwia *et al.* (2004). Mouse limb deformity mutations disrupt a global control region within the large regulatory landscape required for gremlin expression. *Genes & development*, 18(13), 1553–1564.

Zürner, Magdalena, Mittelstaedt, Tobias, Becker, Albert, Schoch, Susanne *et al.* (2011). Analyses of the spatiotemporal expression and subcellular localization of liprin-α proteins. *Journal of Comparative Neurology*, 519(15), 3019–3039.

Zürner, Magdalena & Schoch, Susanne (2009). The mouse and human liprin-α family of scaffolding proteins: Genomic organization, expression profiling and regulation by alternative splicing. *Genomics*, 93(3), 243–253.

Abbreviations

%	percentage
%(v/v)	volume per volume (volume fraction)
%(w/v)	weight per volume (mass fraction)
℃	degree Celsius
μ	micro
β-ME	β-mercaptoethanol
ΔG	Gibbs free energy change
ΔH	reaction enthalpy change
ΔS	reaction entropy change
aa	amino acids
A	ampere
ARM	armadillo repeat
ARR	armadillo repeat region
BSA	bovine serum albumin
CC	coiled-coil
CF	carboxyfluorescein
Da	dalton
DAD	Diaphanous-autoregulatory domain
DAPI	4′,6-Diamidin-2-phenylindol
DBR	DAD-basic region
DCR	DAD-core region
DD	dimerization domain
DID	Diaphanous-inhibitory domain
DMEM	Dulbecco's Modified Eagle's Medium
DNA	deoxyribonucleic acid
dNTP	deoxyribonucleotide
DP	differential power
DRF	Diaphanous-related formin
ϵ	extinction coefficient
e.g.	*exempli gratia* (for example)
et al.	*et alteri/-a/-um* (and others)
FH	formin holomogy domain
g	gravitational acceleration
g	gram
GAP	GTPase-activating protein
GBD	GTPase binding domain

GDP	guanosine diphosphate
GEF	guanine nucleotide exchange factor
GSH	glutathion
GTP	guanosine triphosphate
h	hour
HRP	horseradish peroxidase
IPTG	isopropyl-ß-D-thiogalactopyranosid
ITC	isothermal titration calorimetry
K_A	equilibrium association constant
K_{ass}	association rate constant
K_D	equilibrium dissociation constant
K_{diss}	dissociation rate constant
K_{obs}	observed association rate constants
L	liter
LB	lysogeny broth
ln	natural logarithm
mant	methylanthraniloyl
m	milli
M	molar
mDia	mouse Diaphanous-related protein
min	minute
n	nano
NPF	nucleation promoting factor
O/N	over night
OD	optical density
PBS	phosphate buffered saline
PBST	phosphate buffered saline containing Tween-20
PCR	polymerase chain reaction
pH	pondus hydrogenii
PTM	posttranslational modification
PVDF	polyvinylidene fluoride
R	gas constant
rpm	rounds per minute
RT	room temperature
SDS-PAGE	sodium dodecyl sulfate polyacrylamide gel electrophoresis
sec, s	second
SEC	size exclusion chromatography
Tris	tris(hydroxymethyl)aminomethane ($(HOCH_2)_3CNH_2$)
U	unit
V	voltage
v	volume

Acknowledgments

Meinem Betreuer Dr. Michael Lammers danke ich für die Überlassung des Themas, die Möglichkeit die Arbeit an der Universität zu Köln durchzuführen, die hervorragenden Arbeitsbedingungen und genügend Freiräume. Auch in schwierigen Situationen zeigte er vollstes Verständnis und ermöglichte es mir dadurch immer gerne zur Arbeit zu kommen.

Ich bedanke mich bei Prof. Dr. Kay Hofmann für die Übernahme des Zweitguachtens meiner Arbeit.

Prof. Dr. Ulrich Baumann danke ich für die Übernahme des Vorsitzes in der Prüfungskommission und die Vermessung der Proteinkristalle am SLS.

Allen Mitgliedern der Arbeitsgruppe und des Insituts möchte ich für die schöne Zeit und das angenehme Arbeitsklima danken. Insbesondere danke ich Linda Baldus, Dr. Susanne de Boor, Nora Kuhlmann, Sarah Wroblowski, Philipp Knyphausen und Lukas Scislowski für die hilfreichen aber auch aufmunternden Gespräche beim Mittagessen und in der Kaffeepause. Zudem möchte ich Tobias Tzbik für die sehr gelungene und produktive Zusammenarbeit im Rahmen seiner Masterarbeit danken.

Dr. Astrid Schauss und der gesamten Imaging Facility danke ich für die Hilfe bei der Aufnahme und Auswertung der Zellbilder. Prof. Dr. Ines Neundorf möchte ich für die Synthese der Liprin Peptide danken.

Ein besonders herzlicher Dank geht an meine Eltern und meine Brüder Florian und Kilian, die mich immer außerordentlich geduldig unterstützt und motiviert haben. Danke für euren Rückhalt! Meiner Familie und meinen Freunden möchte ich außerdem für das Verständnis danken, dass Sie mir entgegen brachten, wenn ich mal weniger Zeit für Sie hatte.

Katrin, danke dass du in den letzten vier Jahren so für mich da warst und mich auch in schwierigen Phasen immer wieder motiviert hast. Ohne deine liebevolle und grenzenlose Unterstützung, aber auch konstruktive Kritik wäre die Arbeit in dieser Form nicht möglich gewesen. Danke!

Eidestattliche Erklärung

Ich versichere, dass ich die von mir vorgelegte Dissertation selbständig angefertigt, die benutzten Quellen und Hilfsmittel vollständig angegeben und die Stellen der Arbeit - einschließlich Tabellen, Karten und Abbildungen-, die anderen Werken im Wortlaut oder dem Sinn nach entnommen sind, in jedem Einzelfall als Entlehnung kenntlich gemacht habe; dass diese Dissertation noch keiner anderen Fakultät oder Universität zur Prüfung vorgelegen hat; dass sie - abgesehen von unten angegebenen Teilpublikationen - noch nicht veröffentlicht worden ist sowie, dass ich eine so lche Veröffentlichung vor Abschluss des Promotionsverfahrens nicht vornehmen werde. Die Bestimmungen der Promotionsordnung sind mir bekannt. Die von mir vorgelegte Dissertation ist von Dr. Michael Lammers betreut worden.

_____

Julian Brenig